Electrical Resistance and Natural Convection Heat Transfer Modeling of Shape Memory Alloy Wires

by

Anita Eisakhani

A thesis
presented to the University of Waterloo
in fulfillment of the
thesis requirement for the degree of
Master of Applied Science
in
Mechanical Engineering

Waterloo, Ontario, Canada, 2012

AUTHOR'S DECLARATION

I hereby declare that I am the sole author of this thesis. This is a true copy of the thesis, including any required final revisions, as accepted by my examiners.

I understand that my thesis may be made electronically available to the public.

Abstract

Shape memory alloy (SMA) wires are becoming increasingly popular as actuators in automotive applications due to properties such as large recovery strain, low weight, and silent actuation. The length change and thus actuation in SMA wires occur when the wire is heated, usually by passing a direct current through them. One of the difficulties in controlling electrically-heated SMAs occurs in monitoring their temperature, which is done to control the transformation and hence, actuation and avoid possibly permanent damage due to overheating. The temperature of a SMA wire is usually calculated theoretically based on the wire's natural convection heat transfer coefficient (h). First-order convective heating models are typically used to calculate the natural convection heat transfer coefficient for SMA wires, but there is often significant uncertainty in these calculations due to a lack of existing correlations for thin cylinders, where curvature effects are significant.

The purpose of this investigation is to develop models for SMA wires that may be used to predict the temperature of a current-carrying SMA wire without using direct temperature measurement methods. The models were developed based on experimental results for 0.5 mm diameter NiTi SMA wire. First the effect of various parameters such as wire inclination angle, wire length, ambient pressure, phase transformation time rate and applied external stress were investigated on the SMA wire's electrical resistance. The electrical resistance of the SMA wire was monitored during one complete heating and cooling cycle. Later, based on the experimental results, a resistance model was developed for the current-carrying SMA wires that can be used to predict the wires' temperature

based on electrical resistance. Second, a natural convection heat transfer correlation was developed for NiTi SMA wire, in the range $2.6\times 10^{-8} \leq Ra_D \leq 6\times 10^{-1}$, which is appropriate for modeling natural convection in most practical applications at ambient conditions. A pressure variation method was used to obtain a range of Rayleigh number for a heated SMA wire. The ambient pressure was controlled within a vacuum chamber, from 1 atm to 2×10^{-4} atm (0.1 MPa to 2×10^{-5} MPa). Data were collected for the wire at various angles under both 100 MPa and stress-free conditions between horizontal to vertical at each set pressure. The new correlation can be used to determine the convective heat transfer coefficient of an SMA wire of known diameter and inclination angle. The convection coefficient (h) is determined using the correlation along with the Prandtl number (Pr), air dynamic viscosity (μ), air compressibility factor (Z), air thermal conductivity (k), and gas constant (R_c). The wire temperature can then be determined by substituting this coefficient into the convective heat transfer equation.

Acknowledgements

First, for the opportunity that they gave me to work in the interesting field of shape memory alloys, I would like to thank my supervisors: Professor J. R. Culham for his trust, support, guidance and freedom he gave me during the course of this research, and Professor R. Gorbet for his guidance, support and valuable suggestions throughout this study. Working with them has been a rewarding experience for me.

I would like to thank the Natural Science and Engineering Research Council and General Motors Research Center at Warren Michigan for providing financial support for this work.

I would also like to thank Jay Gao for his help and technical suggestions during the course of this research.

My thanks to machine shop at Mechanical Engineering department, especially Rick Forgett for careful fabrication of the test parts. My sincere thanks extend to Eric Kubica for his help with experimental test setup.

I am grateful to all the members of the Microelectronics Heat Transfer Laboratory for creating a pleasant environment in which to work, especially Elmer Galvis for many valuable discussions that we shared together.

Finally, I would like to thank my parents for their unconditional love and support during past years, which without their encouragements and support the completion of this thesis was not possible for me.

Table of Contents

List of Figures

List of Tables

Nomenclature

A	equation coefficient
A_a	area $[m^2]$
A_{SMA}	SMA wire surface area $[m^2]$
A_{ss}	surface area $[m^2]$
A_c	fin cross sectional area $[m^2]$
A_s	austenite start phase transformation temperature $[℃] or\ [K]$
A_f	austenite finish phase transformation temperature $[℃] or\ [K]$
a	equation coefficient $[\Omega]$
B	equation coefficient
b	equation coefficient [℃]
C	equation coefficient
c	equation coefficient $[\Omega]$
ct_r, ct_I, cs	equation constants
D, d	diameter $[m]\ or\ [mm]$
d_0	SMA wire undeformed cross-section diameter $[m]$
d_c	equation coefficient
G	Gibbs free energy $[J]$
Gr_D, Gr_L	Grashof number
g	acceleration due to gravity $[{}^{m}/_{s^2}]$
H	enthalpy $[J]$

H_M	equation constant
h	convective heat transfer coefficient $[{}^{W}/_{m^2K}]$
I	electric current $[A]$
I_{SMA}	SMA wire current $[A]$
k	thermal conductivity $[{}^{W}/_{mK}]$
k_m	equation coefficient $[{}^{1}/_{\circ\mathrm{C}}]$
k_w	thermocouple wire thermal conductivity $[{}^{W}/_{mK}]$
L, l	length $[m]$ or $[cm]$
L_0	SMA wire undeformed length $[m]$
M_s	martensite start phase transformation temperature $[\mathrm{°C}] or [K]$
M_f	martensite finish phase transformation temperature $[\mathrm{°C}] or [K]$
m	equation coefficient
m_c	equation coefficient
m_3	simulation constant parameter [°C]
$Nu,\ Nu_L,\ Nu_D$	Nusselt number
n	equation coefficient
n_3	simulation constant parameter [°C]
P	pressure $[Pa]$
P_f	fin perimeter $[m]$
Pr	Prandtl number
p_1, p_2	simulation constant parameters $[\Omega m]$

p_3	simulation constant parameter $[{}^{1}/_{\circ\mathrm{C}}]$
Q	heat transfer rate $[W]$
$Q_{conv.}$	convection heat transfer rate $[W]$
$Q_{cond.}$	conduction heat transfer rate $[W]$
$Q_{rad.}$	radiation heat transfer rate $[W]$
Q_f	fin heat transfer rate $[W]$
q_1	simulation constant parameter $[\Omega m]$
q_2	simulation constant parameter $[{}^{\Omega m}/_{\circ\mathrm{C}}]$
R, R_{SMA}	SMA wire electrical resistance $[\Omega]$
$R_{amb.}$	SMA wire electrical resistance at ambient temperature $[\Omega]$
R^a	austenite electrical resistance $[\Omega]$
R^m	martensite electrical resistance $[\Omega]$
R_c	gas constant $[{}^{J}/_{kg\ K}]$
$Ra,\ Ra_L,\ Ra_D$	Rayleigh number
S	entropy $[{}^{J}/_{K}]$
S_A	austenite entropy $[{}^{J}/_{K}]$
S_M	martensite entropy $[{}^{J}/_{K}]$
s	equation constant
T, T_{SMA}	SMA wire temperature $[K]\ or\ [°C]$
T_a	absolute temperature $[K]$
T_0	thermodynamic equilibrium temperature $[K]$

T_{0a}	equation coefficient [℃]
T_{aa}	equation coefficient $[K]$
T_m	mean temperature $[K]$
T_{0m}	equation coefficient [℃]
T_{mm}	equation coefficient $[K]$
T_{RR}	equation coefficient $[K]$
T_s	surface temperature $[K]$
T_∞	ambient temperature $[K]$ or $[°C]$
V	electric voltage $[V]$
V_{SMA}	SMA wire voltage $[V]$
Z	compressibility factor
z	equation constant

Greek Letters

α	thermal diffusivity $[{m^2}/{s}]$
α_i	simulation constant parameter $[{\Omega m}/{°\mathrm{C}^i}]$
α_R	R-phase rhombohedral distortion
β	thermal expansion $[{1}/{K}]$
ϵ	total strain
ε	strain
ε_I, ε_r	strain values correspond to a temperature input

ε_m^{tr}	martensite transformation strain
ε_R^{tr}	R-phase transformation strain
ε_r	emissivity
ξ_m	martensite volume fraction
ξ_R	R-phase volume fraction
θ_b	base temperature [K]
μ	dynamic viscosity $[{}^{kg}/_{ms}]$ or $[{}^{Ns}/_{m^2}]$
ν	kinematic viscosity $[{}^{m^2}/_{s}]$
ν_P	Poisson's ratio
ρ	density $[{}^{kg}/_{m^3}]$
ρ_a	austenite electrical resistivity $[\Omega m]$ or $[\mu\Omega cm]$
ρ_m	martensite electrical resistivity $[\Omega m] or$ $[\mu\Omega cm]$
ρ_i	resistivity $[\Omega m]$
σ	applied stress $[MPa]$
σ_r	Stefan-Boltzmann constant $[{}^{W}/_{m^2K^4}]$
φ	inclination angle $[rad]$ or $[deg]$

Chapter 1
Introduction

Shape memory alloys (SMAs) have attracted attention in recent years because of their ability to undergo a phase transformation at near-room temperature. A shape memory alloy that is deformed at a low temperature (martensite phase) can be returned to its original shape when heated to a higher temperature (austenite phase) [1]. The change between martensite and austenite phases occurs without diffusion, with only the crystal structure of the material changing during this process. Additionally, the phase transformation occurs with strain recovery associated with a large force and mechanical work that gives the alloy the potential to be used as an actuator [1].

The phase transformation in these materials causes a change in physical properties in the two phases, high temperature (austenite) and low temperature (martensite). Studying these changes can help to characterize the behavior of these materials, which may lead to the development of thermophysical models for use in industrial applications such as automotive, aerospace and electrical areas.

In order to observe a physical change in shape memory alloys, the material must be heated under an external applied stress. The SMAs are usually heated via a Joule effect by passing an electric current through the wire, while cooling is achieved by natural or forced convection. At certain temperatures, called phase transformation temperatures, during one heating and cooling cycle, reversible movement of atomic interfaces produce the shape change [1]. The phase transformation temperatures in shape memory alloys depend on the composition of the alloys used for the memory effect and also on the stress

applied to the material. Since phase transformation in SMAs depends strongly on temperature which is difficult to measure directly, a reliable model is required to predict wire temperature, in order to protect the wire from overheating and control the time required to generate a shape recovery motion.

1.1 Motivation

In recent years many studies have been done to efficiently use waste energy and to discover new alternative energy sources in order to improve technologies that do not rely on fossil fuels. Shape memory alloys have the potential to be used as actuators or heat engines in different industries and help save energy. Where a large source of waste heat is available SMAs can save energy by converting waste heat into mechanical work [2]. The advantages of using these materials as a source for mechanical work are that SMA actuators are safe, noiseless, low weight and have a large recovery strain [3]. Although, using these materials commercially as actuators is in its early stage, a lot of research is going on to better understand the behavior of these materials and to overcome the barriers that are preventing their use in commercial applications [2,4-6].

Using shape memory alloys in real applications requires mathematical models that can help predict their behavior. The literature lacks accurate thermal models developed specifically for SMA wires. The thermal models available in the literature cannot be used to calculate natural convection heat transfer coefficients for the SMA wires precisely since they are based on approximations or are developed for other types of wires or cylinders [6-9]. Therefore, this work proposes a heat transfer correlation for SMA wires

that can be used to predict the temperature of current-carrying wires. Also proposed is a model to predict the wire's temperature based on measured electrical resistance.

1.2 Problem Statement

In real applications as opposed to laboratory conditions, it is usually hard to measure the temperature of shape memory alloy wires directly due to practical difficulties in direct temperature measurement methods, such as in spot welding the thermocouples onto the wire or in using infrared thermal imaging while the wire is actually in use. A reliable model is thus important in predicting the SMA wire's temperature so that the stage in the wire's transformation can be determined and potential degradation due to overheating, which can cause permanent damages to the wire such as loss of cyclic behavior in the material, can be avoided. The objectives of this work are

1. To investigate the effect of temperature change and other control parameters such as applied external stress or wire length on its electrical resistance, and to develop a model that can predict the temperature of SMA wires based on their electrical resistance for different wire lengths and under different external applied stresses.

2. To develop a natural convection heat transfer correlation for the SMA wires that can be used to predict the temperature of a current carrying SMA wire at different inclination angles.

3. To develop a natural convection heat transfer coefficient (h) equation for shape memory alloy wires by using the two proposed models.

1.3 Overview

In Chapter 2, a literature review is presented which presents background information about phase transformation and martensite transformation phenomena in materials, shape memory alloys and their applications and also fundamentals of shape memory alloy actuators. Later existing electrical resistance models for shape memory alloy wires and natural convection heat transfer correlations for wires and cylinders available in the literature are reviewed.

In Chapter 3, the experimental apparatus and setup and the data collection procedures for natural convection heat transfer and resistance modeling of the shape memory alloy wire are described.

Chapter 4 presents experimental results for SMA wire electrical resistance and strain under various conditions. Later, a resistance model is proposed for the shape memory alloy wires based on experimental results and can be used to predict wire temperature based on electrical resistance.

Chapter 5 presents experimental results for natural convection heat transfer from SMA wire to air. An empirical natural convection heat transfer correlation is developed for the SMA wire. The newly developed correlation is compared with the existing correlations in the literature for horizontal and vertical orientations.

In Chapter 6, explanations are given of how to use the proposed models for predicting the temperature and natural convection heat transfer coefficient (h) for shape memory alloy wires.

Chapter 7 presents the conclusions for this work and recommendations are made.

Chapter 2
Literature Review

This chapter presents background information about phase transformation phenomena in shape memory alloy wires and fundamentals of SMA actuators are presented. Later a review of existing electrical resistance models for SMA wires is presented along with some reviews of available heat transfer correlations for wires and cylinders.

2.1 Background

2.1.1 Phase Transformation

A closed system under fixed external conditions will naturally transform from its initial state to its equilibrium or stable state. The different states or phases can be distinguished by variations in their physical properties, structural arrangement, or composition. At equilibrium or stable state the system is at its minimal energy level. This level, at a constant temperature and pressure can be defined by the Willard Gibbs theory of equilibrium as [10]

$$G = H - T_a S \tag{2.1}$$

where

T_a = absolute temperature

S = molar entropy

H = molar enthalpy

Based on this theory the system is at its stable state whenever the Gibbs free energy of the system is at its minimum level. The force required for the system to transform from its higher energy level to lower energy level is called the driving force. This force is shown by ΔG (Fig. 2.1), which is the energy difference between the higher and lower energy level in the system and can be shown as [11]

$$\Delta G = G_{end} - G_{begin} \tag{2.2}$$

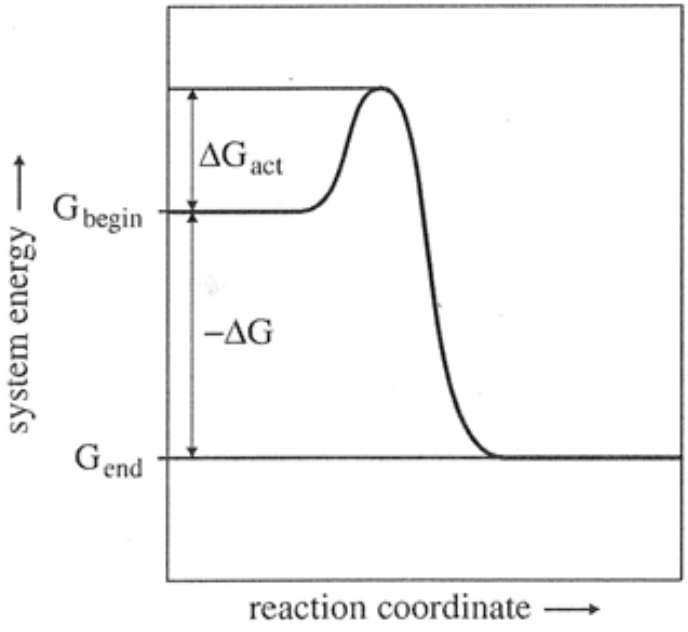

Figure 2.1 The driving force of phase transformation [11]

During phase transformation, the system must overcome an energy barrier (Fig. 2.1) since extensive rearrangement of the atomic structures usually happens under the influence of thermal activation, external stress or surface energy and not only because of

the energy difference between the higher and lower energy levels. The energy barrier (ΔG_{act}) can be defined as

$$\Delta G_{act} = \Delta H_{act} - T\Delta S_{act} \tag{2.3}$$

where

$\Delta S_{act} =$ entropy of activation

$\Delta H_{act} =$ enthalpy of activation also called activation energy

The phase transformation process from a microstructural point of view can be divided into two types: “nucleation and growth” and “martensitic” [12]. Nucleation is the formation of stable particles or nuclei of the new phase. Growth is the growth process of the product phase, during which the nuclei grow and increase their size at the expense of the old phase. The transformation is complete once the growth reaches an equilibrium state. The nucleation and growth type transformation is a time dependent process, meaning that the amount of new phase or nuclei increases with time (Fig. 2.2) [13]. This type of transformation can happened in solids, liquids and gases. In contrast martensite transformation happens in solids only and the rate of transformation is independent of time.

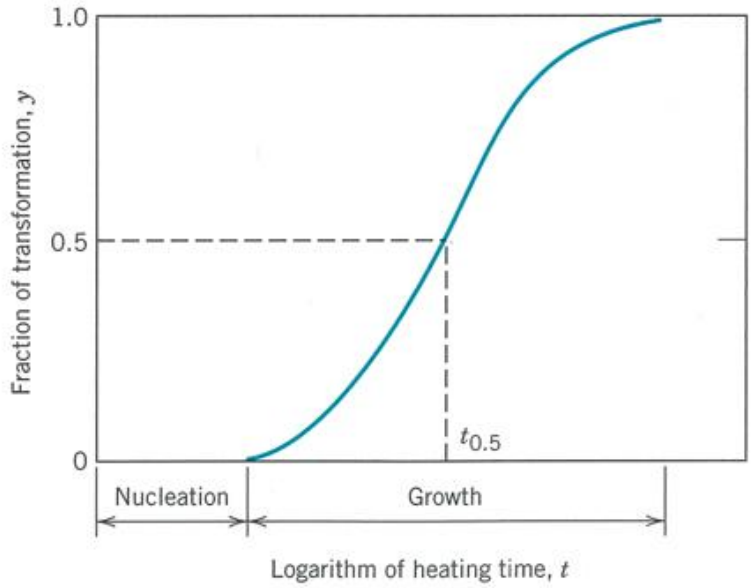

Figure 2.2 Time dependent solid-state phase transformation in which temperature is held constant [13]

2.1.2 Martensite Transformation

Martensite refers to a crystal structure named after metallographer A. Martin, who first observed this microstructure in different steels under a microscope in the 1890s and explained the mechanical properties of steels by expanding the discovery of H. Sorby [14].

Martensite crystal structure in materials is a result of diffusionless growth mechanisms that occur without diffusion by homogeneous movement of atoms in the crystal structure in which the neighbors of most atoms remain unchanged [15]. Martensite transformation is an athermal transformation, meaning the growth mechanism is independent of time and is a function of temperature. The martensite transformation starts at a specific

temperature called the martensite start temperature (M_s) and does not grow with time. Decreasing the temperature from the M_s temperature increases the martensite fraction. The material involved becomes fully martensitic at the M_f temperature. If the cooling process is interrupted before the M_f temperature the phase transformation will be stopped and will not grow with isothermal holding, which means that the temperature is kept constant during the phase transformation process [10]. During the return transformation when martensite is heated it starts to change to austenite at the austenite start temperature (A_s), and this austenite transformation is completed at a certain temperature called the austenite finish temperature (A_f), although in some circumstances, such as small driving force, martensite transformation can be isothermal and increases with time at a constant temperature. When the applied stress is small, the isothermal martensite transformation can be observed, but this process can be controlled by increasing the applied stress that leads back to athermal transformation [16]. In 1948, Kurdjumov and Maximova [17] become the first to observe the isothermal martensite transformation in steel containing magnesium and carbon. Bunshah and Mehl [18] in 1953 found that martensite plates form in about 10^{-7}s and the growth velocity for martensite transformation is about 1 $km/_S$, which is near the velocity of sound in solids. Regardless of athermal or isothermal martensite transformation, the martensite plates form by sudden movement of atoms near the velocity of sound in solids [15].

The temperature at which the free energies of austenite phase and martensite phase are equal can be quantified as $T_0 = \frac{1}{2}(M_s + A_s)$, which is also called the *thermodynamic equilibrium temperature* [10]. At a temperature below T_0, the free energy of martensite becomes less than the free energy of austenite, and that is the point when martensitic transformation occurs [19].

Since no atomic diffusion occurs during martensite transformation, the chemical composition of the two phases remains the same. The mechanical properties such as resistivity and Young's modulus that depend on material crystal structure change between high temperature cubic austenite and low temperature monoclinic martensite phases [19]. Each of these physical properties such as electrical resistance or strain have a hysteresis curve between M_s, M_f, A_s and A_f temperatures. This hysteresis shape is one of the main characteristics of martensite transformation (Fig. 2.3) [1, 20].

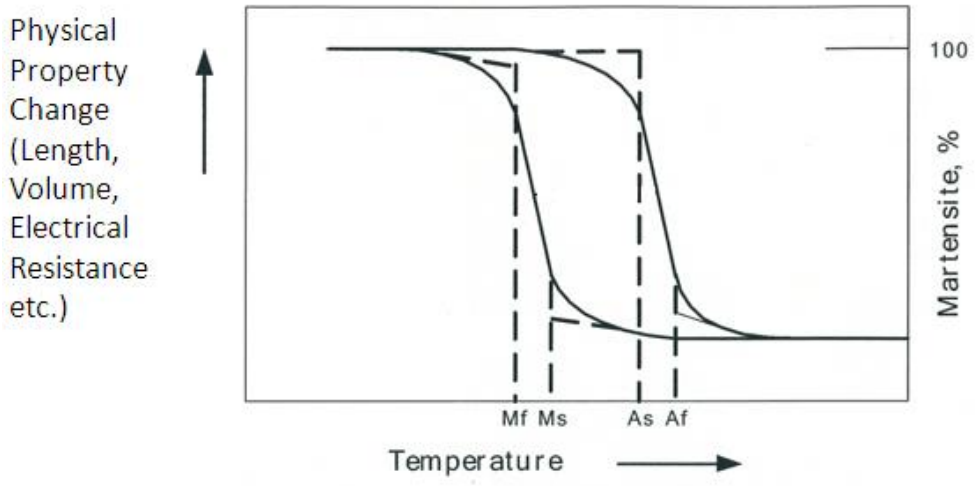

Figure 2.3 Hysteresis curve for martensite phase transformation [20]

Certain conditions such as heat treatment, chemical composition, extreme deformation, or cyclic effects can result in a two stage martensite transformation [21], meaning that during the cooling process from the austenite phase, a new phase, called the R-phase, can appear prior to the martensite phase. The R-phase has different properties, such as higher electrical resistance and lower strain, than the martensite phase [22, 23] and forms in small temperature hysteresis, approximately between 2 to 5℃ [23]. There remains considerable debate in the literature about the origin of the R-phase and its properties [21-25].

Movement of atoms during the transition from the martensite to the austenite phase can be accompanied with a shape change, an important characteristic of martensite transformation that makes it important in technology.

2.1.3 Shape Memory Alloys

The discovery of martensite in steel crystalline structures in the 1890s was an important step in the discovery of shape memory alloys [26]. The first shape recovery capability was observed in Au-Cd alloy by Olander in 1932 [27]. Greinger and Mooradian [28] observed the formation and disappearance of martensite phases in Cu-Zn alloy by decreasing and increasing the temperature of the alloy in 1938. A decade later, Kurdjumov and Khandros [29] observed the shape memory effect governed by reversible martensite transformation in Cu-Zn and Cu-Al alloys. The main interest in using alloys that have shape memory effect and undergo martensitic phase transformation for engineering applications occurred in 1963, when W.J. Buehler and his co-workers [30] at the Naval Ordnance Laboratory discovered the shape memory effect in nickel-titanium

(Ni-Ti) alloys. The commercial name NITINOL was chosen for NiTi materials in honor of its discovery at the Naval Ordnance Laboratory (NOL). The shape memory effect of SMA alloys is a result of the martensitic transformation phenomena in these materials. A typical stress-strain loading path is shown in Figure (2.4), where the stress (σ) is the load applied to the material, and strain (ε) is its length change with respect to its original length.

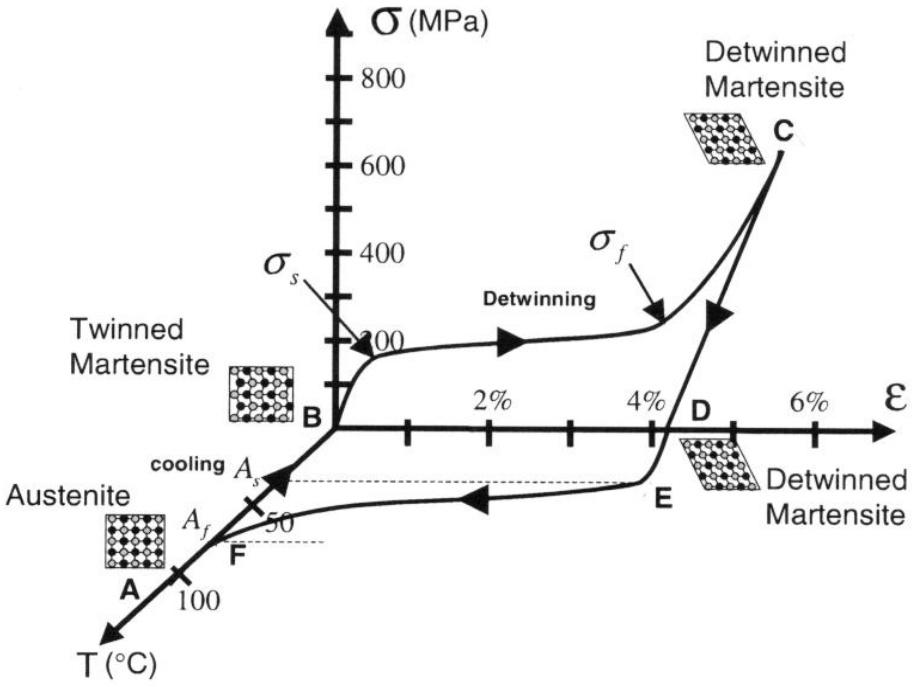

Figure 2.4 Stress-strain-temperature curve for shape memory alloys [26]

When the austenite phase is cooled the crystal structure changes from austenite to twinned martensite, with no macroscopic shape change (A→ B). If the applied load to the material is sufficient, the twinned martensite can be transformed to detwinned martensite by reorientation of the martensite variants, which produces a macroscopic shape change

(B→ C). The minimum stress of detwinning is called the *detwinning start stress* (σ_s), and is lower than the permanent yield stress of martensite. At σ_f stress level the detwinning process is complete. During the cooling process, if the material is cooled with a stress or applied load larger than σ_s it can be directly transformed from austenite to detwinned marteniste. During the heating process (C→ D) the detwinned martensite structure remains and no strain recovery occurs until the temperature reaches the A_s temperature where the austenite phase initiates and the crystal structure starts to change to cubic austenite. This is accompanied by strain recovery until the A_f temperature, where the process is completed (E→ F) [19, 26].

The atomic crystal structure changes that result in the length change of the material are shown in Figure (2.5).

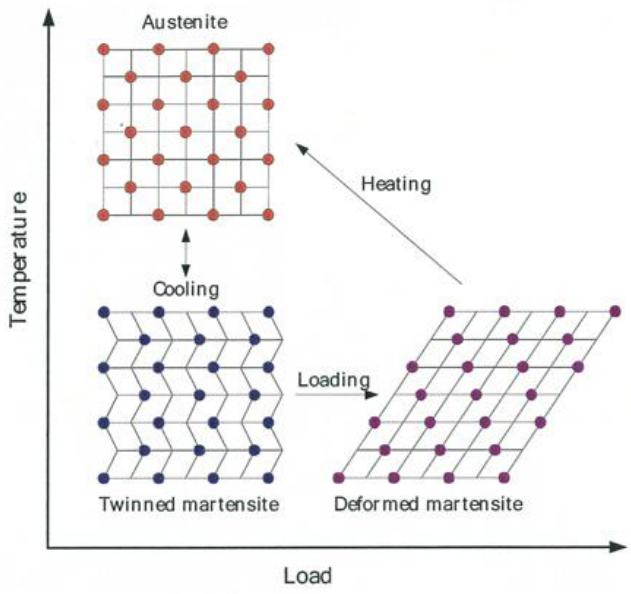

Figure 2.5 Atomic crystal structure changes during martensite phase transformation [20]

The reverse transformation from austenite to martensite that occurs with a shape recovery is called the pseudoelastic effect in shape memory alloys [26]. This shape change is not reversible under stress-free conditions; therefore, it is called a one-way shape memory effect. However, if the phase transformation from austenite to martensite happened under a stress larger than σ_s, then the shape recovery can be achieved in the reverse transformation from austenite to martensite as well, which is called the bias shape memory effect [26]. The cyclic behavior of shape change can be repeated by the bias shape memory effect, giving the material the ability to work as an actuator in cyclic applications.

2.1.3.1 Shape Memory Alloy Actuators

The generated strain associated with a large force and the ability to perform mechanical work makes SMAs a potential material for use in actuators. Some advantages of SMA actuators compared to other types of actuators are small size, low weight, small number of mechanical parts, silent actuation and the large recovery strain that provides large motion [3]. One difficulty with SMA actuators is hysteresis, which makes modeling difficult. Also affected is temperature control, which requires a single data point of position, associated with a temperature. Due to the temperature–strain hysteresis relationship in shape memory alloys there are two strain positions for each temperature point; therefore, it is required to know whether the point is on the cooling or heating curve [31]. There is also only a limited range of transformation temperatures, and in

addition, the slower cooling than heating process precludes applications where fast actuation in both heating and cooling processes are required [32].

Figure (2.6) shows a simple SMA actuator where a shape memory wire or spring is lifting a weight. When the wire is heated, the weight will be lifted and the work done can be defined as $\int \sigma d\varepsilon$ or $\sigma \Delta \varepsilon$. This is the work of an SMA wire on an external load during the heating process. If the applied external stress is greater than σ_s, the applied load will do the same amount of work on the SMA wire while stretching it back during the cooling process. Therefore, if the stress remains the same during heating and cooling, and neglecting the energy losses, the net output $W = \oint \sigma d\varepsilon$ per cycle is zero, which makes it possible to reset the system and use it in cyclic applications [32].

For springs made from traditional materials such as steel when it is obeying Hook's law, the Young's modulus remains constant; therefore, the spring rate, which is proportional to Young's modules, remains constant as well, but in NiTi springs, the shear modulus changes with phase transformation from austenite to martensite [33]. The Young's modulus of the austenite phase is higher than that of the martensite phase due to the different crystal structure, which means the spring rate changes while changing the spring temperature.

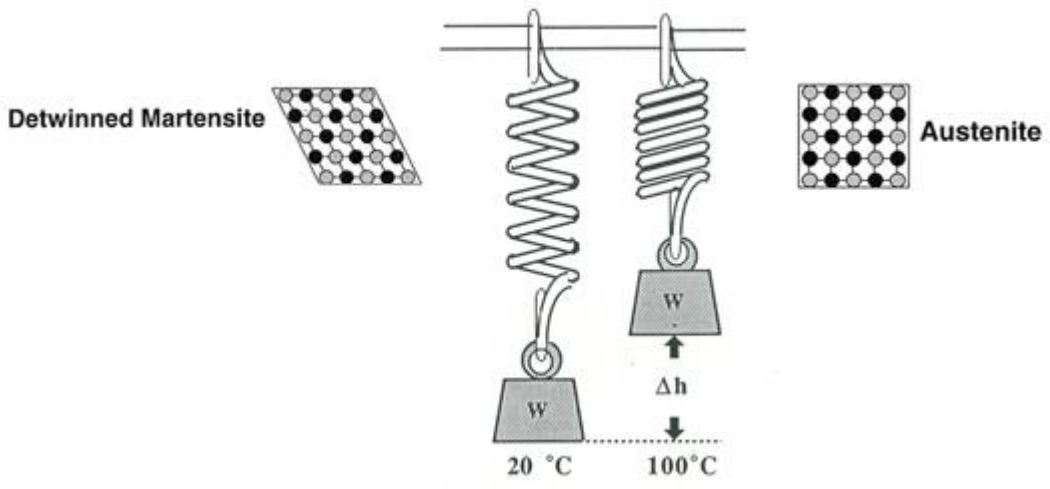

Figure 2.6 Classic shape memory alloy actuator [26, 32]

SMA actuators are usually in one of two types: thermal or electrical. The thermal actuation of an SMA alloy is initiated through a change in temperature of the ambient medium which, in turn, results in a phase transformation of the material and a change of shape. Thermal actuators are mainly used as sensors in which the SMA senses the ambient change and actuates or responds by generating a force [3]. NiTi and Cu based alloys such as Cu-Zn-Al and Cu-Al-Ni can be used as thermal actuators. The limitation of using binary NiTi alloys in thermal actuators is their low transformation temperatures, but they have advantages such as stability, higher fatigue lifetime and strain recovery [3]. Cu based alloys have higher phase transformation temperatures and are less expensive but have lower thermal stability and are difficult to deform. In electrical actuators the SMA alloy wire is heated by passing a current through the wire [3]. These actuators are mainly used to do work by moving a load or performing a task like those used in vehicles for the central locking system. NiTi alloys are mainly used in these types of actuators since an

A_s above room-temperature is required. In addition, NiTi alloys have a higher fatigue lifetime and electrical resistivity than other Cu base SMA alloys, properties that are important in electrical actuators [3]. Usually NiTi used in electrical actuators are with one-way shape memory effect under an external applied load. The parameters that can affect performance of electrical actuators are applied stress, electrical current or power input, ambient temperature and fatigue [3] [32-34].

2.1.3.2 Shape Memory Alloy Applications

SMA alloys are used for various applications in different fields such as robotics, control, automotive, aerospace and biomedicine devices. SMAs can be used in vibration and damping applications because of their pseudoelasticity and memory effects. The high damping capacity in SMAs and their ability to dissipate the vibration energy of structures subjected to loading comes from reversible martensitic transformation in these materials [35]. The damping capacity of shape memory alloys can be improved by applying appropriate thermomechanical treatment or increasing the amplitude of vibration [36]. In automotive applications SMAs can be used both as thermal and electrical actuators in various parts of vehicles such as seat-belt adjustment, central locking and valve actuators in different parts [3]. SMAs can also be used in heat engines to convert thermal energy to mechanical energy [2, 32]. Their damping property can be used for impact absorption in vehicles. There are many examples of SMA materials used in aerospace applications such as embedding SMA beam components inside chevrons in Boeing 777-300ER Quiet Technology Demonstrator 2 design (Fig. 2.7) [37, 38]. During high speed or high altitude flights, the SMA beam components increase engine performance by undergoing

martensitic transformation and straightening the chevrons. For low speed and low altitude flights the SMA beam components increase mixing of exhaust gas flow by bending the chevrons into the flow and thus reducing take off and landing noise [26, 38].

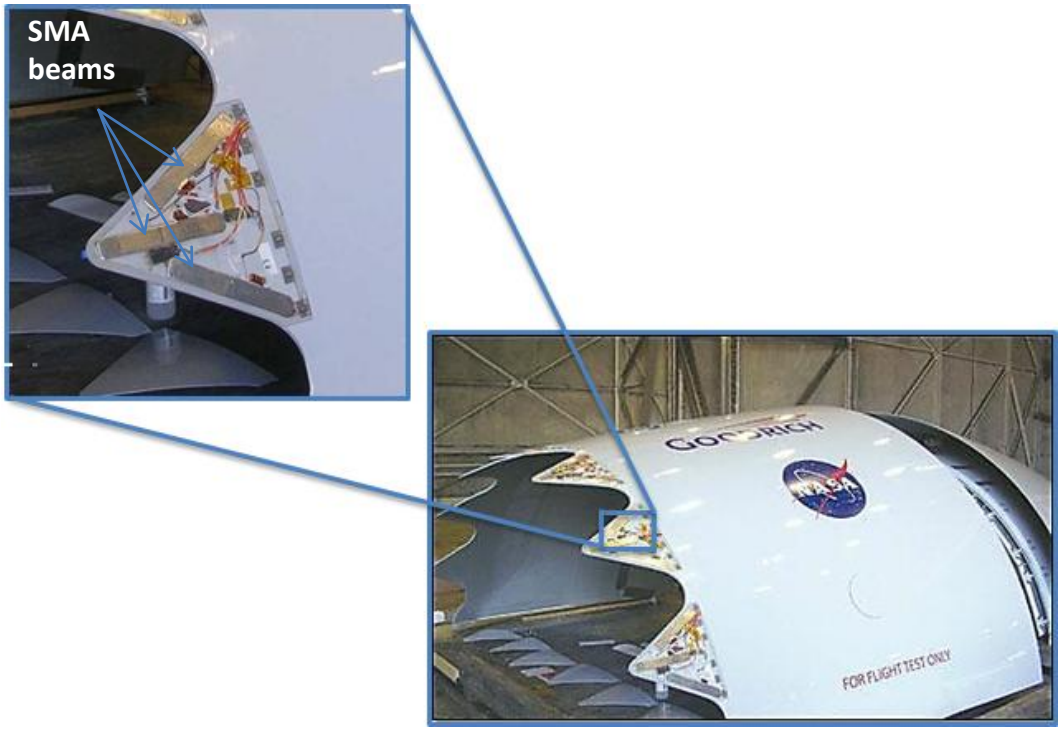

Figure 2.7An inner look at a Boeing 777 chevron; each chevron includes three Ni-Ti actuators [37, 38]

SMAs are also used in different aerostructures such as variable geometry airfoils where the foil changes its configuration from symmetric to camber (Fig. 2.8) by SMA actuation [26, 38]. NASA used SMA actuators in the Mars Pathfinder in order to rotate a dust cover to protect the solar panel from dust and allow the panel to get its required power [26].

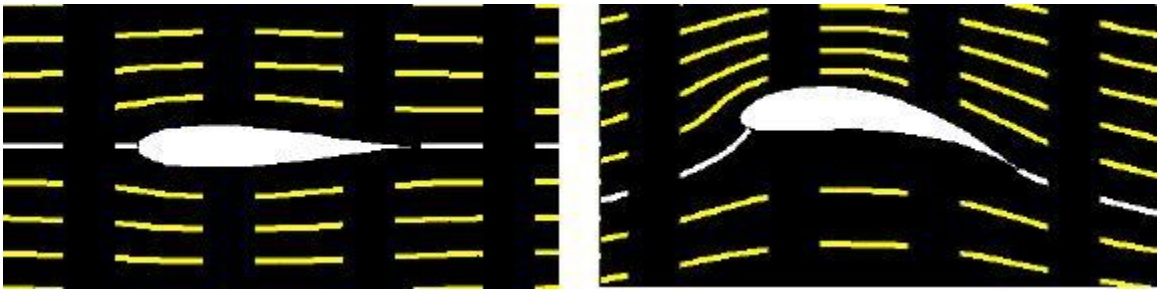

Figure 2.8 Airfoil geometry change from symmetric to camber [39]

SMAs have numerous applications in different medical fields such as dentistry and orthodontistry or in heart and cardiovascular surgery for different applications, such as using NiTi wires in artificial heart muscles or using self-expanding NiTi for opening heart blood vessels [26, 40].

2.2 Review of Shape Memory Alloys Electrical Resistance

Electrical resistance studies for SMA wires can be used to develop a model that relates SMA wire electrical resistance and temperature in order to predict the temperature of the wire based on its electrical resistance. Carballo et al. [41] studied the electrical resistance of NiTi wires under various constant stresses and reported on the effects of applied stress on electrical resistance. Their results show that stress has a significant effect on the resistance-temperature curve and the resistance of SMA materials increase as the applied stress increases. Wu et al. [42] studied the electrical resistance and resistivity of NiTi wires, and their results show that the electrical resistance and its variation range is small for NiTi wire. Their result for electrical resistivity of NiTi wire was 70-100 $\mu\Omega cm^{-1}$. Nascimento et al. [9] studied electrical resistance of NiTi wire for different applied

stresses and reported that the electrical resistance decreases by 17 to 18% during phase transformation from martensite to austenite for all applied loads.

Ikuta et al. [43] proposed a mathematical model of NiTi SMA wires electrical resistance-temperature for design of micro actuators for a transformation temperature range $M_f < T < A_f$ as

$$R(T) = \frac{1}{1 + \exp\left[k_m(T - T_{0m})\right]} \tag{2.4}$$

where in the cooling process

$$T_{0m} = \frac{(M_s + M_f)}{2} \quad and \quad k_m = \frac{6.20}{(M_s - M_f)}$$

in the heating process

$$T_{0m} = \frac{(A_s + A_f)}{2} \quad and \quad k_m = \frac{6.20}{(A_f - A_s)}$$

Dutta and Ghorbel [6] modeled electrical resistance of NiTi SMA wires over the phase transformation temperature range as

$$\frac{1}{R} = \frac{\pi d_0^2}{4L_0(1 + 2\epsilon)}\left[\frac{1 - R^m}{\rho_a(T)} + \frac{R^m}{\rho_m(T)}\right] \tag{2.5}$$

where electrical resistivity of austenite ($\rho_a(T)$) is shown as

$$\rho_a(T) = p_1 + p_2 \exp\left(-p_3(T - T_{amb})\right) \tag{2.6}$$

and electrical resistivity of martensite ($\rho_m(T)$) is

$$\rho_m(T) = (q_1 - q_2\mathrm{T})\left[1 + \mathrm{erf}\left(\frac{T - m_3}{n_3}\right)\right] + \sum_{i=0}^{i=9} \alpha_i\,(T - T_{amb})^i \tag{2.7}$$

where $p_1, p_2, p_3, q_1, q_2, m_3, n_3$ and $\alpha_i (i = 0, \ldots 9)$ are constant parameters. R^m is the electrical resistance of martensite which is shown as

$$R^m = \frac{4L_0(1 + 2\epsilon)}{\pi d_0^2}\rho_m(T) \tag{2.8}$$

and ϵ is total strain defined by the author [6] and L_0 and d_0 are undeformed length and diameter of the wire respectively.

Novak et al. [44] modeled electrical resistivity of SMA wires as

$$\rho_{tot} = \rho_a(1 - \xi_R - \xi_m) + \rho_R\xi_R + \rho_m\xi_m \tag{2.9}$$

where ξ_R and ξ_m are the volume fractions of the R-phase and martensite phase respectively and

$$\rho_a = \rho_{aa} + (T_{aa} - T)\frac{\partial \rho_a}{\partial T} + \sigma\frac{\partial \rho_a}{\partial \sigma} \tag{2.10}$$

$$\rho_R = \rho_{RR} + (T_{RR} - T)\frac{\partial \rho_R}{\partial T} + \sigma\frac{\partial \rho_R}{\partial \sigma} + (90 - \alpha_R)\frac{\partial \rho_R}{\partial \alpha_R} + \varepsilon_R^{tr}\frac{\partial \rho_R}{\partial \varepsilon_R^{tr}} \tag{2.11}$$

$$\rho_m = \rho_{mm} + (T_{mm} - T)\frac{\partial \rho_m}{\partial T} + \sigma\frac{\partial \rho_m}{\partial \sigma} + \varepsilon_m^{tr}\frac{\partial \rho_m}{\partial \varepsilon_m^{tr}} \tag{2.12}$$

T is temperature, σ is applied stress, $\rho_{ii}\,(i = a, R, m)$ are electrical resistivity of individual phases, ε_m^{tr} and ε_R^{tr} are transformation strain. All the values for parameters introduced above are given by the authors [44].

Cui et al. [4] modeled the change in electrical resistance of the shape memory alloy wires based on strain as

$$\frac{\Delta R}{R} = \frac{\Delta \varepsilon}{\varepsilon} + (1 + 2\nu_P)\varepsilon \tag{2.13}$$

where ν_P is Poisson's ratio, ε is the strain and $\Delta\varepsilon/\varepsilon$ is the strain change which is further defined by the authors [4]. Kirkpatrick and Valasek [5] mathematically modeled the strain-temperature hysteresis curve in NiTi SMA wires based on a hyperbolic tangent curve as

$$\varepsilon_I = H_M/2\tanh\big((T - ct_I)z\big) + s(T - (ct_I + ct_r)/2) + H_M/2 + cs \tag{2.14}$$

$$\varepsilon_r = H_M/2\tanh\big((T - ct_r)z\big) + s(T - (ct_I + ct_r)/2) + H_M/2 + cs \tag{2.15}$$

where H_M, ct_r, ct_I, z, s and cs are constant coefficients [5]. ε_I and ε_r are the strain values that correspond to the temperature input [5].

2.3 Review of Natural Convection Heat Transfer Correlations

An important factor in natural convection heat transfer is to determine the convection heat transfer coefficient (h). h can be calculated for SMA wires using natural convection heat transfer correlations between dimensionless variables Rayleigh (Ra) and Nusselt (Nu) numbers. Natural convection heat transfer correlations can be obtained

experimentally for a specific type of geometry under controlled laboratory conditions in terms of dimensionless parameters that later may be used for different fluids, velocities and length scales [45]. There is no specific type of heat transfer correlation for SMA wires readily available in the literature therefore, some authors such as Nascimento et al. [9] obtained natural convection heat transfer coefficient (h) between SMA wire and its surrounding based on experiments and the Ljung identification method. Others used heat transfer correlations for cylinders or wires for heat transfer modeling of the SMA wires. Shahin et al. [7] suggested using the Incropera and DeWitt [45] empirical correlation for long horizontal cylinders to determine natural convection heat transfer coefficient (h) in their work to enhance SMA wires response time. Pathak et al. [8] used Morgan's [46] correlation for horizontal cylinders in their work to calculate (h) for SMA wires based on a strain recovery method. None of the above mentioned methods can be used to calculate (h) for the SMA wires precisely since they are based on approximations or are developed for other types of wires or cylinders. Some of these existing correlations proposed in the literature for wires and cylinders are reviewed in this section.

2.3.1 Horizontal

Incropera and DeWitt [45] show results of Churchill and Chu [47] natural convection heat transfer correlation for long horizontal cylinders developed in 1974 for all Pr values and $10^{-5} < Ra_D < 10^{12}$ as

$$Nu_D = \left(0.6 + \frac{0.387{Ra_D}^{1/6}}{[1 + (0.599/Pr)^{9/16}]^{8/27}}\right)^2 \tag{2.16}$$

Morgan [46] introduced a power form of the natural convection heat transfer correlations for long horizontal cylinders as

$$Nu_D = B(Ra_D)^m \tag{2.17}$$

where

B = 0.675 m = 0.058 for $10^{-10} < Ra_D < 10^{-2}$

B = 1.02 m = 0.148 for $10^{-2} < Ra_D < 10^{2}$

B = 0.85 m = 0.188 for $10^{2} < Ra_D < 10^{4}$

Jaluria [48] developed a natural convection heat transfer correlation for long horizontal cylinders for Pr=0.7 and $10^{-10} \leq Ra_D \leq 10^{7}$as

$$Nu_D = 0.436(Ra_D)^{1/4} \tag{2.18}$$

McAdams [49] reported results of Herman's correlation for natural convection heat transfer from single horizontal cylinders to gases for $Gr_D > 10^4$ and Pr= 0.74 as

$$Nu_D = 0.4(Ra_D)^{0.25} \tag{2.19}$$

Kyte et al. [50] proposed a correlation for natural convection heat transfer from long horizontal cylinders to gases for $10^{-7} \leq Ra_D \leq 10^{1.5}$ as

$$Nu_D = \frac{1}{\ln\left[1 + \frac{7.09}{Ra_D^{0.37}}\right]} \tag{2.20}$$

Tsubouchi and Masuda [51] developed a correlation for thin horizontal cylinders in which oil was used as the cooling fluid for a cylinder diameter range of $0.015\,mm \leq D \leq 0.063\,mm$ and $10^{-6} < Ra_D < 10$ as

$$Nu_D = 0.36 + 0.56Ra_D^{0.25} \tag{2.21}$$

Fujii et al. [52] introduced a correlation for natural convection heat transfer from long horizontal thin platinum wire of 50.4 μm in diameter and 270 mm in length to air for $10^{-8} < Ra_D < 10^6$ as

$$\frac{2}{Nu_D} = \ln\left(1 + \frac{3.3}{C(Pr)Ra_D^m}\right) \tag{2.22}$$

where

$$C(Pr) = {0.671}\Big/{\left\{1 + \left({0.492}/{Pr}\right)^{9/16}\right\}^{4/9}} \tag{2.23}$$

$$m = 0.25 + 1/(10 + 5Ra_D^{0.175}) \tag{2.24}$$

2.3.2 Vertical

Yang [53] introduced a natural convection heat transfer correlation for vertical cylinders for all Pr values and $Ra_D < 10^9$ as

(2.25)

$$Nu_D = 0.36 + \frac{0.670[Ra_D \frac{D}{l}]^{1/4}}{[1 + \left(\frac{0.492}{Pr}\right)^{9/16}]^{4/9}}$$

Mueller [54] introduced a correlation for vertical wires for $10^{-6} \leq Ra_D \leq 10^{-2}$ as

(2.26)

$$Nu_D = (Ra_D)^{0.11}$$

Nagendra et al. [55] introduced a correlation for natural convection heat transfer from 0.5 mm, 1 mm and 1.25 mm diameter platinum wires to water as

(2.27)

$$Nu = 0.87(Ra\frac{D}{l})^{0.05}$$

where D/l is the ratio of wire diameter to its length.

For vertical cylinders Fujii et al. [56] introduced a correlation for natural convection heat transfer from long horizontal thin platinum wire of 0.470 mm in diameter and 238 mm in length to air for $Pr = 0.7$ as

(2.28)

$$Nu_D = C\ (Pr)(Gr_D \Pr D/1)^{1/4} + \ 0.763C(Pr)^{1/6}(Gr_D \Pr D)/1)^{1/24}$$

for

$C\ (Pr)(Gr_D \Pr D/1)^{1/4} > 2\ \times\ 10^{-3}$

where the authors [56] conclude that Equation (2.28) can be used for vertical wires as well.

Janna [57] introduced a natural convection heat transfer correlation based on experimental work as

(2.29)

$$Nu_D = 0.6\left(Ra_D \frac{D}{l}\right)^{0.25} \qquad Ra_D \frac{D}{l} \geq 10^4$$

(2.30)

$$Nu_D = 1.37\left(Ra_D \frac{D}{l}\right)^{0.16} \qquad 0.05 \leq Ra_D \frac{D}{l} \leq 10^4$$

(2.31)

$$Nu_D = 0.93\left(Ra_D \frac{D}{l}\right)^{0.05} \qquad Ra_D \frac{D}{l} \leq 0.05$$

2.3.3 Inclined

Oosthuizen [58] proposed a convective heat transfer correlation for inclined cylinders based on experimental study for $10^4 < Gr_D < 10^9$as

(2.32)

$$Nu_D/(Gr_D cos\varphi)^{0.25} = 0.42 \qquad l^* > 10$$

(2.33)

$$Nu_D/(Gr_D sin\varphi)^{0.25} = 0.55 \qquad l^* < 10$$

(2.34)

$$Nu_D/(Gr_D cos\varphi)^{0.25} = 0.42\left[1 + \left(\frac{1.31}{l^{*0.25}}\right)^8\right]^{0.125} \qquad 1 < l^* < 10$$

where $l^* = l/(D\ tan\varphi)$

Chand and Vir [59] showed results of the Kato and Ito natural convection heat transfer correlation for inclined cylinders for $Pr = 0.733$ and $1.95 \times 10^5 < Gr_D < 8.62 \times 10^6$ as

$$Nu_D = 0.399(Ra_D)^{1/4} \qquad \varphi = 0 \tag{2.35}$$

$$Nu_D = 0.403(Ra_D)^{1/4} \qquad \varphi = 30 \tag{2.36}$$

$$Nu_D = 0.410(Ra_D)^{1/4} \qquad \varphi = 45 \tag{2.37}$$

Fujii et al. [56] improved its relation for horizontal wires Equation (2.22) that corresponds to the correlation method by Oosthuizen [58] and Raithby and Hollands [60] proposed a correlation for inclined wires in the range of $10^{-4} \leq Ra_D \leq 10^{-3}$ and $0° < \varphi \leq 85°$ as

$$\frac{2}{Nu_D} = \ln\left(1 + \frac{3.3}{C(Pr)(Gr_D Pr cos\varphi)^n}\right) \tag{2.38}$$

2.3.4 Summary of Natural Convection Heat Transfer Correlations

There are few correlations in the literature for wires; therefore, most of the presented correlations are for cylinders. Some of the presented correlations for cylinders in horizontal and vertical orientations are used to verify the newly developed correlation for

SMA wires shown in Section 5.2. There are very few correlations for inclined wires and cylinders, and none of them are in the Rayleigh number range used in this work. Therefore, the developed correlation for SMA wires contains a wire inclination angle that can be used for SMA wires at any inclination angle from horizontal to vertical.

Chapter 3
Experimental Study

Two main experiments were conducted in this work:

1. The first experiment was designed to collect the data necessary for developing a natural convection heat transfer correlation between Nusselt and Rayleigh numbers for the SMA wire. The SMA wire is heated via a Joule effect method by passing direct current through the wire. Heat transfer occurs between the wire and its surrounding by convection, conduction and radiation. The Nusselt numbers are calculated for the SMA wire based on the convection heat transfer rate, and a range of Rayleigh number is obtained by varying of the ambient pressure. The summary of this process is shown in Figure (3.1).
2. The next experiment was designed to collect data necessary for electrical resistance modeling of SMA wires. The SMA wire is heated though its phase transformation temperatures via a Joule effect method and its electrical resistance is measured using Ohm's law based on a voltage drop across the wire and the current input.

The procedures performed during these experiments are presented in this chapter. The uncertainties in collected experimental data are presented in Appendix A.

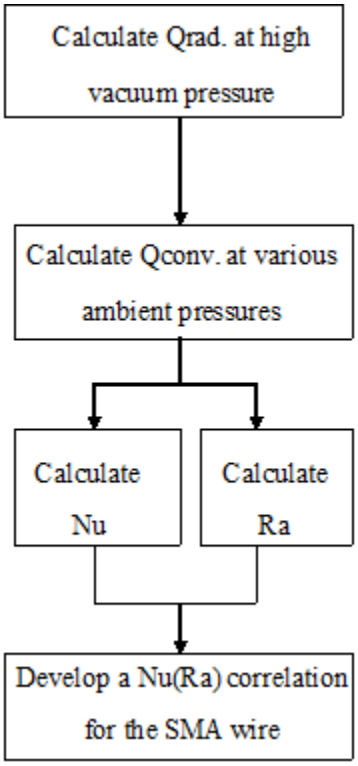

Figure 3.1 Flow chart of natural convection heat transfer experiment process

3.1 Apparatus

All experiments were carried out in an NRC 3117 vacuum chamber composed of an 18" dia × 30" tall Pyrex bell jar. The system allows control of the ambient pressure from 1 atm (760 torr) down to 10^{-7}torr by using mechanical and diffusion pumps. The ambient pressure was measured using a CeramiCel pressure gauge and Stokes gauge. A Keithley Model 2700 data acquisition system was used to collect the data, and then the data were recorded using a computer running an ExceLINX program. The 0.5 mm diameter Flexinol Ni-Ti SMA wire with $A_s = 90℃$ was heated with a BK PRECISION 1760A power supplier, its current determined using a 0.05 Ω shunt resistor (Fig. 3.3). The SMA

wire inclination angle was controlled by connecting one end of the wire test fixture to another plate with a hinge and a rod is connected to the both plates. The top plate can be inclined and fixed at any angle from horizontal to vertical. The rod is marked at intervals so that the devices' fixed angles can be measured to show its inclination angle (Fig. 3.2). The SMA wire strain was determined using a BOURNS square single turn panel control by reading a resistance signal through the Keithley data acquisition system.

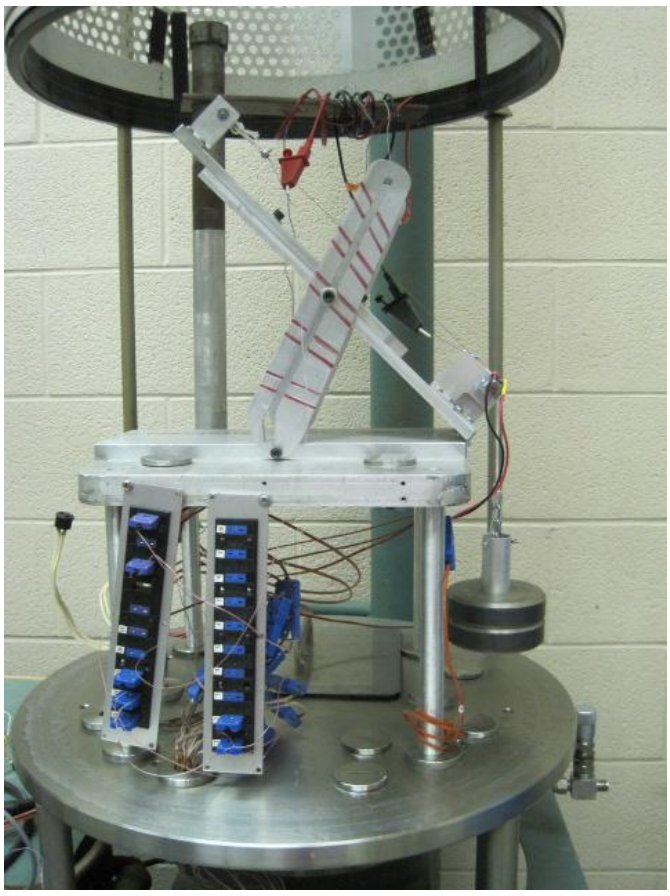

Figure 3.2 SMA wire inclination angle modifier

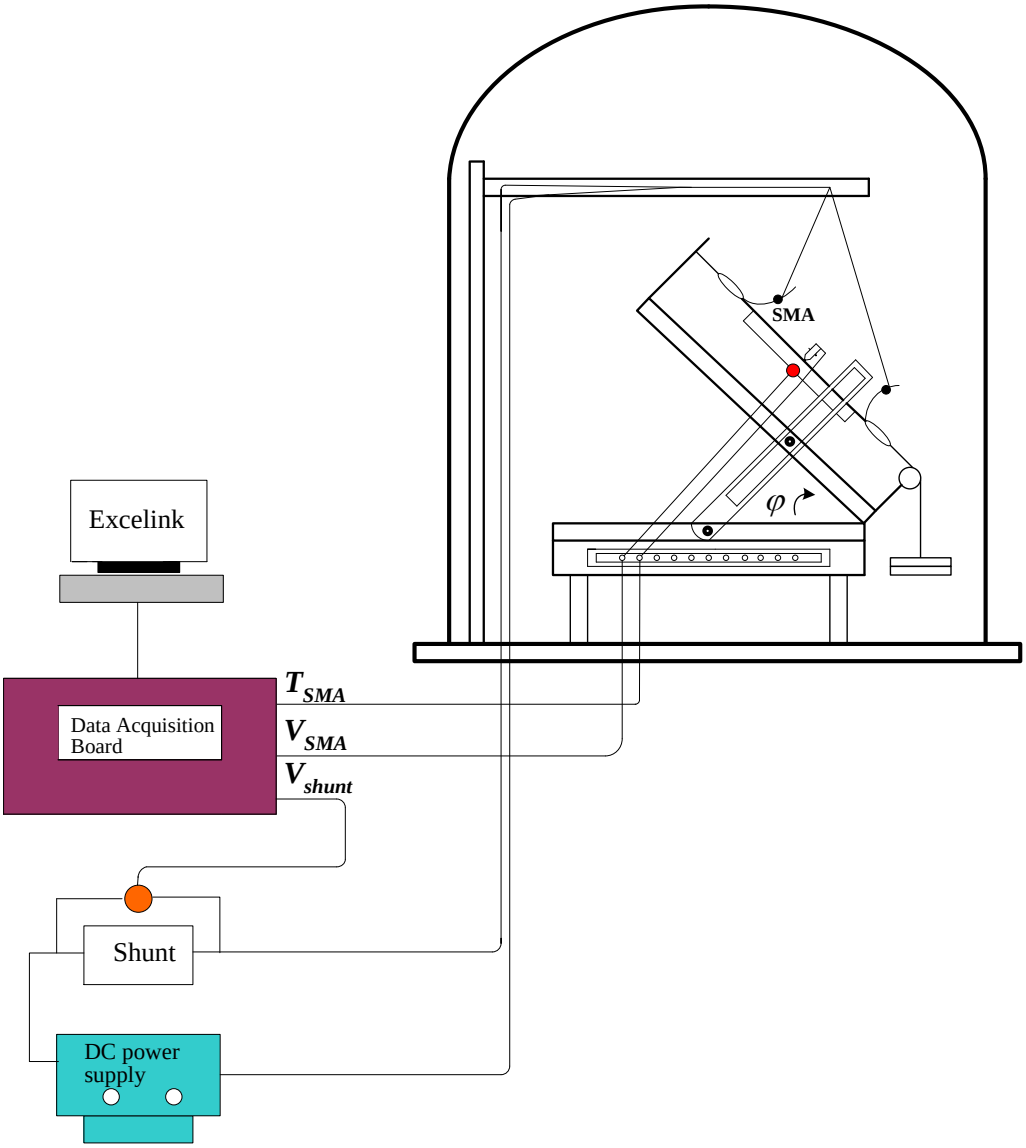

Figure 3.3 Experimental setup

3.2 Specimen Preparation

1. A sample Dynalloy, Inc. Flexinol nickel-titanium (Ni-Ti) SMA wire of 50 cm total length and 0.5 mm diameter with $A_s = 90℃$ was sanded with a fine sandpaper sheet to achieve a better electrical contact.

2. Both ends of the SMA wire were doubled over and clamped with screws, leaving 8.5cm loop at each end to hold higher loads (Fig. 3.4).

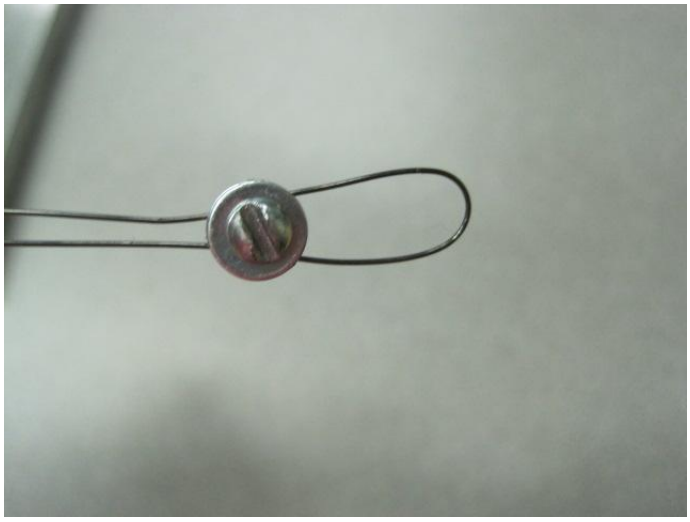

Figure 3.4 Crimping of the shape memory alloy wire

3. An E type, 40AWG Chromega and Constantan thermocouple was spot welded to the center of the sample wire for temperature readings. The thermocouple was spot welded with a capacitor-discharge spot-welder using a two step spot weld method [61]. In this method the first thermocouple wire is spot welded onto the SMA wire then the second thermocouple wire is spot welded exactly at the same point where the

first weld is in a way that the two thermocouple wires are welded at a single point onto the SMA wire [61].

4. Two constantan 40 AWG thermocouple wires were spot welded 2.5 cm in from both ends of the screw clamps for the wire's voltage measurements.

5. The SMA wire was set up in the test fixture with one loop attached to the fixture's left side screw by a string and the other loop connected to a string attached to a weighted pulley. The test fixture was then placed inside the vacuum jar.

3.3 Experimental Procedure for Natural Convection Heat Transfer Correlation

The experiments in this section were designed to develop a natural convection heat transfer empirical correlation for the SMA wires that relates Rayleigh number (Ra) to Nusselt number (Nu).

The Nusselt number (Nu) is a dimensionless number named after Wilhelm Nusselt and is the ratio of convective heat transfer to conductive heat transfer and can be shown as [45]

$$Nu_L = \frac{hL}{k} \tag{3.1}$$

where

h= convective heat transfer coefficient [$^{W}/_{m^2K}$]

L = characteristic length [m]

k = thermal conductivity of the fluid [$^{W}/_{mK}$]

The convective heat transfer coefficient can be defined based on Newton's law of cooling as

$$h = \frac{Q_{conv}}{A_{ss}(T_s - T_\infty)} \tag{3.2}$$

where

Q_{conv} = convective heat flow rate $[W]$

A_{ss} = heat transfer surface area $[m^2]$

T_s = solid surface temperature $[K]$

T_∞ = ambient fluid temperature $[K]$

The Nusselt number for the SMA wire can be defined as

$$Nu_D = \frac{Q_{conv}D}{kA_{SMA}(T_{SMA} - T_\infty)} \tag{3.3}$$

where

Q_{conv} = convective heat flow rate $[W]$

D = SMA wire diameter $[m]$

k = thermal conductivity of the fluid $[{}^{W}/_{mK}]$

A_{SMA} = SMA wire surface area $[m^2]$

T_{SMA} = SMA wire surface temperature $[K]$

T_∞ = wire ambient fluid temperature $[K]$

Q_{conv} for the SMA wire can be calculated when the wire is heated by passing a current through it. Heat transfer occurs between the heated wire and its surroundings, by convection, conduction and radiation. When the wire reaches a steady state condition with its surroundings, the power input to the wire (VI) is equal to the convection, conduction and radiation heat transfer rate (Fig. 3.5), and it can be shown as

$$Q_{in} = V.I = Q_{rad.} + Q_{conv.} + Q_{cond.} \tag{3.4}$$

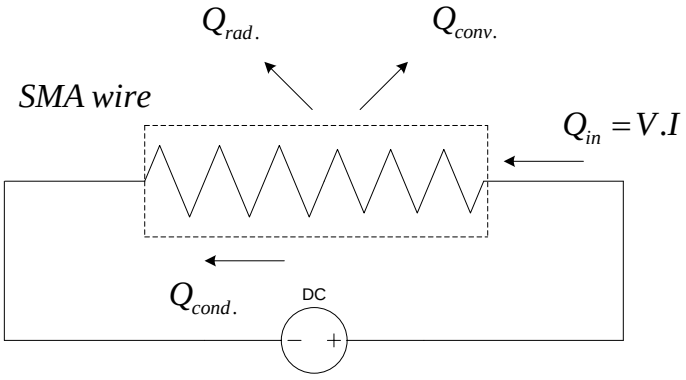

Figure 3.5 Heat transfer from SMA wire to its surroundings at steady-state condition

The conduction heat transfer rate is minimized by choosing thin thermocouple wires. Since conduction heat transfer rate is proportional to thermocouple wire cross sectional area selecting smaller radius thermocouple wires can help to reduce the conduction heat transfer rate. The 40 AWG (Constantan and Chromega) E type thermocouple used in this work is one of the thinnest thermocouples available and additionally has lower conductivity than other thermocouples. The thermal conductivity of Constantan and Chromega are 21 [$^{W}/_{mK}$] and 19 [$^{W}/_{mK}$], respectively, at 100℃ , which are much

lower values than those for the thermal conductivity of Copper (337 $^{W}/_{mK}$) and Iron (68 $^{W}/_{mK}$) that are found in T type and J type thermocouples, respectively [62]. In order to minimize the error for conduction heat transfer losses from the wire ends, the thermocouples for voltage measurements were spot welded 2.5 cm in from both ends of the screw clamps. The heat losses through the attached thermocouples are calculated using fin heat transfer rate as [45]

$$Q_f = \sqrt{hP_f k_w A_c}\ \theta_b \tag{3.5}$$

where

Q_f = fin heat transfer rate $[W]$

θ_b = base temperature $[K]$

k_w = thermal conductivity of thermocouple wire $[^{W}/_{mK}]$

h = convective heat transfer coefficient $[^{W}/_{m^2K}]$

P_f = fin perimeter = πD $[m]$

A_c = fin cross sectional area = $\pi D^2/4$ $[m^2]$

The heat transfer losses from the attached thermocouples based on the convective heat transfer coefficient range in this work is calculated as $0.005[W] \leq Q_f \leq 0.01[W]$. Additionally, the SMA wire is heated using the Joule effect method by passing a direct current through the wire. In this method the wire particles are heated simultaneously and act as a heat source themselves. Therefore, based on the calculated Q_f range and

Joule effect heating method it can be assumed that there is a uniform temperature distribution across the wire and the conduction heat transfer rate can be neglected. For the SMA wire at steady state conditions by neglecting conduction heat transfer rate the power input is the sum of the convection and radiation heat transfer rates and can be shown as

$$V_{SMA}I_{SMA} = Q_{conv} + Q_{rad} \tag{3.6}$$

Q_{rad} can be calculated for the wire through an experiment procedure as described in Section 3.3.2.1, therefore

$$Q_{conv} = V_{SMA}I_{SMA} - Q_{rad} \tag{3.7}$$

3.3.1 Pressure Variation Method

In order to develop a heat transfer correlation for the wire, the natural convective heat transfer coefficient must be measured over a wide range of Rayleigh numbers. The Rayleigh number is a dimensionless number named after Lord Rayleigh and it is defined as a product of Grashof number, which is the relationship between fluid buoyancy and viscosity, and Prandtl number which is the relationship between momentum diffusivity and thermal diffusivity. The Rayleigh number for a fluid can be shown as [45]

(3.8)

$$Ra_L = Gr_L . Pr = \frac{g\beta(T_s - T_\infty)L^3}{v^2} . \frac{v}{\alpha} = \frac{g\beta(T_s - T_\infty)\, L^3}{v\alpha}$$

where

Gr_L = Grashof number

Pr = Prandtl number

g = acceleration due to gravity $[{}^{m}/_{s^2}]$

T_s = surface temperature $[K]$

T_∞ = ambient fluid temperature $[K]$

L = characteristic length $[m]$

α = thermal diffusivity $[{}^{m^2}/_{s}]$

v = kinematic viscosity $[{}^{m^2}/_{s}]$

β = thermal expansion $[{}^{1}/_{K}]$

The Rayleigh number for the SMA wire based on Equation (3.8) can be defined as

(3.9)

$$Ra_D = \frac{g\beta(T_{SMA} - T_\infty)D^3}{v^2} . Pr$$

g is a constant. Pr can be assumed to be constant for ideal gases such as air. Thermal expansion is a function of ambient temperature and can be defined as $\beta = \frac{1}{T_\infty}$. Kinematic viscosity ($v$) by definition is

$$v = \frac{\mu}{\rho} \tag{3.10}$$

where

μ = air dynamic viscosity [$^{kg}/_{ms}$]

ρ = air density [$^{kg}/_{m^3}$]

By considering air as an ideal gas its density can be defined as

$$\rho = \frac{P}{R_c T_m Z} \tag{3.11}$$

where

P = air pressure [Pa]

R_c= gas constant [$^{J}/_{kgK}$]

$T_m = \frac{T_{SMA}+T_\infty}{2}$ average temperature of air [K]

Z = air compressibility factor

By substituting Equations (3.10) and (3.11) into Equation (3.9)

(3.12)

$$Ra_D = \frac{g(T_{SMA} - T_\infty)D^3P^2}{\mu^2 T_\infty R_c^2 Z^2 T_m^2}.Pr$$

According to Equation (3.12), a range of Rayleigh number can be obtained by:

- Changing SMA wire surface temperature (T_{SMA})
- Changing SMA wire diameter (D)
- Changing SMA wire ambient pressure (P)
- Changing air properties

Varying the temperature of the SMA wire does not allow for a wide range of Rayleigh number to be simulated given the first order dependence of Rayleigh number on temperature. A large variation of temperature is required to obtain a sufficient Rayleigh number range and there are limitations of increasing the temperature of the SMA wire over 400℃ that can cause permanent damage to the wire, such as losing its cyclic effect. As an example by changing the wire temperature from 50℃ to 200℃ the obtained Rayleigh number range is approximately $0.2 \leq Ra_D \leq 1$.

The diameter of the SMA wire cannot be used to simulate a range of Rayleigh number since there are limited diameters of SMA to choose from. The SMA wire diameter various from 0.5 mm to 0.025 mm and there are limitations in spot welding the thermocouples at the small diameter wires for monitoring temperature. By changing the

wire diameter from 0.1 mm to 0.5 mm the obtained Rayleigh number range is approximately $0.005 \leq Ra_D \leq 0.59$.

The compressibility factor Z and gas constant R_c are assumed to be constant for air. μ and Pr vary in a small range over a large range of temperature. μ and Pr vary only from $1.846 \times 10^{-5}\ [Ns/m^2]$ to $2.301 \times 10^{-5}\ [Ns/m^2]$ and 0.707 to 0.690 respectively with temperature changes from $300K$ to $400K$ [45]. Therefore, changing the wire ambient pressure was selected to obtain a wide range of Rayleigh number. By changing the air pressure from atmospheric pressure (760 torr) down to 0.1 torr the obtained Rayleigh number range is $2.6 \times 10^{-8} \leq Ra_D \leq 6 \times 10^{-1}$.

3.3.2 Data Collection for the SMA Wire Natural Convection Heat Transfer Correlation

This section describes the experimental procedures used to collect data for Q_{rad} and Q_{conv} . The specimen was prepared as described in Section 3.2. The SMA wire was set up in the test fixture and placed inside the vacuum jar. The wire was connected to the power supply circuit. The power supply circuit, the shunt resistor and the sample SMA wire were connected in series (Fig. 3.3). The wire was heated via a Joule effect heating method by passing DC current through the wire. Q_{conv} data were collected for the wire under stress-free and 100 MPa applied stress conditions.

3.3.2.1 Data Collection for Radiation Heat Transfer rate Q_{rad}

The air pressure inside the vacuum jar was reduced to 10^{-7} torr. The SMA wire was heated up in a horizontal orientation by applying current step by step (60 mA, 100 mA, 200 mA and 250 mA) until the temperature of the SMA wire reached 100℃. The current was then discontinued, and the wire was cooled. A time step after each incremental change allowed the temperature to reach a stable condition (when the temperature readout on ExceLINX does not increase more than 1% in 20 temperature readings with 5s time step). The voltage of the wire was measured using the Keithley 2700 data acquisition system when the wire had reached a steady state temperature at 100℃. At 10^{-7} torr, it can be assumed that the power input to the wire will be only equal to the radiation heat transfer rate and it can be calculated as:

$$Q_{rad} = V_{SMA(Vaccu\,m)} I_{SMA(\,Vacuum)} \tag{3.13}$$

3.3.2.2 Data Collection for Convective Heat Transfer rate Q_{conv}

The experiments were carried out at different air pressures using the vacuum station in order to get a wide range of Rayleigh number. At different air pressures (700 torr, 600 torr, 500 torr, 400 torr, 300 torr, 200 torr, 100 torr, 60 torr, 30 torr, 5 torr and 0.1 torr) the SMA wire in a horizontal orientation was heated by applying current in 200 mA increments, starting from 60 mA, until the temperature of the wire reached 100°C .The current was then discontinued and the wire was cooled. A time step after each

incremental change allowed the temperature to reach a stable condition (when the temperature readout on ExceLINX does not increase more than 1% in 20 temperature readings with 5s time step). The voltage of the wire was measured using the Keithley 2700 data acquisition system when the wire reached a steady state at 100℃. At each set pressure, the data for Q_{conv} were collected for the wire at 0°, 15°, 30°, 45°, 60°, 75° and 90° inclination angles. As mentioned in Section 3.3, Q_{conv} at each set pressure will be equal to the power input to the wire minus Q_{rad} Equation (3.13), and it can be calculated as $Q_{conv} = V_{SMA}I_{SMA} - Q_{rad}$.

3.4 Experimental Procedure for Resistance and Strain Measurements of SMA Wire

In this section, experiments were carried out to generate electrical resistance–temperature curves and strain-temperature curves for the SMA wire. Electrical resistance was calculated for the wire based on experiment results to investigate the effect of temperature change on the wire resistance.

The properties of SMA wires such as electrical resistance and strain have a hysteretic behavior due to phase transformation of the wire. In order to generate these hysteretic curves for the SMA wire electrical resistance and strain, the temperature of the wire must be changed through four key phase transformation temperatures: A_s and A_f, which are the phase transformation temperatures from martensite to austenite; and M_s and M_f, which are the phase transformation temperatures from austenite to martensite.

The experiments in this section were carried out for the SMA wire at stress-free conditions and under 50 MPa, 100 MPa and 150 MPa applied stresses.

3.4.1 Data Collection for the SMA Wire Electrical Resistance and Strain

Inside the vacuum station at 10^{-7} torr air pressure the SMA wire in a horizontal position was heated by passing direct current through the wire using a DC power supply, and T_{SMA}, V_{SMA} and V_{shunt} were measured with the Keithley data acqusition system. The resistance of the wire was then calculated based on Ohm's law equation $R_{SMA} = {V_{SMA}}/{I_{SMA}}$.

The current was applied in 100 mA increments, from 100 mA to 400 mA, then back to 100 mA. A time step after each incremental change allowed the temperature to reach a stable condition (when the temperature readout on ExceLINX does not increase more than 1% in 20 temperature readings with a $5s$ time step). For the heating process, the current was increased by 100 mA increments until the temperature of the wire reached approximately to 130℃. For the cooling process, the current was decreased by 100 mA increments until the wire temperature reached near room temperature. The heating and cooling processes were repeated in two different current directions by changing the current flow polarity through the wire. In order to investigate the effect of pressure and inclination angle on electrical resistance and strain of the wire the experiments were carried out at 700 torr, 500 torr, 300 torr, 100 torr and 30 torr pressures and at different wire inclination angles from horizontal ($\varphi = 0$) to vertical ($\varphi = 90°$) under 100 MPa applied stress.

Chapter 4

Electrical Resistance of Shape Memory Alloy Wires

The memory effect in shape memory alloys is due to phase transformation phenomena in these materials. The phase transformation between the austenite and the martensite phases is diffusionless transformation that occurs only by crystallographic structure changes between the two phases. Therefore, the physical properties that depend on the crystal structure of the atoms, such as electrical resistance, vary during the phase change and show a hysteresis behavior with a change in wire temperature during one complete cycle of the heating and cooling process. In this chapter, the variation of electrical resistance and strain of SMA wire with temperature are investigated. Hysteresis curves are generated for the SMA wire electrical resistance and strain under various conditions, including wire inclination angle, wire length, ambient pressure, phase transformation time rate and applied external stress. Later, a resistance model is proposed for SMA wires based on experimental results in order to predict the temperature of the wire based on its electrical resistance.

4.1 Electrical Resistance and Strain of SMA Wire

The changes of the SMA wire's electrical resistance and strain with change of the wire temperature are investigated under various conditions, and the following effects of these conditions are studied:

- Effect of applied stress on SMA wire electrical resistance and strain

- Effect of wire length on SMA wire electrical resistance and strain
- Effect of wire inclination angle on SMA wire electrical resistance and strain
- Effect of ambient pressure on SMA wire electrical resistance and strain
- Effect of phase transformation time on SMA wire electrical resistance and strain

The investigated effects help to better clarify the electrical resistance behavior of the SMA wire during the phase transformation process when the wire temperature is changed. This investigation leads to developing a resistance-temperature model for the wire.

The effect of different parameters as listed above are investigated by generating the electrical resistance-temperature and strain-temperature hysteresis curves based on experimental results for the SMA wire. The 0.5 mm Dynalloy SMA wire with $A_s = 90℃$ in a horizontal orientation is first heated from ambient temperature to above the A_f temperature via a Joule effect method by passing a direct current through the wire. It is then cooled down below the M_s temperature by natural convection heat transfer. The results are recorded for two different current flow directions through the SMA wire. A sample generated resistance-temperature (R-T) hysteresis curve is shown in Figure (4.1). During the heating process the resistance of the wire starts to increase as the wire temperature increases, until it reaches its austenite start phase transformation temperature (A_s). The phase transformation from martensite to austenite happens as the wire absorbs thermal energy. The wire's resistance then decreases suddenly during the phase

transformation. When the phase transformation is completed, the resistance of the wire starts to increase again as the temperature increases. As the wire cools, its resistance starts to decrease until it reaches its martensite start temperature (M_s). During the phase transformation from austenite to martensite, the wire's resistance increases and returns to that of the starting point. The resistance difference between the two phases is due to their different crystallographic structures. The martensite phase has a low-symmetry crystal structure; it is soft and can be deformed easily, while the cubic austenite phase has a high-symmetry crystal structure with high strength [19]. Therefore, the phase transformation happens with a large change in electrical resistance of the wire [19]. The change in electrical resistance between the two phases can also be explained by the SMA wire length change during the phase transformation. When the wire is transformed from martensite to austenite, its length decreases, and during the martensitic transformation, the wire length extends back to its original length. The resistance of the wire is proportional to its length as given in Equation (4.1); therefore, it changes when the wire length changes during the phase transformation process. The resistance of the wire is lower in the austenite phase than in the martensite phase.

As mentioned, in order to investigate the current direction effect on wire electrical resistance, the experimental results are recorded for the SMA wire under various conditions, in two different current directions. As shown in Figure (4.1), current direction does not have a significant effect on wire electrical resistance. The electrical resistance of the SMA wire change less than 2% in two different current directions, which is in the range of experimental error calculated for this work.

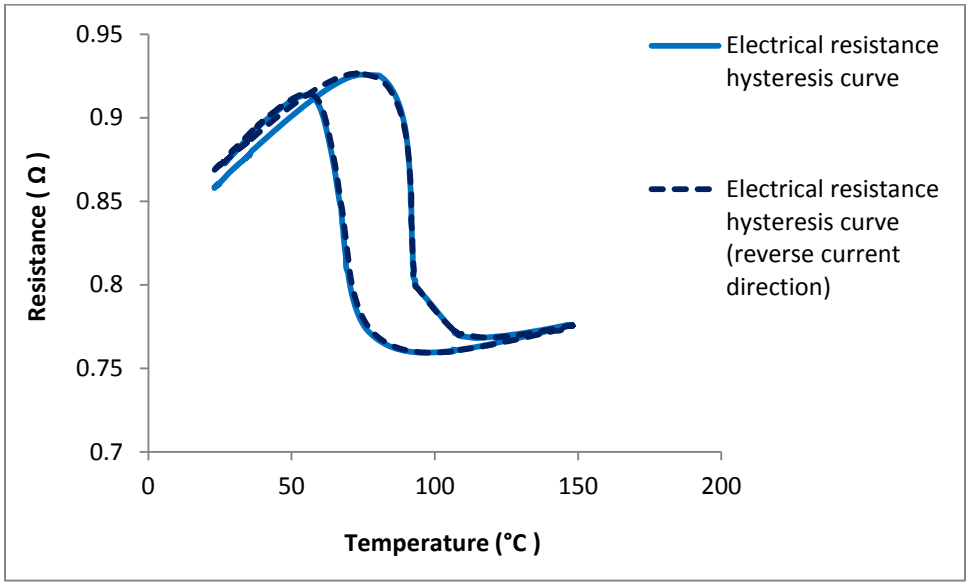

Figure 4.1 Electrical resistance-temperature hysteresis curves for 0.5 mm diameter NiTi SMA wire under 150 MPa applied stress in two different current directions

4.1.1 The Applied Stress Effect on the SMA Wire Electrical Resistance

The electrical resistance and temperature hysteresis curves are generated for the SMA wire under different applied stresses. At each applied stress, as mentioned in Section 4.1, the wire is heated from ambient temperature to above the A_f temperature then cooled down below the M_s temperature in two different current directions. The electrical resistance-temperature (R-T) hysteresis curves for the SMA wire under different applied stresses are shown in Figure (4.2). As the phase transformation from martensite to austenite starts, the wire absorbs thermal energy and its resistance starts to decrease. The SMA wire resistance decrease, by about 14%, 15% and 16% under 50 MPa, 100 MPa and 150 MPa applied stress, respectively, during this transformation. During the phase

transformation from austenite to martensite, the wire's resistance increases and returns to that of the starting point. As mentioned the change in the electrical resistance of the SMA wire occurs because of changes in the atomic crystal structure inside the wire caused by the phase transformation process.

Applied stress has a significant influence on the martensitic phase transformation. It can increase the amount of transformation and complete the phase transformation process [15, 19]. The electrical resistance of the SMA wire and the gap between heating and cooling curves as seen in Figure 4.2 increase with increasing stress. As the applied stress increases the frictional forces due to movement of the interfaces during martensite transformation increases as well, the increase of these frictional forces causes a larger power input during one cycle of heating and cooling process which this leads to a larger gap in the wire hysteresis curves [41, 63]. Since the applied stresses to the wire are tensional, as the stress increases the atomic distance inside the wire increases as well, this makes the wire longer and leads to higher electrical resistance.

When there is no stress on the wire (stress-free condition) or the applied stress is low the hysteresis curves for the SMA wire show different behavior in each of the two different current directions, as seen in Figure (4.2). This may be due to self-accommodating martensite transformation, which can be explained by the plate appearance nature of martensite transformation [40]. The transformation of austenite grains to martensite occurs by formation of thin martensite plates. In low stress or stress-free conditions, the martensitic transformation produces randomly oriented martensite plate variants while, under stress, the martensite plates are forced to produce a single

preferred variant [15, 40]. In a self-accommodating microstructure, martensite plates arrange themselves in a manner that minimizes strain energy without crystal deformation [64]. The conjecture is that this random plate orientation leads to a less repeatable resistance response in the case of low or zero-stress conditions.

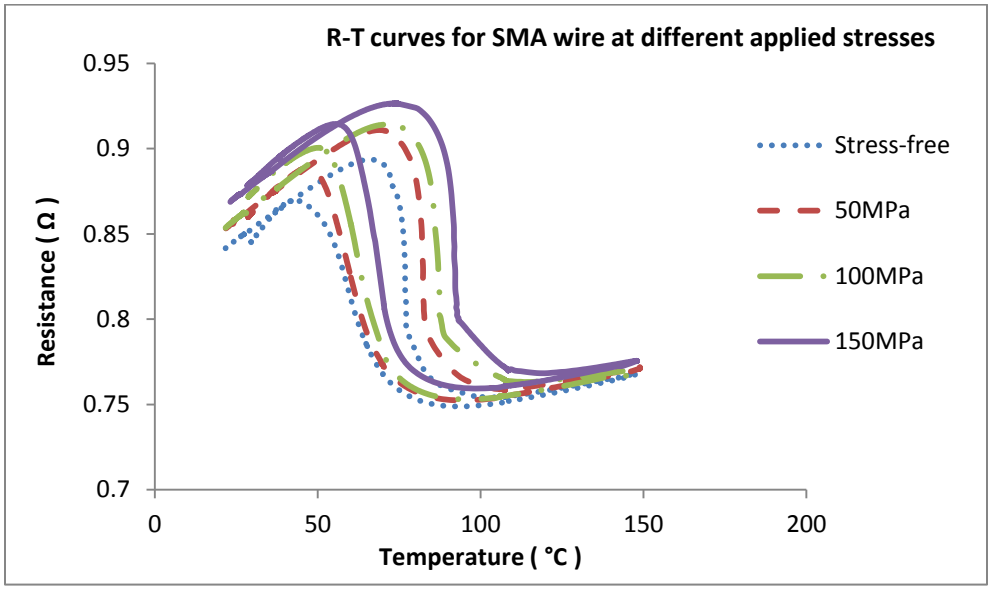

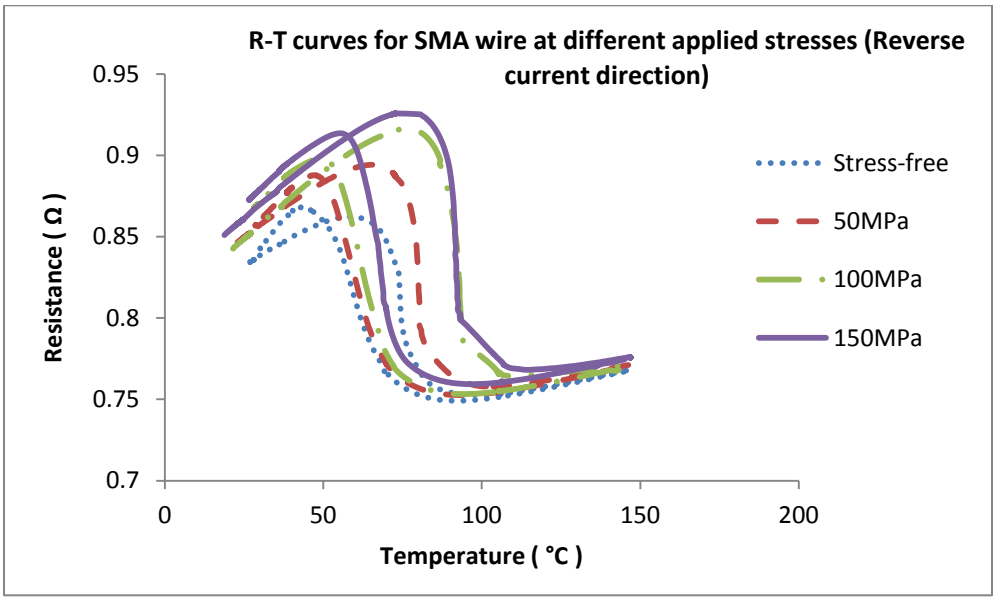

Figure 4.2 Electrical resistance-temperature curves for horizontal NiTi SMA wire with 0.5 mm diameter and 500 mm total length at different applied constant stresses in two different current directions

4.1.2 The Wire Length Effect on the SMA wire Electrical Resistance

The electrical resistance of NiTi SMA wire with 0.5 mm diameter is plotted against wire temperature for different wire total lengths at each applied stress in two different current directions (Fig. 4.3, 4.4, 4.5, 4.6). As shown in Figures (4.3), (4.4), (4.5) and (4.6) the wire electrical resistance is not changing significantly with changing current direction but the wire's total length plays a significant role in its electrical resistance. The wire electrical resistance can be written as [4]

(4.1)

$$R = \rho_i \frac{l}{A_a}$$

where

l= wire total length

ρ_i = resistivity

A_a = wire cross sectional area

The wire's electrical resistance increases if the wire's total length is increased, but the phase transformation temperatures remain the same; therefore, increasing the wire's total length only shifts the R-T hysteresis curves vertically in the plots.

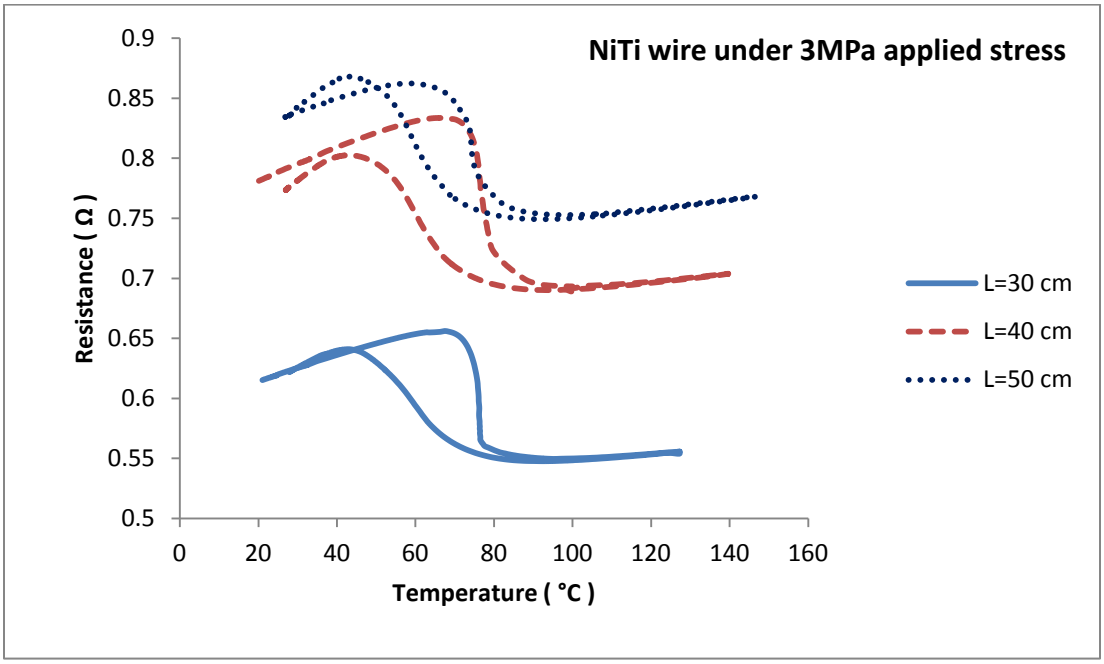

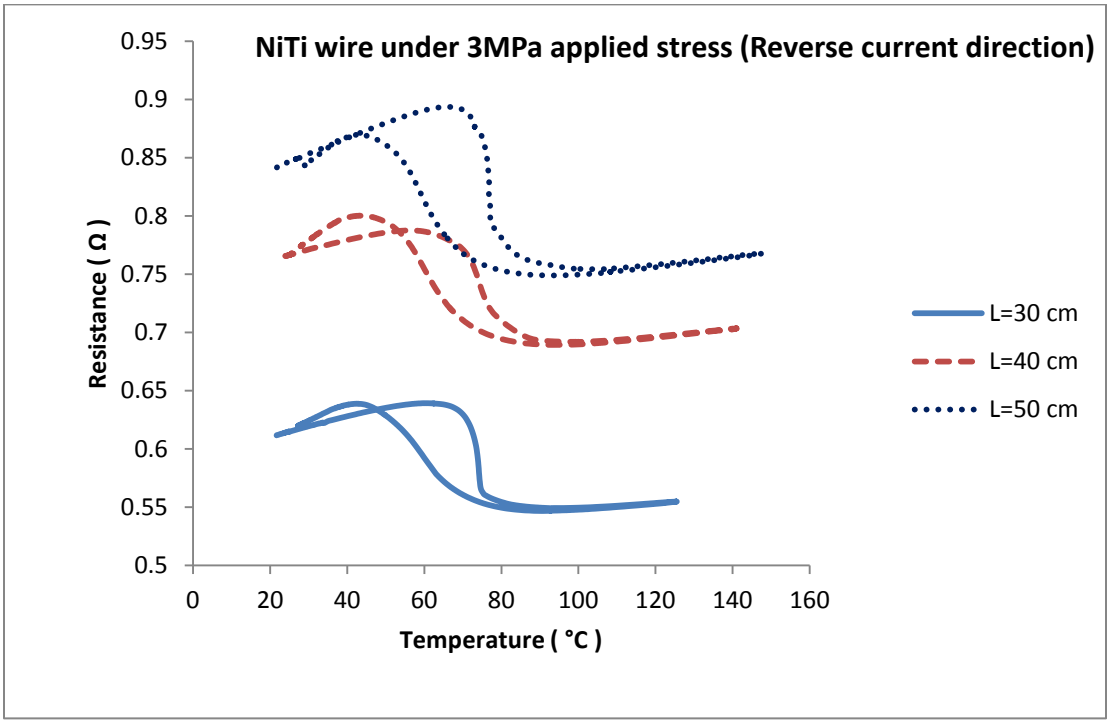

Figure 4.3 Electrical resistance-temperature curves for different total lengths NiTi SMA wire with 0.5 mm diameter under 3 MPa applied stress in two different current directions

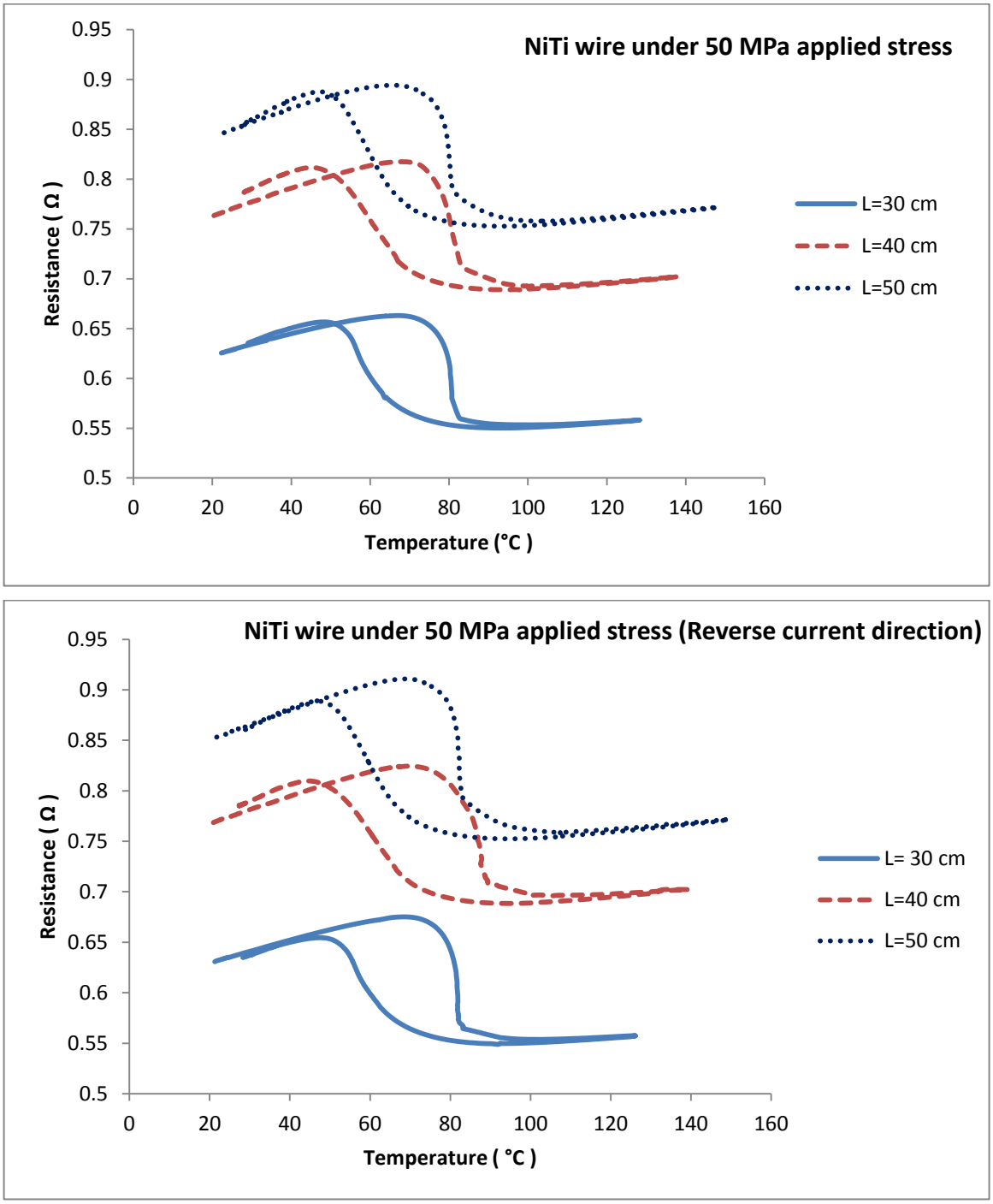

Figure 4.4 Electrical resistance-temperature curves for different total lengths NiTi SMA wire with 0.5 mm diameter under 50 MPa applied stress in two different current directions

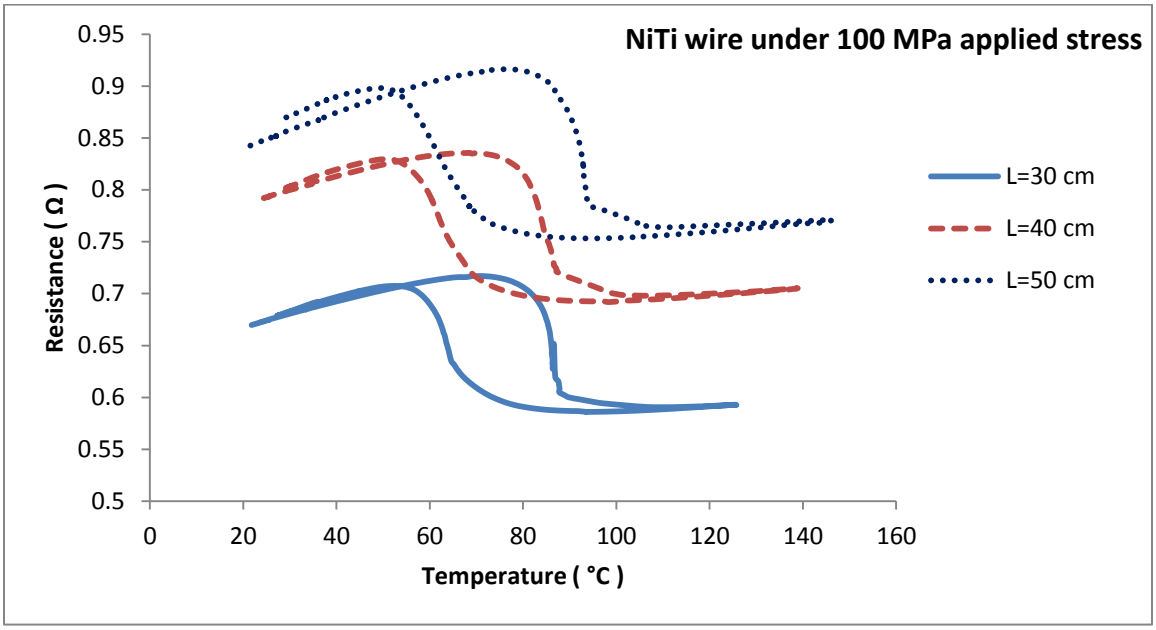

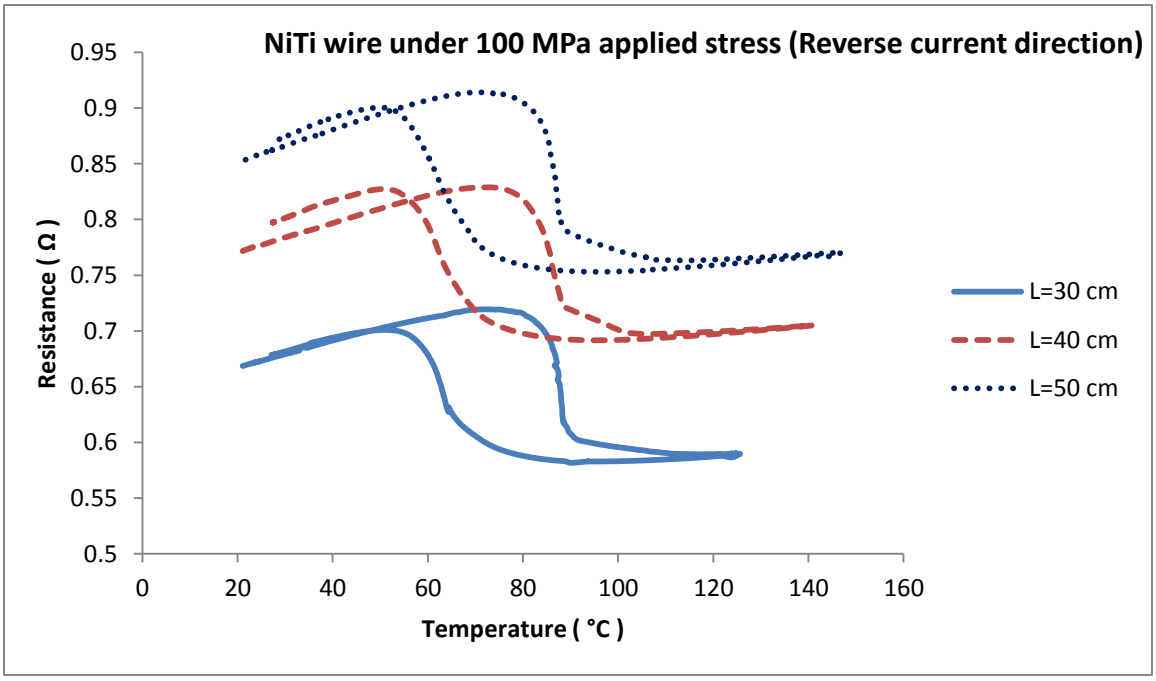

Figure 4.5 Electrical resistance-temperature curves for different total lengths NiTi SMA wire with 0.5 mm diameter under 100 MPa applied stress in two different current directions

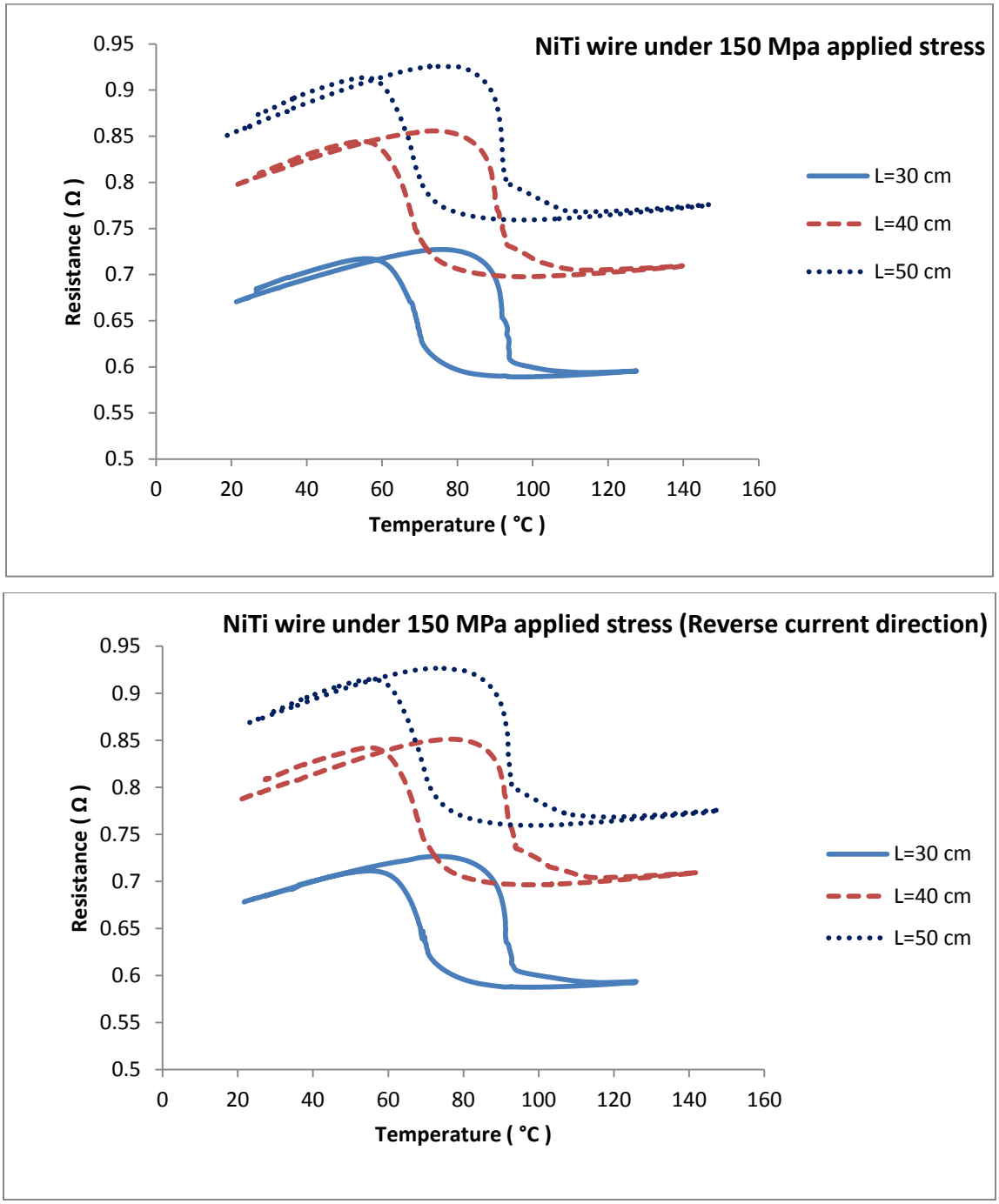

Figure 4.6 Electrical resistance-temperature curves for different total lengths NiTi SMA wire with 0.5 mm diameter under 150 MPa applied stress in two different current directions

As shown in Figures (4.3), (4.4), (4.5) and (4.6) the electrical resistance of the SMA wire increases with an increase in the applied stress. As mentioned, this increase is due to an increase in atomic spacing inside the wire or the wire length associated with an increase in the external applied stress, which, in turn leads to higher electrical resistance. As seen in Figures (4.3) to (4.6) the SMA wire resistance-temperature hysteresis curves are not showing a unique behavior under 3 MPa applied stress, as mentioned, the conjecture is that the self-accommodating martensite transformation leads to this different resistance response.

4.1.3 The Applied Stress and Wire Length Effect on the SMA Wire Strain

As mentioned, the phase transformation in shape memory alloy wires under applied stress is accompanied by the wire length change. As electrical resistance, the wire length change also has a hysteresis relation with its temperature. The strain-temperature hysteresis curves are generated for the SMA wire under different constant applied stresses and wire lengths. As for the electrical resistance measurements, at each applied stress the wire is first heated via a Joule effect method from ambient temperature to above A_f temperature then cooled down below the M_s temperature by natural convection in two different current directions. The strain-temperature (ε-T) hysteresis curves are shown in Figures (4.7) and (4.8) for two different wire lengths.

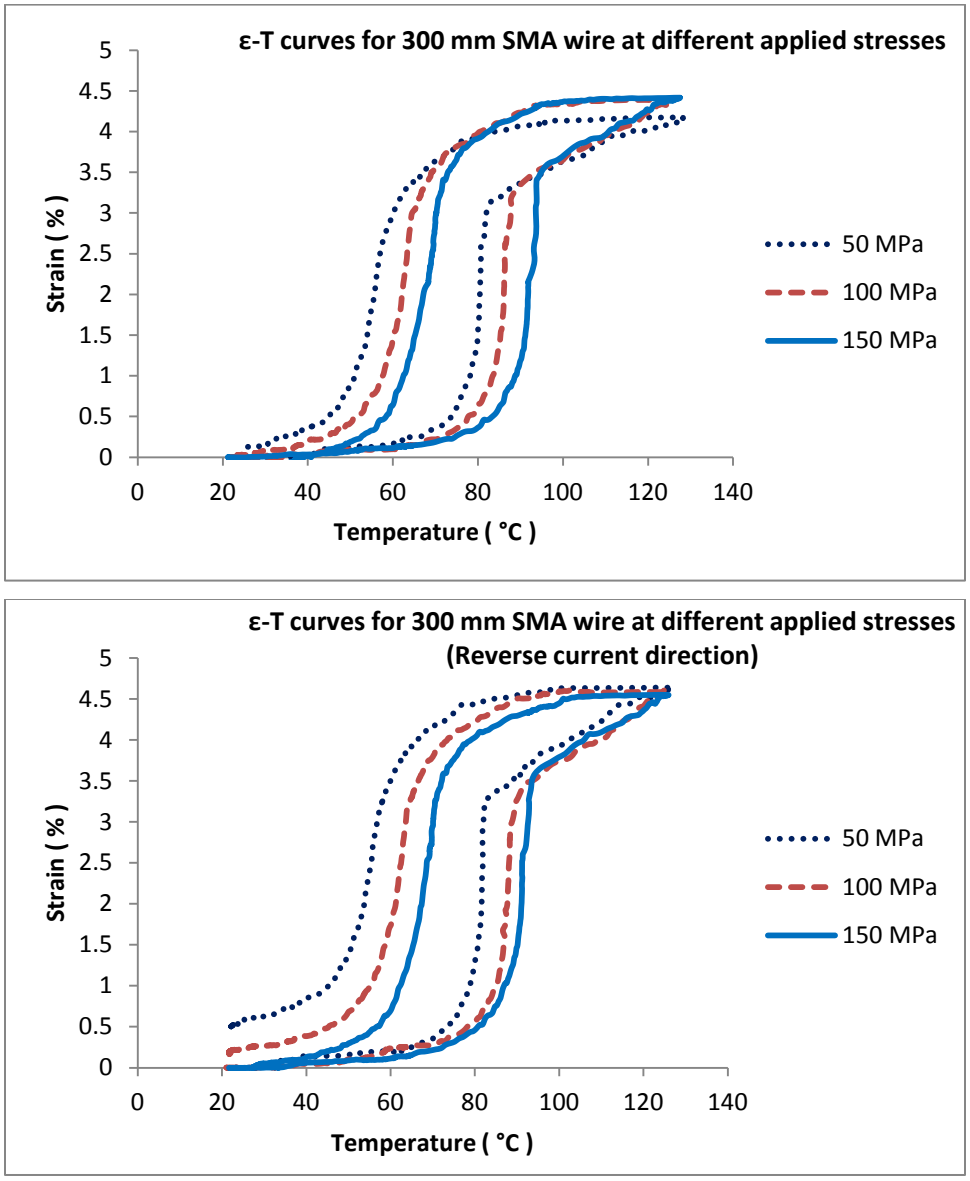

Figure 4.7 Strain-temperature curves for horizontal SMA wire with 0.5 mm diameter and 300 mm total length under different applied stresses in two different current directions

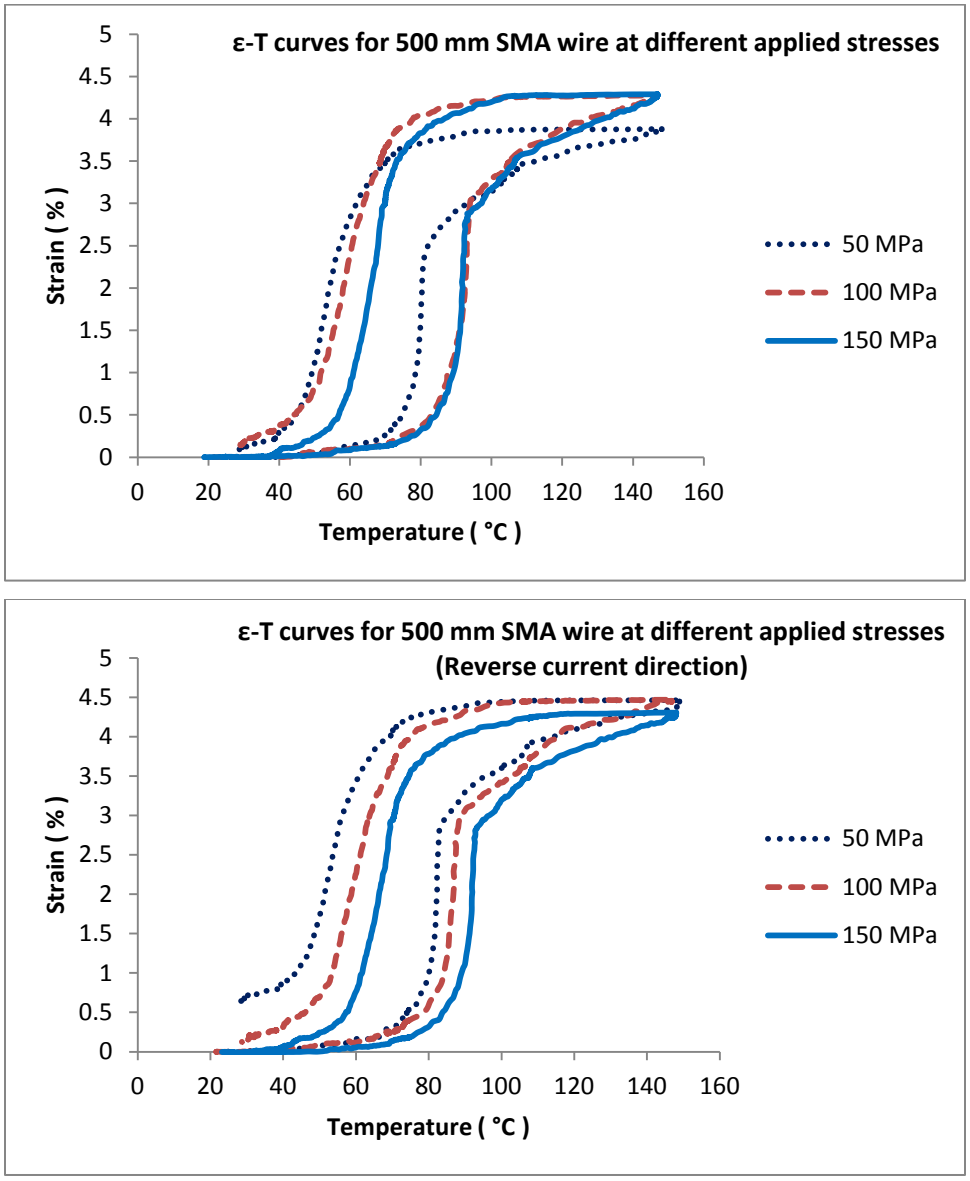

Figure 4.8 Strain-temperature curves for horizontal SMA wire with 0.5 mm diameter and 500 mm total length under different applied stresses in two different current directions

Under applied external stress the SMA wire martensite plate variants are forced to reorient themselves through the movement of their boundaries into a single variant with a large macroscopic strain change and when the wire is heated up to the A_f temperature the boundaries move back to their initial position and the strain is recovered [19]. For SMA wires with 300 mm and 500 mm total lengths around 4.5% strain or length change is recorded. The strain of the SMA wire is not changing significantly (less than 0.5 %), by changing the applied stress from 50 MPa to 150 MPa in two different current directions as shown in Figures (4.7) and (4.8). When the applied stress becomes high enough (larger than σ_s) to create a complete detwinned martensite phase, which for NiTi SMA wire with $A_s = 90℃$ is around 100 MPa, the martensite plates do not grow further significantly by increasing the applied stress [15]. The horizontal shift of the hysteresis (ε-T) curves in the plots are due to changes in the SMA wire phase transformation temperatures by changing the external applied stress. Hysteresis (ε-T) curves are not plotted for the wire under stress-free conditions since at low stress levels the wire undergoes a self-accommodating martensite transformation which occurs with no visible strain change. In a self-accommodating martensite transformation the martensite plate groups or variants arrange themselves in a way that minimize the strain energy and produce zero net shape change meaning although there is a deformation in the microstructural level, no shape change or strain change can be observed in macroscopic level during the transformation from austenite to martensite [64, 65].

4.1.4 The SMA Wire Inclination Angle and Ambient Pressure Effect on the Electrical Resistance and Strain

The SMA wire electrical resistance and strain were measured for the wire under 100 MPa applied stress at different inclination angles and ambient pressures to investigate the effect of the wire's inclination angle and ambient pressure on its electrical resistance and strain. The results are shown in Figures (4.9) and (4.10). The electrical resistance and strain of the SMA wire were monitored at each wire inclination angle from horizontal to vertical and set ambient pressure from atmospheric pressure down to 10^{-7}torr. The wire was heated by a Joule effect method to above the A_f temperature and cooled by natural convection below the M_s temperature in two different current directions.

The wire's ambient pressure and its inclination angle have an effect on natural convection heat transfer from the wire to its ambient and on the formation of boundary layers around the wire [45], but they have no significant effect on the wire's physical properties such as electrical resistance and strain. As seen in Figures (4.9) and (4.10) the electrical resistance of the wire is not changed by wire inclination angle and ambient pressure changes. The total strain change for the SMA wire at different pressures is 4.5% but the strain values during the phase transformation is 1% lower at 10^{-7}torr than the strain at higher pressures as seen in Figure (4.10). This might be due to the high vacuum condition. At 10^{-7}torr the SMA wire temperature changes gradually in respect to the temperature changes at higher pressures which results in a longer elapsed time for the wire to reach a 4.5% strain change. As seen in Figure (4.10) the strain of the wire is changed approximately 0.5% in response to a change in its inclination angle from

horizontal to vertical orientation; this change in strain might be due to an error in strain measurement values for the wire in a vertical orientation.

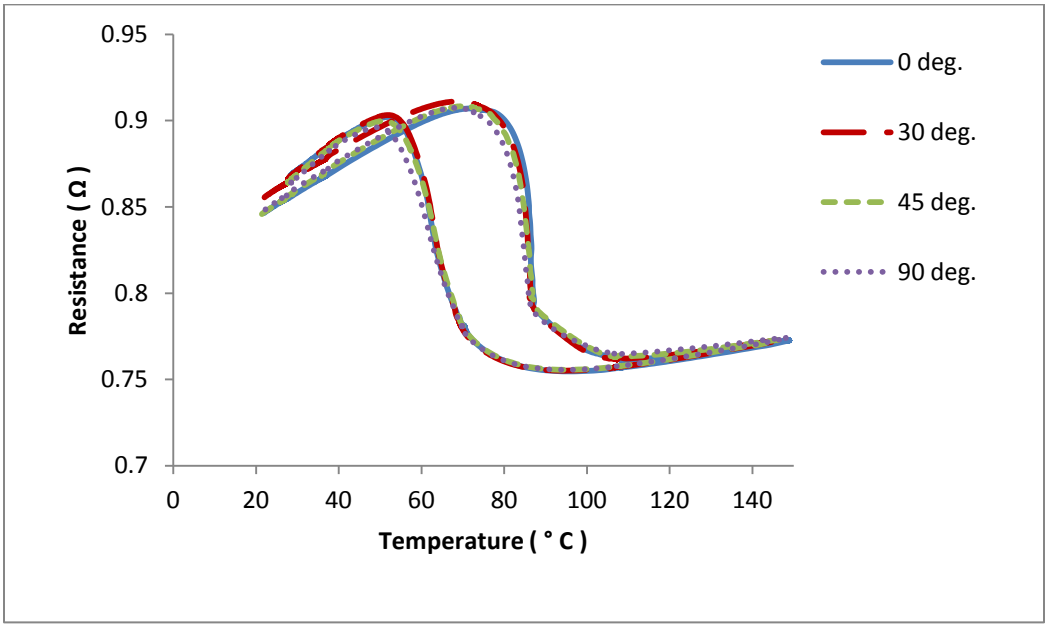

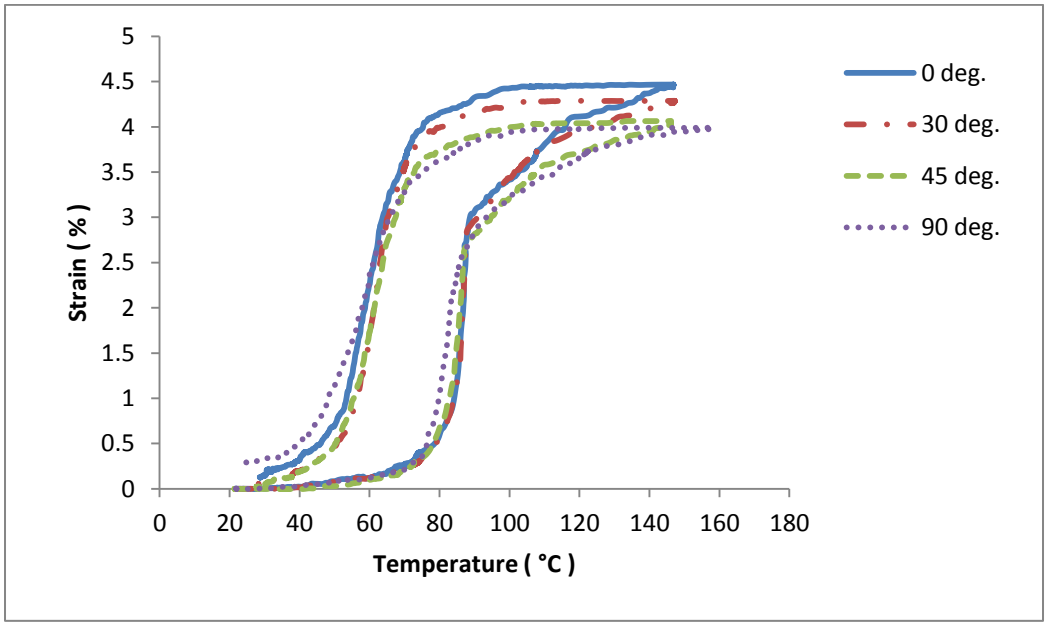

Figure 4.9 Electrical resistance and strain of NiTi SMA wire with 0.5 mm diameter and 500 mm total length at different wire inclination angles under 100 MPa applied stress

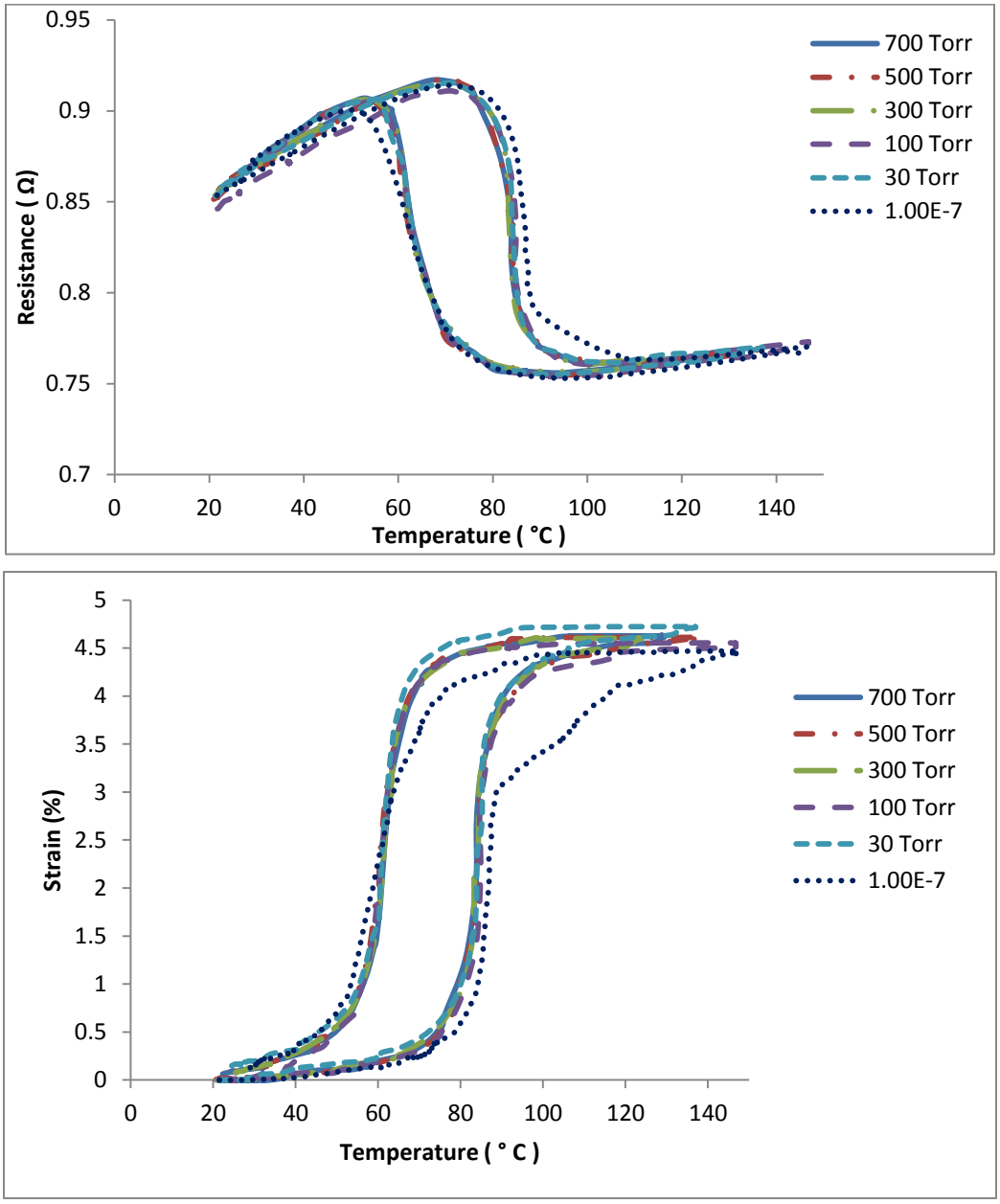

Figure 4.10 Electrical resistance and strain of NiTi SMA wire with 0.5 mm diameter and 500 mm total length at different ambient pressures under 100 MPa applied stress

4.1.5 Phase Transformation Time Effect on the SMA Wire Electrical Resistance

In order to investigate the effect of phase transformation time on SMA wire electrical resistance and strain the wire electrical resistance and strain are monitored at different heating and cooling time intervals and the results are presented in Figure (4.11).

Martensite transformation is an athermal or time independent transformation which happens with sudden movement of atoms at a certain temperatures. Therefore, there is no time effect on the hysteresis behavior of electrical resistance and strain curves for the SMA wire under applied 100 MPa external stress as shown in Figure (4.11). In martensite transformation the atoms move with a velocity near sound waves inside the crystal and the new phase does not grow with time [15, 19]. Therefore, at a constant temperature the amount of transformation is independent of time and the production of the new phase is due to a rapid lowering of the system free energy [15].

When the SMA is under stress-free conditions or the applied stress to the wire is low, sometimes a different hysteresis behavior can be observed (Fig. 4.12). This behavior is a result of fast heating and cooling, during which the hysteresis gap between the R-T heating and cooling curves tries to minimize itself. A small driving force or a small applied stress to the wire can cause isothermal martensite transformation, meaning that the martensite plates grow slowly with time [15, 16]. This isothermal martensite transformation can be controlled by increasing the applied stress that leads back to athermal transformation [16]. In both athermal and isothermal martensite transformation, the martensite plates formed with a speed near sound velocity in solids. The difference is in isothermal martensite transformation the number of transformed martensite plates

grows with time while in athermal martensite transformation the number of transformed plates depends on temperature and does not grow with time.

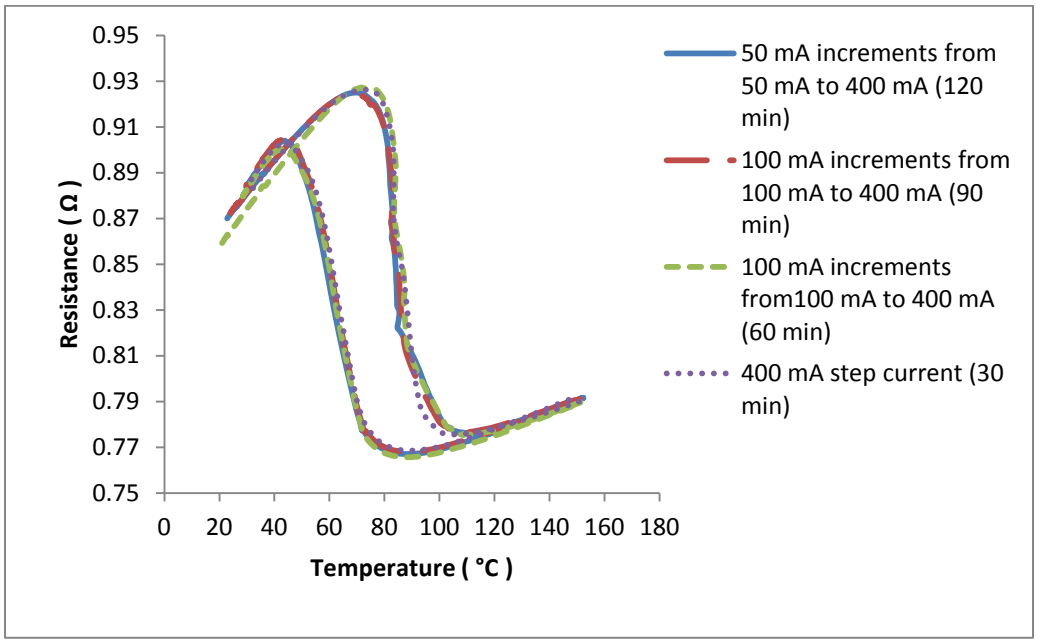

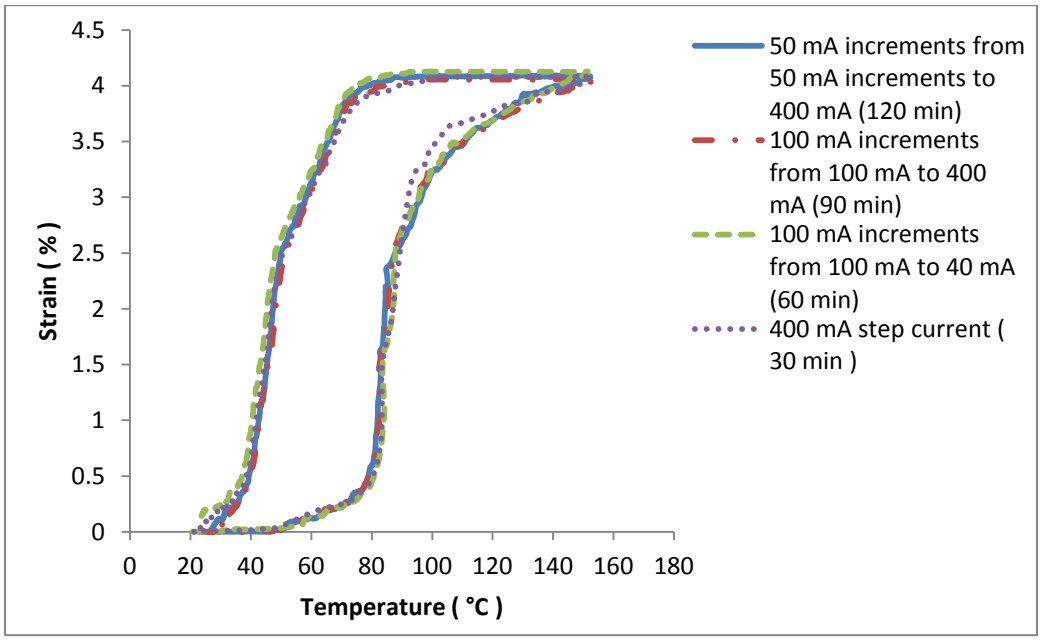

Figure 4.11 Electrical resistance and strain of NiTi SMA wire with 0.5 mm diameter and 500 mm total length at different time rates under 100 MPa applied stress

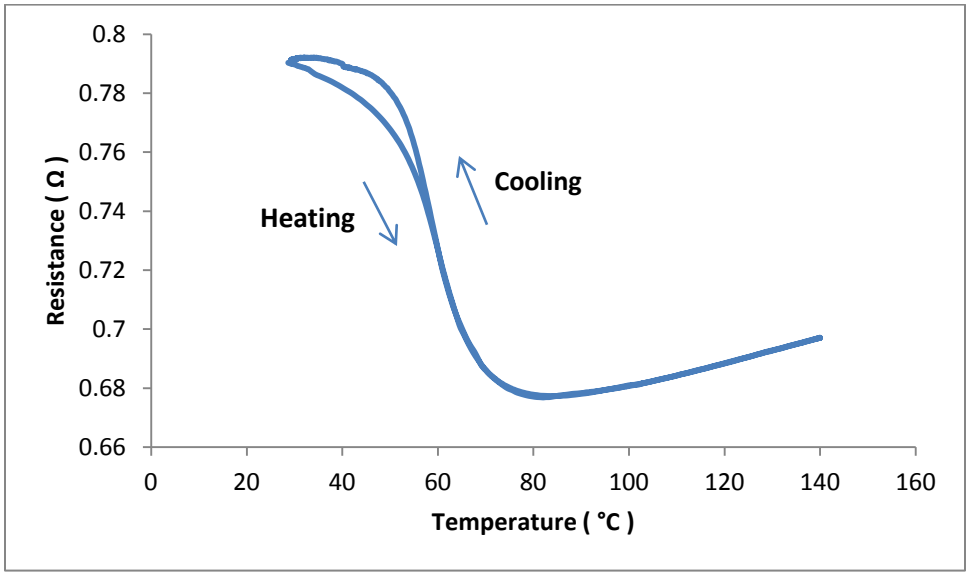

Figure 4.12 Electrical resistance-temperature hysteresis curve for NiTi SMA wire under stress-free condition with rapid heating and cooling process

4.1.6 Relation between SMA Wire Electrical Resistance and Strain

There is very little published literature about the relation between SMA wire strain and its electrical resistance [4, 9]. The strain of SMA wire is a function of phase transformation and can be used to detect the phase state of the wire during heating and cooling [41]. As mentioned, it is hard to measure the temperature of the SMA wire precisely in real applications, and it is much more convenient to measure the wire's electrical resistance. Therefore, instead of temperature, the relationship between electrical resistance and strain can be used to predict the strain of the SMA wire based on its electrical resistance [4, 66]. Figure (4.13) shows strain-electrical resistance ($\varepsilon - R$) curves for the SMA wire at different applied stresses.

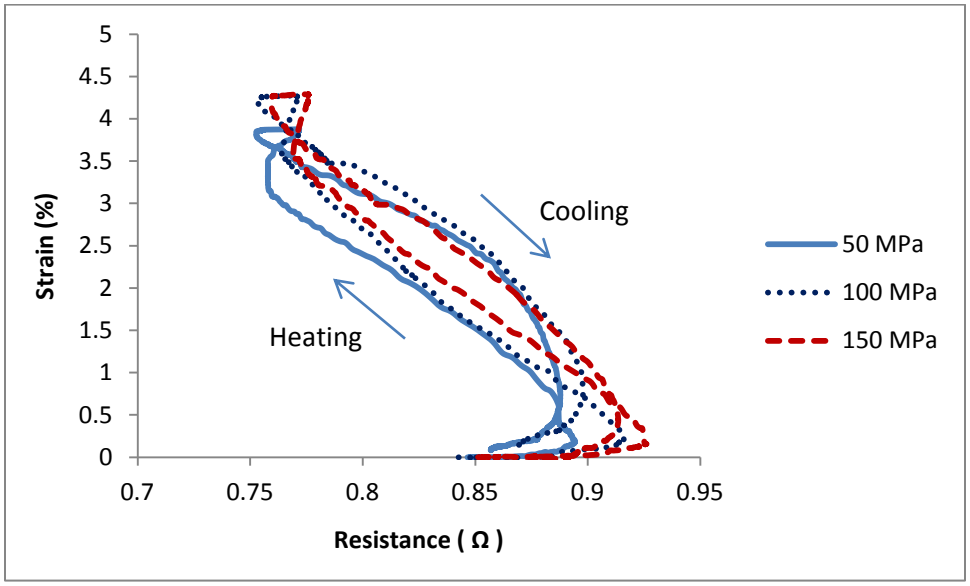

Figure 4.13 ε-R relation for NiTi 0.5mm diameter and 500 mm total length horizontal SMA wire at different applied stresses

As seen in Figure (4.13) the relationship between SMA wire electrical resistance and strain is hysteretic. Before phase transformation the electrical resistance of the SMA wire is increasing, but the wire strain is almost constant; therefore, the slope of the curve is zero. Then during the heating process as the transformation advances, the electrical resistance decreases because of the phase change in the SMA wire as the strain increases. In the cooling process before martensite phase transformation, the electrical resistance of the wire increases with the strain. As a result of martensite phase transformation, as the phase transformation starts, the resistance of the wire increases as the strain decreases. The hysteresis width for the $(\varepsilon - R)$ curve is smaller than the (R-T) and (ε-T) curves, since the temperature variations in SMAs are much larger than the resistance changes during the phase transformation.

4.2 Resistance Modeling of Shape Memory Alloy Wires

In this section an electrical resistance model is proposed for SMA wires based on experimental results presented in this chapter. The proposed model can be used to predict the temperature of the SMA wire based on its electrical resistance when direct temperature measurement methods are not possible. In real applications it is more convenient to measure electrical resistance of SMA wires than temperature due to difficulties in direct temperature measurement methods. An example of this difficulty is spot welding the thermocouples to the wire. Based on experimental results presented in this chapter the two main factors affecting the SMA wire electrical resistance were wire length and applied external stress. Therefore, the proposed electrical resistance model is based on wire length and applied stress. In order to calculate the constant coefficients of the proposed empirical resistance model the wire phase transformation temperatures for various applied stresses must be known. Therefore in the next section the effect of applied stress on phase transformation temperatures is investigated and linear relations between applied stress and wire phase transformation temperatures are developed.

4.2.1 The Variation of Phase Transformation Temperatures under Various Applied Stresses

In any application it is important to know the phase transformation temperatures (PTTs) of a shape memory alloy wire. Before designing any SMA actuator the PTTs of the wire must be determined. PTTs depend strongly on the stress applied to the wire. It is important to know the relation between applied stress and PTTs in order to determine PTTs for SMA wires under different applied stresses for a specific application. There are

several ways to calculate PTTs for the SMA wires: constant stress, differential scanning calorimetry (DCS), and active A_f. For the constant stress method a constant stress is applied to the wire and its electrical resistance (R) or strain (ε) is monitored while heating and cooling the wire through its PTTs range. Then the PTTs can be obtained based on hysteresis strain-temperature ($\varepsilon - T$) or electrical resistance-temperature ($R - T$) curves. DSC testing is a precise method for determining the PTTs but it can only be used for the wire under zero stress or stress-free conditions. In active A_f method, also known as the water bath or alcohol bath method, the wire is bent below its M_s temperature and then its shape recovery is monitored while it is heated slowly in the liquid bath [67-69]. In this work the DSC experimental technique was used to obtain the PTTs for the SMA wire under stress-free conditions. For the wire under different stresses the PTTs were obtained using the constant stress technique, from the ($R - T$) hysteresis cycles conducted for each applied stress. A DSC Q2000 (TA Instruments, New Castle, DE) machine was used to collect the data for the NiTi 0.5 mm diameter shape memory alloy wire. The sample wire was cut into 3 mm long pieces with 20.93 mg sample size, which were then placed side by side on the aluminium DSC pan and pressed with the DSC encapsulation press. The sample pan was placed on the test pedestal and an empty pan on the reference pedestal. The measurement was carried out in a nitrogen atmosphere with 50 ml/min flow rate. The test was conducted between -75℃ to 110℃ with a heating and cooling rate of 5 $℃/min$ during a period of 98 minutes [70]. The single peaks for heating and cooling on the DSC curves also show that the wire undergoes one stage of

transformation, meaning that there is no significant R-phase present in the tested sample wire.

The PTTs are determined from the $(R - T)$ curves by tangent line intersection method as shown in Figure (4.14) and from the DCS curve by intersection of the straight line fitted to the steepest sides of the peaks (the base line) with a line tangent to the slope of the peaks [70] (Fig. 4.15).

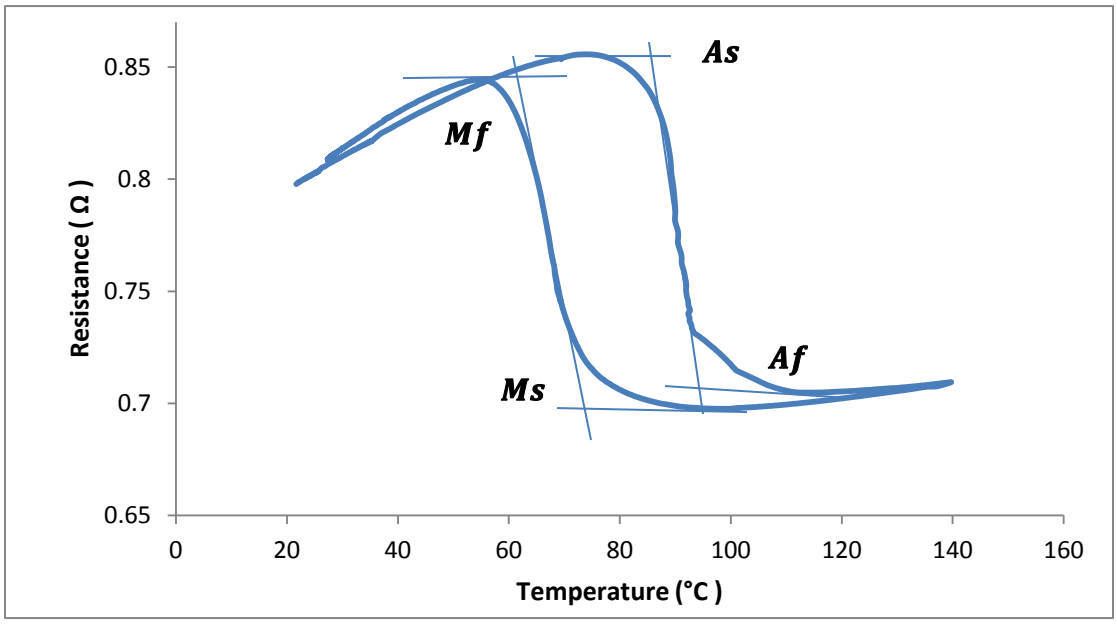

Figure 4.14 Electrical resistance-temperature curve for NiTi SMA wire under 150 MPa applied stress

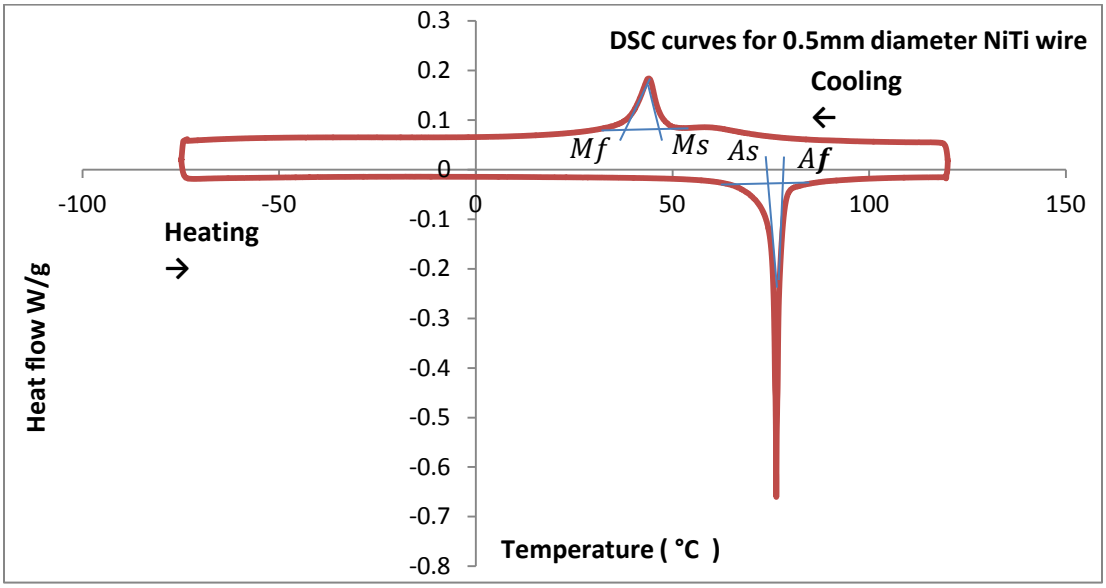

Figure 4.15 DSC curve for 0.5 mm diameter NiTi SMA wire

The variation of transformation temperatures with applied stress is shown in Figure (4.16). It is seen that the PTTs increase as the applied stress is increased. The increase in the PTTs can be described by the Clausius-Clapeyron equation by assuming linearity in the M_s temperatures. The Clausius-Clapeyron equation can be written as a function of enthalpy as follows [41]

$$\frac{dT}{d\sigma} = -\frac{T_0 \Delta\varepsilon}{\Delta H} \tag{4.2}$$

where

$\Delta\varepsilon$ = phase transformation strain

ΔH = phase transformation enthalpy [J]

T_0 = characteristic temperature [K] or [℃]

or it can be written as a function of entropy as [15]

$$\frac{dT}{d\sigma} = -\frac{\Delta\varepsilon}{\Delta S} \tag{4.3}$$

where

$\Delta S =$ phase transformation entropy $[{}^{J}/_{K}]$

The negative sign in the formula is because $S_M < S_A$.

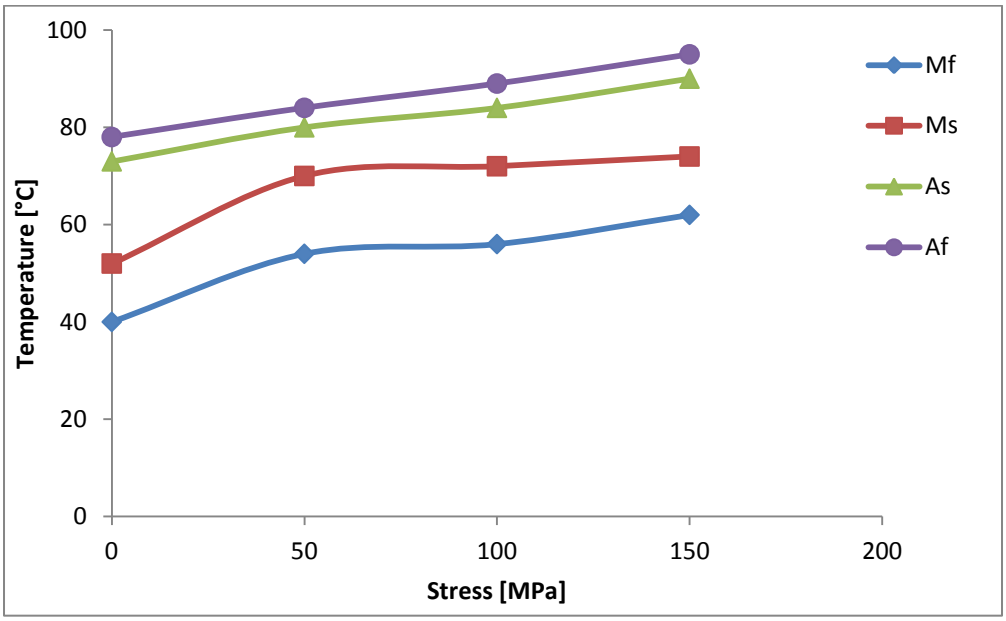

Figure 4.16 Effect of applied stress on the phase transformation temperatures

The PTTs for the 0.5 mm NiTi Flexinol wire with $A_s = 90℃$ are shown in Table (4-1).

Table 4-1 Phase transformation temperatures for NiTi Flexinol wire with As=90℃

Stress (MPa)	M_f(℃)	M_s(℃)	A_s(℃)	A_f(℃)
0	40	52	73	78
50	54	70	80	84
100	56	72	84	89
150	62	74	90	95

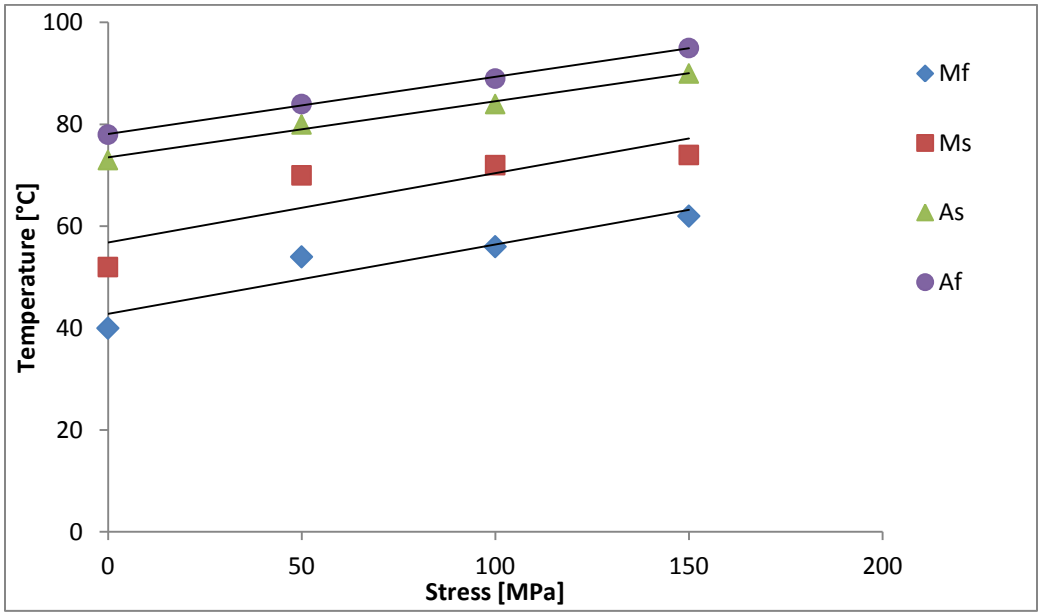

Figure 4.17 Linear fits of phase transformation temperatures under different applied stresses for NiTi Flexinol wire with As=90℃

The lines shown on the stress-temperature curve (Fig. 4.17) are called the transformation lines and slopes of each transformation line are increasing with rate of $dT/d\sigma$ [71]. Therefore, by assuming linearity in the M_s temperatures the relation between applied stress and PTTs for 0.5 mm diameter NiTi Flexinol wire with $A_s = 90℃$ can be shown by the following equations

$$M_f\ (℃) = 0.136\sigma\ (MPa) + 42.8 \tag{4.4}$$

$$M_s\ (℃) = 0.136\sigma\ (MPa) + 56.8 \tag{4.5}$$

$$A_s\ (℃) = 0.11\sigma\ (MPa) + 73.5 \tag{4.6}$$

$$A_f\ (℃) = 0.112\sigma\ (MPa) + 78.1 \tag{4.7}$$

where σ is the applied stress to the SMA wire.

4.2.2 Resistance Model Development for Shape Memory Alloy Wires

The electrical resistance of the SMA wire is modeled based on the wire surface temperature during phase transformation process as

$$R(T) = a/(1 + \exp\left(\frac{T_{SMA} - T_{0a}}{b}\right)) + c \tag{4.8}$$

where a model similar to the Boltzmann Sigmoid equation is used to fit the experimental data. The equation coefficients can be calculated based on the SMA wire phase

transformation temperatures, Equation (4.4) to (4.7), and the minimum and maximum values of resistance in the heating and cooling process.

For the heating process the coefficients are

$$T_{0a} = \frac{A_f + A_s}{2} \ [℃]$$

$$a = R_{max.heating} - R_{min.heating} \ [\Omega]$$

$$b = \frac{A_f - A_s}{3} \ [℃]$$

$$c = R_{min.heating} \ [\Omega]$$

and for the cooling process the coefficients are

$$T_{0a} = \frac{M_s + M_f}{2} \ [℃]$$

$$a = R_{max.heating} - R_{min.heating} \ [\Omega]$$

$$b = \frac{M_s - M_f}{3} \ [℃]$$

$$c = R_{min.cooling} \ [\Omega]$$

Since the electrical resistance of the SMA wires varies within a very small range in response to temperature changes over a comparatively much larger range, the introduced coefficients are sensitive. Therefore, running one cycle of the heating and cooling process is recommended between ambient temperature to a temperature above the A_f temperature in order to find the maximum and minimum values of electrical resistance. If it is not possible to run a heating and cooling cycle, $R_{max.}$ and $R_{min.}$ are defined based on

experimental results by using curve fit for actual values of $R_{max.}$ and $R_{min.}$ for different SMA wire lengths (30 cm, 40 cm, 50 cm) and for different applied external stresses (50 MPa, 100 MPa, 150 MPa).

For a SMA wire during the heating process $R_{max.}$ and R_{min} are defined as

$$R_{max.heating} = R_{amb.} + (10^{-4}(\sigma) + 6 \times 10^{-4}(l) + 0.0178) \quad (4.9)$$

or

$$R_{max.heating} = (-2 \times 10^{-5}(l) + 0.0012)\sigma + (0.0121(l) + 0.2953) \quad (4.10)$$

and

$$R_{min.heating} = R_{max.heating} - (2.5 \times 10^{-4}(\sigma) + 1.2 \times 10^{-3}(l) + 0.0658) \quad (4.11)$$

and for the cooling process are

$$R_{max.cooling} = R_{max.heating} - 0.012 \quad (4.12)$$

$$R_{min.cooling} = R_{min.heating} - (2 \times 10^{-6}(l) - 4 \times 10^{-5})\sigma + (2 \times 10^{-5}(l) + 0.0032) \quad (4.13)$$

where

$R_{amb.}$= electrical resistance of the SMA wire at ambient temperature ($T_{amb.} = 23℃$) for the heating curve [Ω]

σ = applied external stress [MPa]

l = SMA wire length [cm]

Equation (4.8) is developed to predict the SMA wire temperature based on its electrical resistance during the phase transformation process, and it works with less than 1% error between the A_s to A_f temperatures and the M_s to M_f temperatures for the heating and cooling curves, respectively. Equation (4.8) works with less than 5% error with the actual R_{max} and R_{min} values in the range of $A_s - 10℃ \leq T_{SMA} \leq A_f + 10℃$ for the heating process and $M_s + 18℃ \leq T_{SMA} \leq M_f$ for the cooling process. By using Equation (4.9) to calculate $R_{max.heating}$, Equation (4.8) works with less than 5% error in the range of $A_s - 6℃ \leq T_{SMA} \leq A_f + 6℃$ for the heating process and $M_s + 10℃ \leq T_{SMA} \leq M_f - 3$ for the cooling process. Using Equation (4.10) to calculate $R_{max.heating}$, Equation (4.8) works with less than 5% error in the range of $A_s - 5℃ \leq T_{SMA} \leq A_f + 5℃$ for the heating process and $M_s + 4℃ \leq T_{SMA} \leq M_f - 4$ for the cooling process. The resistance correlations and their application range are summarized in Table (4-2).

Table 4-2 The introduced resistance correlations and their application range

R_{max} and R_{min} Correlation	Application	Error
Actual R_{max} and R_{min} values	Heating: $A_s - 10℃ \leq T_{SMA} \leq A_f + 10℃$ Cooling: $M_s + 18℃ \leq T_{SMA} \leq M_f$	5%
Equation (4.9)	Heating: $A_s - 6℃ \leq T_{SMA} \leq A_f + 6℃$ Cooling: $M_s + 10℃ \leq T_{SMA} \leq M_f - 3$	5%
Equation (4.10)	Heating: $A_s - 5℃ \leq T_{SMA} \leq A_f + 5℃$ Cooling: $M_s + 4℃ \leq T_{SMA} \leq M_f - 4$	5%

The experimental data and the curve fits based on Equation (4.8) for the SMA wire under different applied stresses are shown in Figures (4.18), (4.19) and (4.20).

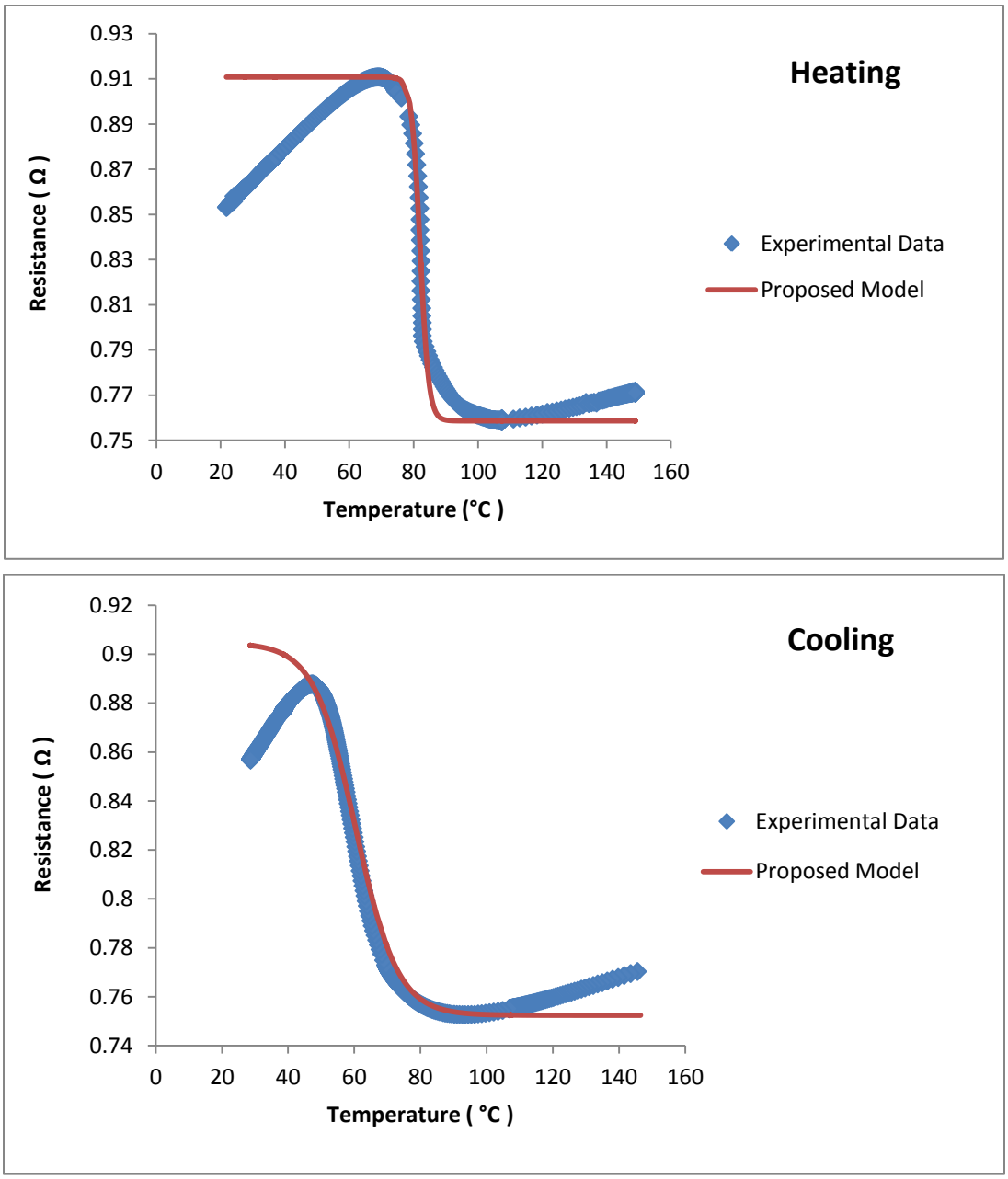

Figure 4.18 Experimental data and proposed model for 500 mm length NiTi SMA wire under 50 MPa applied stress

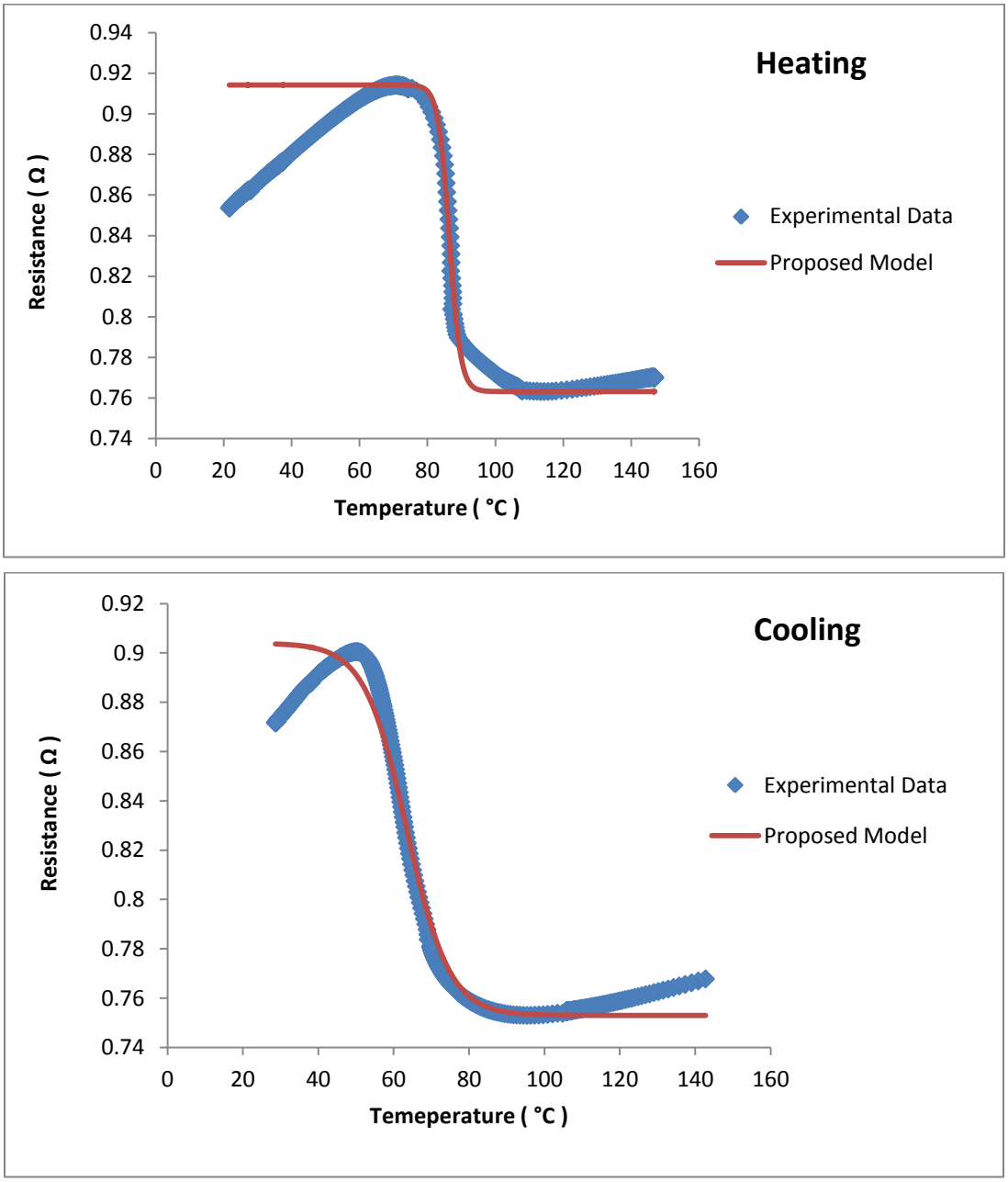

Figure 4.19 Experimental data and proposed model for 500 mm length NiTi SMA wire under 100 MPa applied stress

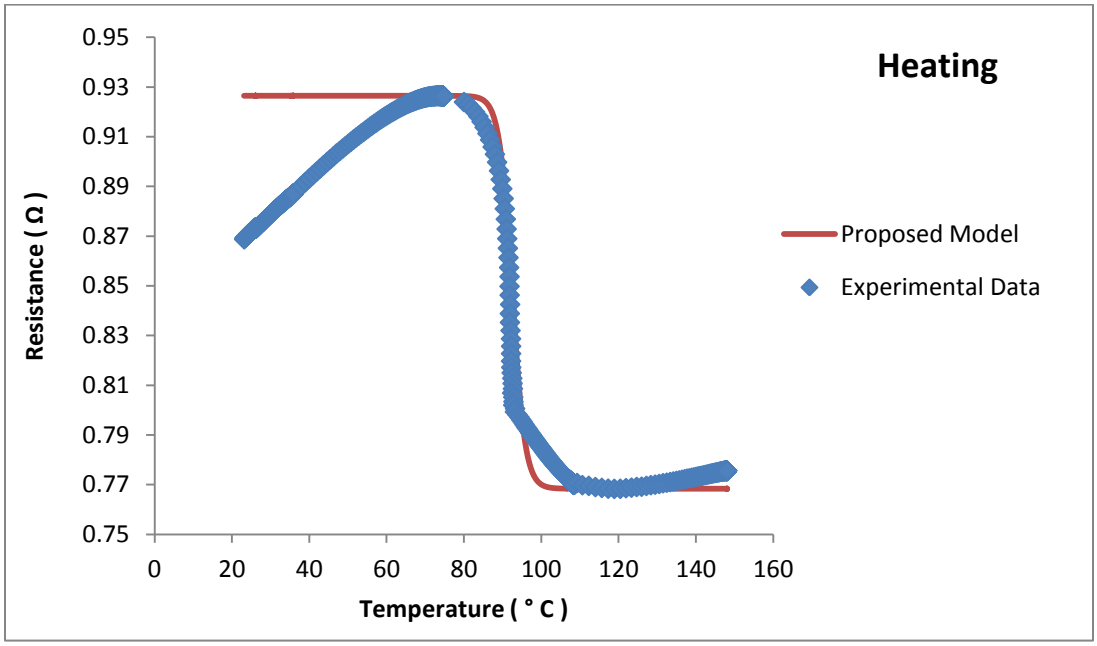

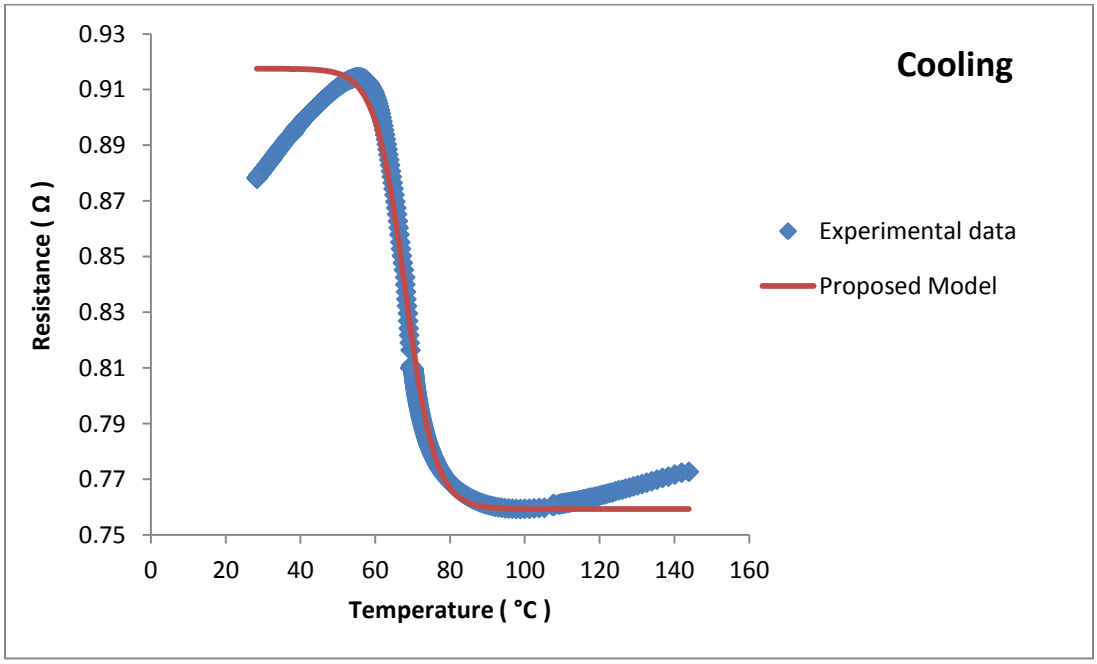

Figure 4.20 Experimental data and proposed model for 500 mm length NiTi SMA wire under 150 MPa applied stress

The heating process of SMA wires from ambient temperature to approximately 70℃ exhibits a linear relation as is the case in most metals upon heating as seen in Figures (4.18) to (4.20). For the cooling process where the temperature is greater than $M_f - 5℃$ down to ambient temperature, the SMA wire resistance is showing a linear relation with its temperature as seen in Figures (4.18) to (4.20). The linear parts of the heating and cooling curves are modeled with a line equation as

$$R_{SMA} = m_c T_{SMA} + d_c \tag{4.14}$$

For the heating process in the temperature range of $T_{amb.} \leq T_{SMA} \leq 70℃$

$$m_c = \frac{R_{max.heating} - R_{amb.}}{70℃ - T_{amb.}} \tag{4.15}$$

or based on experimental results for $30\ [cm] \leq l \leq 50\ [cm]$, m is defined as

$$m_c = \frac{(-17.5 + l)}{(-6250 + 625(l))} \tag{4.16}$$

and

$$d_c = R_{amb.} - (0.0005(l) + 0.005) \tag{4.17}$$

where

l = SMA wire total length $[cm]$

$R_{amb.}$= electrical resistance of the SMA wire at ambient temperature ($T_{amb.} = 23℃$) for the heating curve [Ω]

For the cooling process in the temperature range of $M_f - 5℃ \leq T_{SMA} \leq T_{amb.}$

$$m_c = \frac{R_{max.cooling} - R_{amb.}}{(M_f - 10℃) - T_{amb.}} \tag{4.18}$$

or based on experimental results for $30\ [cm] \leq l \leq 50[cm]$, m is defined as

$$m_c = \frac{(-12.2 + l)}{(3700 + 370(l))} \tag{4.19}$$

and

$$d_c = R_{amb.} - (0.0013(l) + 0.0156) \tag{4.20}$$

where

l = SMA wire total length $[cm]$

$R_{amb.}$= SMA wire electrical resistance at ambient temperature for the cooling curve [Ω]

R-phase transformation is not considered in the developed resistance model for SMA wires.

4.3 Summary

In this chapter, the effects of different parameters such as applied external stress and wire length on electrical resistance and strain of SMA wires were observed. Hysteresis curves between SMA wires electrical resistance and strain are plotted. Later the effect of applied stress on SMA wires phase transformation temperatures is investigated, and linear relations are introduced between the applied stress and phase transformation temperatures for 0.5 mm diameter NiTi Flexinol wire with $A_s = 90℃$. At the end, a resistance model

is proposed for SMA wires, based on the experimental results that can be used to predict the temperature of SMA wire based on electrical resistance.

Chapter 5

Natural Convection Heat Transfer Correlation for Shape Memory Alloy Wires

In this chapter, an empirical natural convection heat transfer correlation is developed for SMA wires based on Ra_D and Nu_D numbers in the range of $2.6\times 10^{-8} \leq Ra_D \leq 6 \times 10^{-1}$ and Pr = 0.702. The proposed correlation is based on experimental results for 0.5 mm diameter NiTi SMA wire under 100 MPa applied stress and stress-free conditions. The SMA wire is heated from ambient temperature up to 100℃ at various pressures. In order to develop a correlation that contains the wire inclination angle at each set pressure, the Ra_D and Nu_D numbers are calculated for the wire from horizontal to vertical inclination angles. The proposed correlation can be used to calculate the natural convection heat transfer coefficient (h) for a heated SMA wire based on its inclination angle.

5.1 Convection Heat Transfer Correlation

The equation used to calculate natural convection heat transfer coefficients comes from correlations of dimensionless numbers. To develop a correlation for natural convection heat transfer, the Nusselt (Nu_D) number must be determined which leads to a calculation of the natural convection heat transfer coefficient (h). Usually for natural convection heat transfer, Nu_D is expressed as a function of Rayleigh (Ra_D) number [45]. The convective heat transfer correlation can be developed experimentally for the SMA wire by heating

the wire to a temperature above the ambient temperature. Convection heat transfer then occurs from the wire to the surrounding ambient fluid. The wire and the ambient temperatures must be measured. The power input to the wire (VI) is equal to the total heat transfer rate (Q) [45]. Under steady state conditions the convective heat transfer coefficient can be calculated from Newton's law of cooling as expressed in Equation (3.2), and then the Ra_D and the Nu_D numbers can be calculated for the wire. As described in Section 3.3, the Ra_D and the Nu_D numbers are calculated for the SMA wire based on experimental results at each inclination angle from horizontal to vertical. The SMA wire under 100 MPa applied stress and stress-free conditions was heated via a Joule effect method by passing a direct current through the wire, from ambient $T_\infty = 296\ K$ (23℃) to $T_{SMA} = 373\ K$ (100℃) temperature, under which the (Nu_D) and (Ra_D) are calculated based on Equations (3.3) and (3.12) respectively. The constants in Equations (3.3) and (3.12) are determined from the heat transfer tables for the calculated mean temperature ($T_m = \frac{T_{SMA}+T_\infty}{2} = 334\ K$ (61.5℃)) as: $k = 0.0288\ [W/m\,.K]$,

Pr=0.702 and μ = 200.648 × 10^{-7} [$N\,s/m^2$] [45]. At each wire inclination angle the (Nu_D) and (Ra_D) numbers are calculated for various air pressures, from 700 torr to 0.1 torr, which results in a Rayleigh number range of $2.6\times 10^{-8} \leq Ra_D \leq 6 \times 10^{-1}$. An empirical correlation for SMA wires is developed in power law form as

$$Nu_D = A + C(Ra_D)^n \tag{5.1}$$

The empirical correlation for the SMA wire under 100 MPa applied stress and Pr = 0.702 in the range of $2.6\times 10^{-8} \leq Ra_D \leq 6 \times 10^{-1}$ is

$$Nu_D = (-0.03\varphi + 0.16) + (-0.1\varphi^2 + 0.03\varphi + 0.8)Ra_D^{(-0.03\varphi+0.16)} \tag{5.2}$$

and for the SMA wire under stress-free conditions and Pr = 0.702 in the range of $2.6\times 10^{-8} \leq Ra_D \leq 6 \times 10^{-1}$ is

$$Nu_D = (-0.04\varphi + 0.19) + (-0.09\varphi^2 + 0.003\varphi + 0.8)Ra_D^{(-0.03\varphi+0.17)} \tag{5.3}$$

where φ is the inclination angle of the SMA wire in radians from 0 to 1.57 radians (0 to 90°). The constant values of A, C, and n decrease with an increase in the wire inclination angle. The relation between Nu_D and Ra_D are shown in Figures (5.1) and (5.2) for the wire at different inclination angles from horizontal ($\varphi = 0$) to vertical ($\varphi = 90°$) with 15° increments based on Equations (5.2) and (5.3).

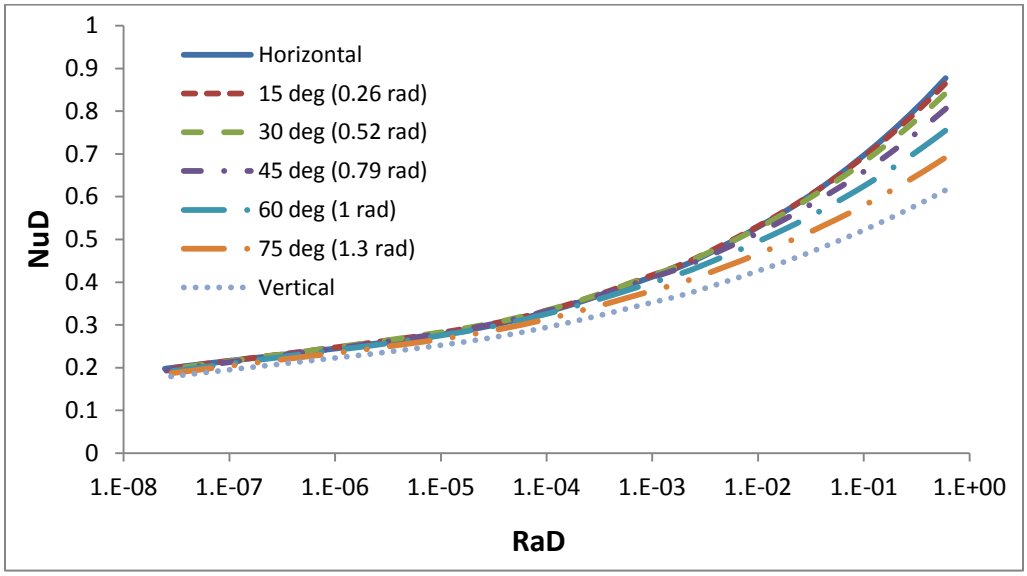

Figure 5.1 Relation between Nu and Ra for the SMA wire at various angles under 100 MPa applied stress

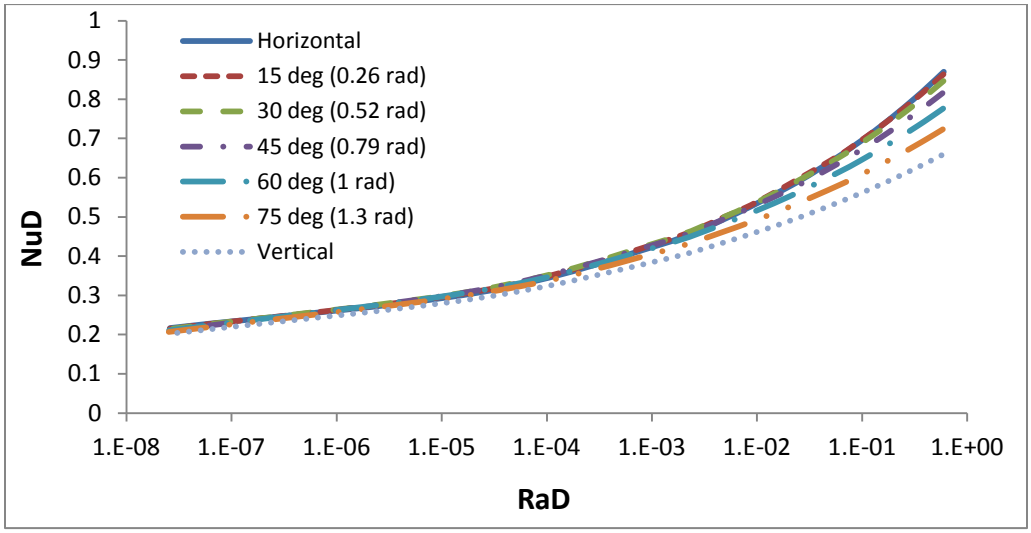

Figure 5.2 Relation between Nu and Ra for the SMA wire at various angles under stress-free condition

As the wire inclination angle changes from horizontal to vertical, the thickness of the boundary layer increases due to an increase in the developing boundary length, which, leads to a decrease in the Nu_D values. At higher Rayleigh values, the Nu_D decreases approximately 25 % when the wire orientation is changed from horizontal to vertical. At lower Rayleigh values, the Nu_D decreases approximately 5% when the wire orientation is changed from vertical to horizontal. The experimental values for Nu_D are plotted against wire inclination angle in Figures (5.3) and (5.4). The Nu_D values decrease with increasing wire inclination angle, but as the Rayleigh number decreases and reaches 2.5×10^{-8}, the Nu_D values flatten almost to a straight line and do not change significantly with changes in the wire inclination angle. At low pressures when $Ra \to 0$ the convection heat transfer rate reduces and the Nusselt number approaches the diffusive limit which is constant for a same geometry and is not affected by wire inclination angle.

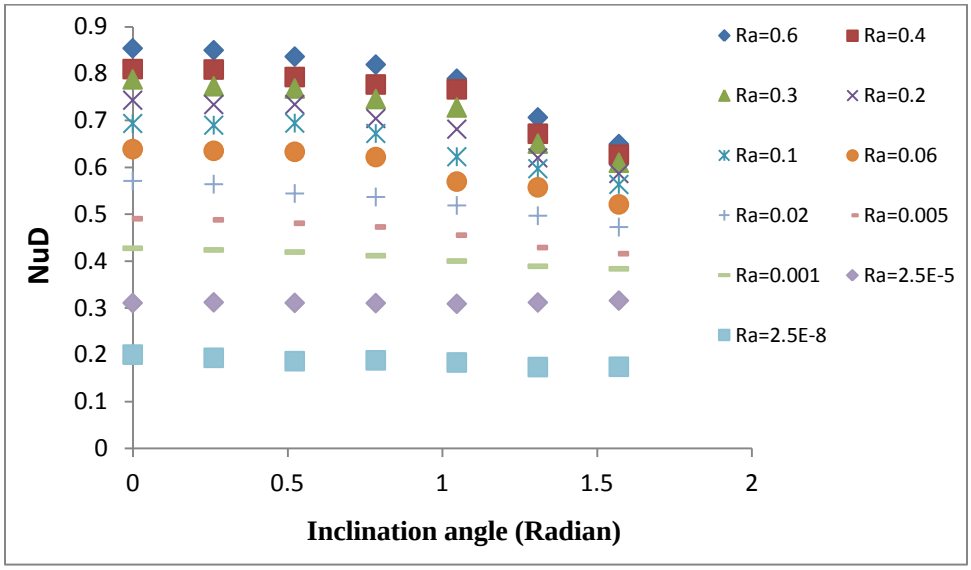

Figure 5.3 Effect of inclination angle on Nu values for the SMA wire under 100 MPa applied stress

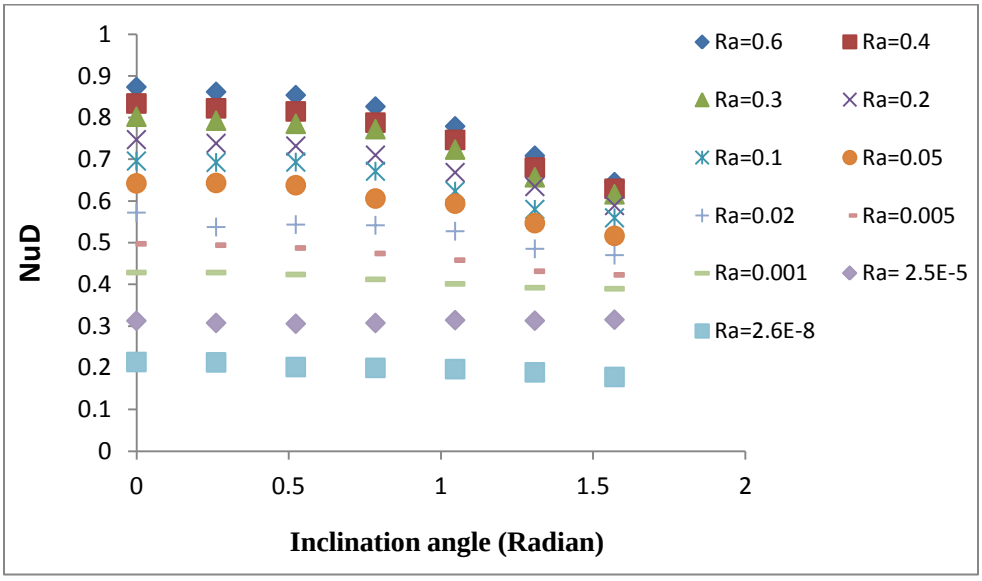

Figure 5.4 Effect of inclination angle on Nu values for the SMA wire under stress- free condition

The experimental results show less than 5% difference in Nu values for the wire under 100 MPa stress and the stress-free condition. Therefore, it can be concluded that the applied external stress to SMA wire does not have a significant effect on its natural convection heat transfer correlation. Therefore, a single natural convection heat transfer correlation is proposed for SMA wires independent of applied stress for the range of $2.6\times 10^{-8} \leq Ra_D \leq 6 \times 10^{-1}$ and Pr =0.702 in the power law form

$Nu_D = A + C(Ra_D)^n$ as

$$Nu_D = (-0.03\varphi + 0.17) + (-0.09\varphi^2 + 0.02\varphi + 0.76)Ra_D^{(-0.03\varphi+0.16)} \quad (5.4)$$

The values for the constants $A, C,$ and n for Equation (5.4) are shown in Table (5-1) for various SMA wire inclination angles $\varphi = 0$ to $\varphi = 90°$ with 15° increments. The wire inclination angles in Equation (5.2), (5.3) and (5.4) are in radians. Equation (5.4) works with approximately 5% error in the introduced Rayleigh number range.

Table 5-1 Constants for the SMA wire in the range of 2.6 E-8 ≤ Ra ≤ 6E-1

$\boldsymbol{\varphi}$ **Radian** $(\boldsymbol{degree})$	$\boldsymbol{A}$	$\boldsymbol{C}$	$\boldsymbol{n}$
0	0.17	0.76	0.16
0.26 (15°)	0.162	0.759	0.152
0.52 (30°)	0.154	0.746	0.144
0.79 (45°)	0.146	0.720	0.136
1.05 (60°)	0.139	0.682	0.129
1.31 (75°)	0.131	0.632	0.121
1.57(90°)	0.123	0.569	0.113

The relation between Nu_D and Ra_D for the SMA wire based Equation (5.4) is shown in Figure (5.5).

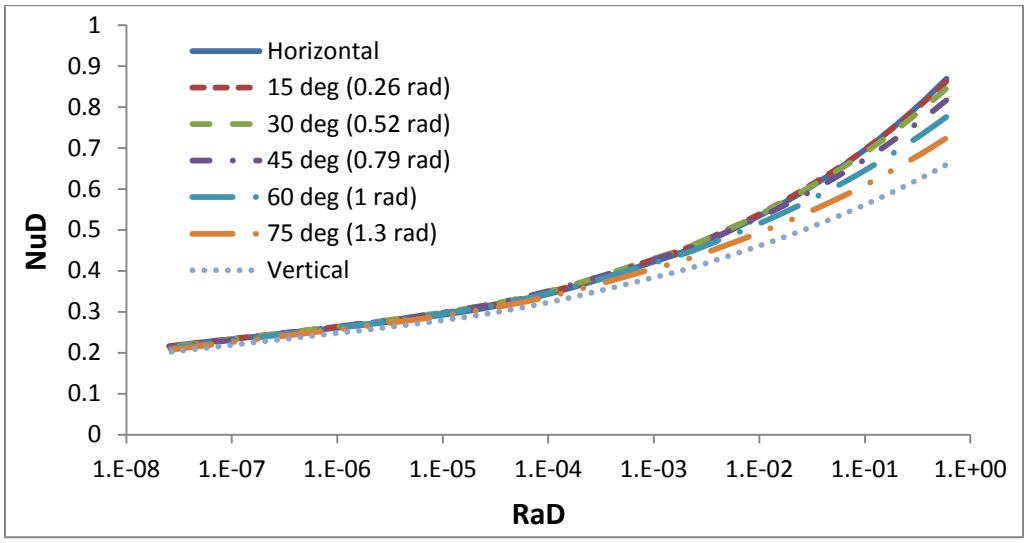

Figure 5.5 Relation between Nu and Ra for the 0.5mm diameter NiTi SMA wire at various angles in the range of 2.6E-8 ≤ Ra ≤ 6E-1

5.2 Verification of Convective Heat Transfer Correlation

The proposed correlation Equation (5.4) is compared with other existing heat transfer correlations available in the literature and introduced in Section 2.3 for wires and cylinders in horizontal and vertical orientations. Very few correlations are available for inclined wires and cylinders, and none of the correlations introduced in Section 2.3.3 are in the working Rayleigh number range under which the new correlation has been developed. Therefore, the verification in this section of the newly developed correlation is compared with other existing correlations in horizontal and vertical orientations. The differences between the new correlation and other existing correlations are due to different methods and conditions used or the errors when the correlations were

developed. There are some limitations in using the available heat transfer correlations in the literature for accurate calculation of the natural convection heat transfer coefficient (h) for SMA wires, since the existing correlations have been developed under different conditions and not specifically for SMA wires. The different conditions affect the boundary layer development around the wires or cylinders due to natural convection heat transfer development which causes the difference between the newly developed correlation and existing correlations. The other limitation of the existing correlations is the inclination angle, in that they are usually developed for vertical or horizontal orientations. The proposed correlation contains the wire inclination angle, which can be used for wires in any inclination angle from horizontal to vertical. As shown in Figures (5.6) and (5.7), the proposed correlation has the same trend as other correlations and is positioned in the middle among the existing correlations. For the horizontal orientation, the proposed correlation agrees with the Fujii et al. [52] correlation for platinum wires and Morgan's [46] correlation for long horizontal cylinders. It is less than 10% lower than Fujii [52] and less than 5% lower than Morgan's [46] correlation. The Churchill and Chu [47] correlation is 8% lower than the proposed correlation from this work.

For the wire in the vertical position, the proposed correlation is lower than Mueller [54] and higher than Fujii et al. [56] and Nagendra [55]. It is less than 10% higher than Nagendra [55] and less than 15% higher than Fujii [56].

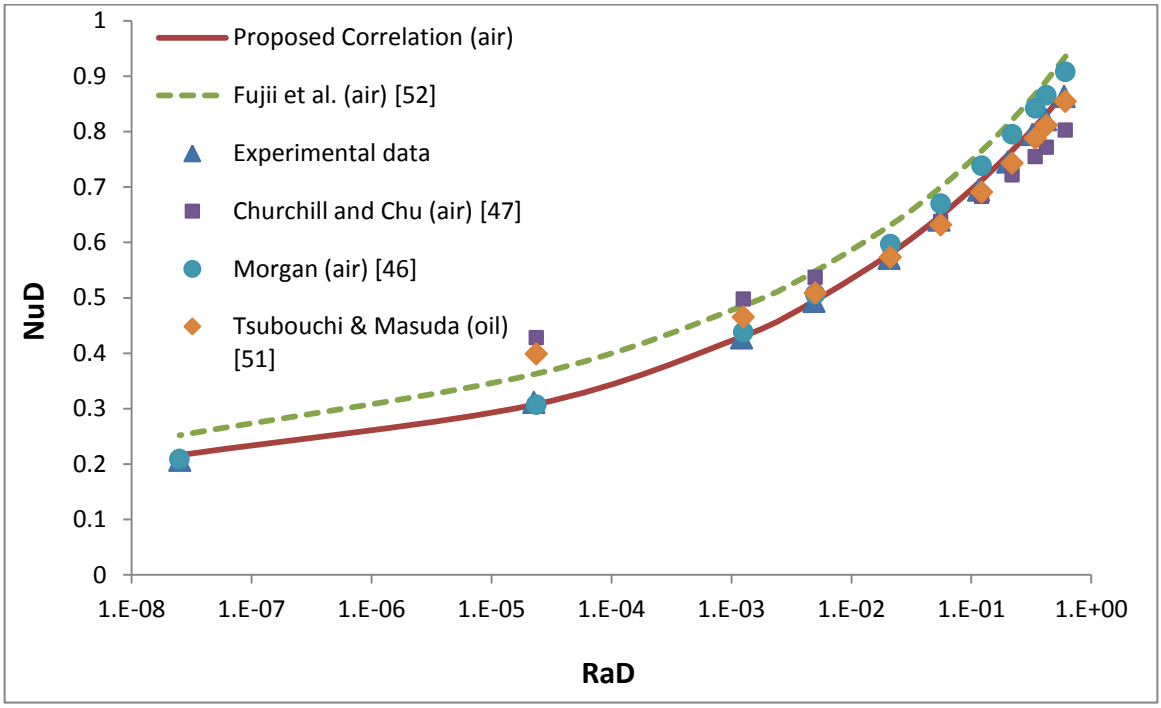

Figure 5.6 Comparison of proposed correlation for the SMA wire at horizontal orientation with existing natural convection heat transfer correlations

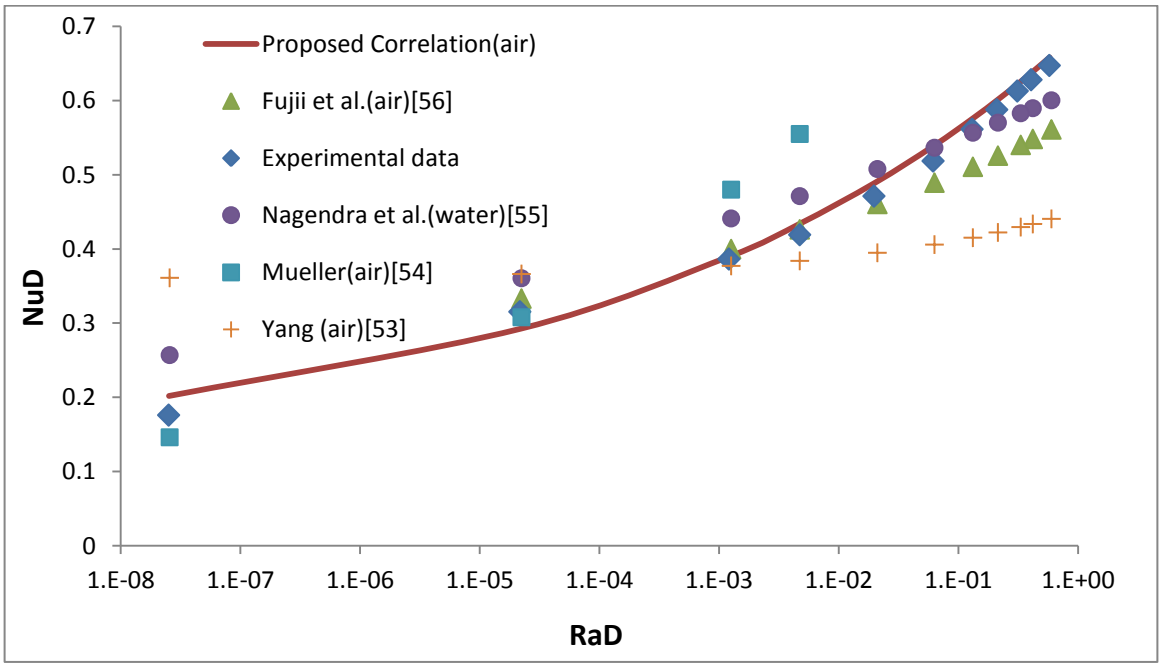

Figure 5.7 Comparison of proposed correlation for the SMA wire at vertical orientation with existing natural convection heat transfer correlations

5.3 Summary

A natural convection heat transfer correlation is developed for the SMA wires for a Rayleigh number range of $2.6\times 10^{-8} \leq Ra_D \leq 6 \times 10^{-1}$. The new correlation is based on inclination angle and can be used for SMA wires with an inclination angle range of $0° \leq \varphi \leq 90°$. The new correlation is compared with other existing correlations in the literature for wires and cylinders.

Chapter 6

SMA Wire Temperature and Heat Transfer Coefficient Calculation through Proposed Models

The temperature of SMA wires can be predicted directly using the resistance model Equation (4.8) or it can be predicted using the standard heat transfer equation and proposed correlation, Equation (5.4). In this chapter a more detailed description is given.

6.1 Temperature Prediction through Proposed Natural Convection Heat Transfer Correlation

As described in Section 3.3, the SMA wire is heated by passing a current through it. At steady state conditions, by neglecting the conduction heat transfer rate, the power input to the wire will be equal to convection and radiation heat transfer rates (Fig. 3.5). Therefore, the standard heat transfer equation as given in Equation (3.4) by neglecting conduction heat transfer rate, can be written for a heated SMA wire when it reaches steady state conditions as

$$I^2R = hA_{SMA}(T_{SMA} - T_\infty) + \varepsilon_r \sigma_r A_{SMA}(T_{SMA}^4 - T_\infty^4) \tag{6.1}$$

where

σ_r = Stefan-Boltzmann constant ($5.67 \times 10^{-8}\ W/m^2K^4$)

ε_r = emissivity

A_{SMA} = SMA wire surface area (πDl)

T_{∞} = ambient temperature

I and R are current input and electrical resistance of the SMA wire respectively. Although the emissivity of the SMA can vary with respect to surface temperature, a value of 0.63 [61] is used based on the average working temperature range for NiTi. The heat transfer coefficient can be calculated for the SMA wires based on Equation (5.1) as

$$Nu_D = \frac{hD}{k} = (A + CRa_D^n) \Rightarrow h = \frac{k}{D}(A + CRa_D^n) \tag{6.2}$$

The procedure for calculating the SMA wire temperature by using the new developed correlation is shown in a flowchart (Fig. 6.1).

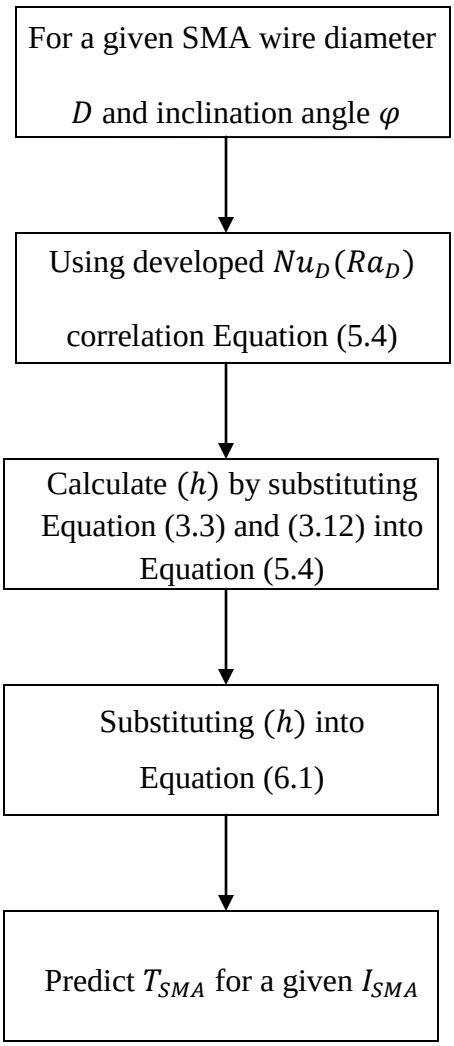

Figure 6.1 Flowchart to determine SMA wire temperature based on proposed natural convection heat transfer correlation

For example when a 0.5 mm diameter current carrying SMA wire in 1 atm air pressure (760 torr) is inclined from horizontal at 15°, Equation (6.2) can be written based on Equation (5.4) or based on defined constant values A, C and n with respect to wire inclination angles in Table (5-1) as

$$Nu_D = 0.162 + 0.759(\mathrm{Ra_D})^{0.152} \tag{6.3}$$

By substituting Equation (6.3) and the Nusselt and Rayleigh number definitions, Equation (3.3) and (3.12) respectively, into Equation (6.2), it becomes

$$h = \frac{k}{D}\left(0.759\left(\frac{g(T_{SMA} - T_\infty)D^3P^2}{\mu^2 T_\infty R^2 Z^2 \left(\frac{T_{SMA} + T_\infty}{2}\right)^2}.Pr\right)^{0.152} + 0.162\right) \tag{6.4}$$

Substituting Equation (6.4) into Equation (6.1) the standard heat transfer equation of the SMA wire becomes

$$I^2R = \frac{k}{D}\left(0.759\left(\frac{g(T_{SMA} - T_\infty)D^3P^2}{\mu^2 T_\infty {R_c}^2 Z^2 (T_m)^2}.Pr\right)^{0.152} + 0.162\right) \times (\pi Dl(T_{SMA} - T_\infty) + \varepsilon_r \sigma_r \pi Dl(T_{SMA}^4 - T_\infty^4)) \tag{6.5}$$

Based on the T_m value Pr, μ and k values can be found from air thermodynamic property tables [45]. Pr, μ and k are correlated based on T_m by using a curve fit of introduced values for Pr, μ and k in air thermodynamic tables [45] for a temperature range $200K \leq T_m \leq 400K$ as

$$Pr = 6 \times 10^{-7} T_m^2 - 0.0006 T_m + 0.8278 \quad (6.6)$$

$$k = -3 \times 10^{-8} T_m^2 + 10^{-4} T_m - 3 \times 10^{-5} \quad (6.7)$$

$$\mu = -3 \times 10^{-11} T_m^2 + 7 \times 10^{-8} T_m + 8 \times 10^{-7} \quad (6.8)$$

where

$$T_m = \left(\frac{T_{SMA} + T_\infty}{2}\right)^2$$

Therefore, by substituting the constant values of $g = 9.8\ [m/s^2]$, $R_c = 287\ [J/kg.K]$, $Z = 1$ by considering air as an ideal gas, $\varepsilon_r = 0.63$, $\sigma_r = 5.67 \times 10^{-8}\ [W/m^2K^4]$, R based on SMA wire resistivity from Dynalloy, Inc.[72] and Equations (6.6), (6.7) and (6.8) into Equation (6.5), the temperature of a known current carrying SMA wire can be predicted. The introduced procedure can be simplified by predicting the wire temperature directly from electrical resistance using the resistance models introduced in Equations (4.8) or (4.14). The procedure of using electrical resistance to calculate SMA wire temperature is described in Section 6.2.

6.2 Through SMA Wire Electrical Resistance

The SMA wire surface temperature (T_{SMA}) can be calculated directly without using the standard heat transfer Equation (6.1) from its electrical resistance by using Equation (4.8) or Equations (4.14) based on the working temperature range. The procedure for calculating the SMA wire temperature directly from wire electrical resistance (R_{SMA}) is shown in flowchart (Fig. 6.2).

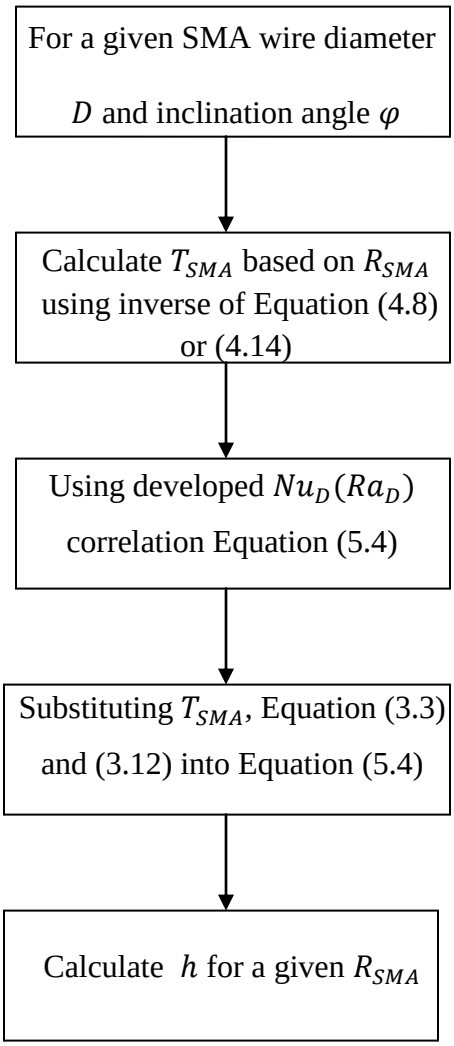

Figure 6.2 Flowchart to determine SMA wire temperature and natural convection heat transfer coefficient based on proposed electrical resistance model

As an example the SMA wire surface temperature (T_{SMA}) during the phase transformation process can be calculated by using Equation (4.8) as

$$T_{SMA} = b.\ln\left(\frac{a}{R_{SMA} - c} - 1\right) + T_{0a} \tag{6.9}$$

where a, b, c and T_{0a} are defined in Section 4.2.2 based on the applied external stress to the wire and its total length.

Based on the calculated T_{SMA} from Equation (6.9), the convection heat transfer coefficient (h) for the SMA wire can be calculated by using the proposed correlation Equation (5.4) and Nu_D and Ra_D definitions Equation (3.3) and (3.12) as

$$h = \frac{k}{D}[A + C(\frac{g\left(\left(b.\ln\left(\frac{a}{R_{SMA} - c} - 1\right) + T_{0a}\right) - T_{\infty}\right)D^3P^2}{\mu^2 T_{\infty} {R_c}^2 Z^2 {T_m}^2}.Pr)^n] \tag{6.10}$$

where $g = 9.8\ [m/s^2]$, $R_c = 287\ [J/kgK]$ and $Z = 1$. A, B, and n can be replaced based on the wire inclination angle using Equation (5.4) or Table (5-1) and Pr, μ and k can be found based on T_m from thermodynamic air property tables or Equations (6.6) to (6.8).

Chapter 7
Conclusions and Recommendations

There are two sections in this chapter. The first section is conclusions for electrical resistance and strain measurements of the SMA wire, the effects of different parameters on wire electrical resistance and development of a resistance-temperature model. The second section is conclusions for natural convection heat transfer from a heated SMA wire to the air and development of a natural convection heat transfer model for the wire.

7.1 Conclusions for SMA Wire Electrical Resistance and Strain

The changes of SMA wire electrical resistance and strain were investigated during the phase transformation process by changing the wire temperature. Due to martensite phase transformation phenomena in the SMA wires, hysteresis relations were observed between SMA wire resistance-temperature and strain-temperature curves. The Electrical resistance of SMA wire changes with changes to the wire temperature, and due to crystal structure change caused by phase transformation the electrical resistance is higher in the martensite (low temperature) phase than in the austenite (high temperature) phase. In order to investigate effects of different parameters on SMA wire electrical resistance and strain the resistance-temperature and strain-temperature hysteresis curves were generated for the wire under various conditions. Applied stress has a significant effect on martensite transformation and also on SMA wire electrical resistance. The electrical resistance change during phase transformation is 14%, 15% and 16% for the SMA wire under 50 MPa, 100 MPa and 150 MPa applied stress, respectively and also the value of electrical resistance increases with an increase in the applied stress to the wire. When the stress is

large enough to create complete, detwinned martensite the electrical resistance of the wire is independent of the phase transformation time rate. The SMA wire ambient pressure and inclination angle have no effect on electrical resistance.

A 4.5% strain is recorded for the SMA wire under applied stress of 50 MPa, 100 MPa and 150 MPa. Self-accommodating martensite transformation is observed for SMA wire under low stress or stress-free conditions in which the shape recovery occurs with no visible strain change.

The SMA wire phase transformation temperatures depend strongly on the external stress applied to the wire. The phase transformation temperatures increase with an increase in the applied stress. Linear correlations are developed based on experimental results for 0.5 mm diameter NiTi Flexinol wire with $A_s = 90℃$ to calculate phase transformation temperatures based on applied stress to the wire.

An electrical resistance model is proposed for SMA wires based on experimental results. The proposed model can predict the temperature of a current-carrying SMA wire during the phase transformation process based on its electrical resistance.

7.2 Conclusions for SMA Wire Natural Convection Heat Transfer Modeling

Natural convection heat transfer from a heated SMA wire to the air is studied for the wire at various angles, from horizontal to vertical, under 100 MPa applied stress and stress-free conditions. Less than 5% difference is observed in Ra_D and Nu_D values for the SMA wire under 100 MPa applied stress and stress-free conditions, from which it can be concluded that the applied stress to the wire has no effect on natural convection heat

transfer from the SMA wire to the ambient. Nu_D values decrease with increases in the wire inclination angle at higher Rayleigh ranges. As the Rayleigh values approach 2.6×10^{-8} no significant changes in the Nu_D values are observed, which means that at lower Rayleigh ranges Nu_D values are independent of wire inclination angle.

A natural convection heat transfer correlation for the SMA wires based on experimental results is proposed which agrees with existing correlations for the range of $2.6 \times 10^{-8} \leq Ra_D \leq 6 \times 10^{-1}$ and $Pr = 0.702$. The new correlation is based on the inclination angle and can be used for SMA wires with an inclination angle range of $0° \leq \varphi \leq 90°$.

7.3 Recommendations

- Carrying out the experiments on different SMA wire diameters is recommended to investigate the effects of wire diameter on electrical resistance and the heat transfer models.
- In this work two different electrical resistance models are used to model the resistance of the SMA wire. First, a linear model is used from ambient temperature to the phase transformation start temperature, and later, an exponential function is used to model the electrical resistance of the wire during the phase transformation. A single resistance model can be developed for the SMA wire that can be used from ambient temperature up to the phase transformation finish temperature.

- The electrical resistance of SMA wire can be modeled based on its strain to predict the position of the SMA wire based on its electrical resistance.

Appendix A
Uncertainty Analysis

A.1 Method

In this section the uncertainty of experimentally measured values are calculated. The Moffat [73] method of uncertainty analysis is used to calculate the random uncertainty of measured data. In this method the result Y of an experiment is assumed to be calculated from measurement data as

$$Y = Y(X_1, X_2, X_3, \dots, X_N) \tag{A.1}$$

where the uncertainty in a single measurement X_i is shown as

$$\delta Y_{X_i} = \frac{\partial Y}{\partial X_i} \tag{A.2}$$

When several variables are used to calculate Y such as

$$Y = X_1^a X_2^b X_3^c \dots X_M^m \tag{A.3}$$

The total error of Y can be calculated by the sum of individual errors as

$$\frac{\delta R}{R} = \sqrt{(a\frac{\delta X_1}{X_1})^2 + (b\frac{\delta X_2}{X_2})^2 + \cdots + (m\frac{\delta X_m}{X_m})^2} \tag{A.4}$$

A.2 Uncertainty in Measured Values

A.2.1 SMA Wire Temperature Measurements

E-type thermocouples were used to measure the temperature of the SMA wire and the temperature readings were through a Keithley 2007 data acquisition system. The uncertainty in the temperature reading based on the Keithley specifications is 1℃. Therefore, the uncertainty in temperature readings is

$$\frac{\delta T}{T} = \pm \frac{1℃}{T[℃]} \tag{A.5}$$

A.2.1.1 SMA Wire Phase Transformation Temperatures

The SMA wire phase transformation temperatures are obtained from the wire DSC curve and electrical resistance-temperature curves using a ruler with $\pm$ 0.1 cm error in reading or $\pm$ 2℃. Therefore, the uncertainty in the reported phase transformation temperatures for the wire is

$$\frac{\delta T}{T} = \pm \frac{2℃}{T[℃]} \tag{A.6}$$

A.2.2 Voltage Measurements

The uncertainty in the SMA wire voltage readings based on the Keithley specifications in the range of 1 V is

(A.7)

$$\frac{\delta V_{SMA}}{V_{SMA}} = \pm\left(3.0 \times 10^{-5} + \frac{7.0 \times 10^{-6} V}{V_{SMA}[V]}\right)$$

and the uncertainty in the voltage readings for the shunt resistor in the range of 100 mV according to the Keithley specifications is

(A.8)

$$\frac{\delta V_{shunt}}{V_{shunt}} = \pm\left(3.0 \times 10^{-5} + \frac{3.5 \times 10^{-6} V}{V(V_{shunt})}\right)$$

A.2.3 SMA Wire Current Measurements

The current of SMA wire is calculated as

(A.9)

$$I_{SMA} = \frac{V_{shunt}}{R_{shunt}}$$

Therefore, the uncertainty for the SMA wire current can be shown as

(A.10)

$$\frac{\delta I}{I} = \pm\sqrt{(\frac{\delta V_{shunt}}{V_{shunt}})^2 + (\frac{\delta R_{shunt}}{R_{shunt}})^2}$$

which is [74]

(A.11)

$$\frac{\delta I}{I} = \pm\sqrt{(3.0 \times 10^{-5} + \frac{3.5 \times 10^{-6} V}{V_{shunt}[V]})^2 + (0.0014)^2}$$

A.2.4 Pressure Measurements

A CeramiCel pressure gage was used to measure the air pressure and pressure readings were through the Keithley data acquisition system as a voltage signal. The air pressure is calculated as [74]

$$p = C.V_{pressure} \tag{A.12}$$

where C is a constant coefficient. Therefore, the uncertainty in the pressure readings can be shown as

$$\frac{\delta p}{p} = \pm \sqrt{(\frac{\delta C}{C})^2 + (\frac{\delta V_{pressure}}{V_{pressure}})^2} \tag{A.13}$$

The $(\frac{\delta C}{C})$ based on the CeramiCel pressure gage specification is 0.25% of full scale where full scale for the device is 1000 torr = 1.33322×10^5 Pa therefore

$$\frac{\delta C}{C} = \pm \frac{333.305\ Pa}{p\ [Pa]} \tag{A.14}$$

and $\frac{\delta V_{pressure}}{V_{pressure}}$ according to the Keithley specifications for $10V$ range can be shown as

$$\frac{\delta V_{pressure}}{V_{pressure}} = \pm \left(3 \times 10^{-5} + \frac{5 \times 10^{-5}\ V}{V_{pressure}\ [V]} \right) \tag{A.15}$$

By substituting Equation (A.14) and (A.15) into Equation (A.13) the uncertainty in pressure reading can be calculated as

$$\frac{\delta p}{p} = \pm \sqrt{\left(\frac{333.305\ Pa}{p\ [Pa]}\right)^2 + \left(3 \times 10^{-5} + \frac{5 \times 10^{-5}\ V}{V_{pressure}\ [V]}\right)^2} \tag{A.16}$$

A.2.5 Dimensions

An electronic digital caliper with a resolution of $\pm\, 0.005\ mm$ was used to measure the dimensions. Therefore the uncertainty in the diameter and length measurements can be shown as

$$\frac{\delta D}{D} = \pm \frac{0.005}{D[mm]} \tag{A.17}$$

$$\frac{\delta l}{l} = \pm \frac{0.005}{l[mm]} \tag{A.18}$$

Since A $\alpha\ D^2$ the uncertainty in the calculated area can be shown as

$$\frac{\delta A}{A} = \pm \sqrt{\left(\frac{0.005}{D[mm]}\right)^2 + \left(\frac{0.005}{l[mm]}\right)^2} = \pm \frac{0.01mm}{D[mm]} \tag{A.19}$$

A.2.6 Wire Inclination Angle

The angle intervals at the angle measurement device rod are marked with a protractor with a $\pm$ 0.1 cm reading error. Therefore, the uncertainty of wire angle measurements is

$$\frac{\delta\varphi}{\varphi} = \pm\frac{1^\circ}{\varphi\ (^\circ)} \tag{A.20}$$

A.2.7 Properties

The uncertainty for air properties μ, k and Pr can be shown as [75]

$$\frac{\delta k}{k} = \frac{\delta\mu}{\mu} = \frac{\delta Pr}{Pr} = 1.5 \times 10^{-3} \tag{A.21}$$

A.2.8 SMA Wire Electrical Resistance

The resistance of SMA wire is calculated as

$$R_{SMA} = \frac{V_{SMA}}{I_{shunt}} \tag{A.22}$$

Therefore the uncertainty in the calculated wire resistance can be shown as

$$\frac{\delta R_{SMA}}{R_{SMA}} = \pm\sqrt{(\frac{\delta V_{SMA}}{V_{SMA}})^2 + (\frac{\delta I_{shunt}}{I_{shunt}})^2} \tag{A.23}$$

The uncertainty in the SMA wire voltage and current is shown in Equations (A.7) and (A.11) respectively. By substituting Equations (A.7) and (A.11) into Equation (A.23) the uncertainty in electrical resistance of the SMA wire can be shown as

$$\frac{\delta R_{SMA}}{R_{SMA}} = \pm \sqrt{(3.0 \times 10^{-5} + \frac{7.0 \times 10^{-6} V}{V_{SMA}[V]})^2 + (3.0 \times 10^{-5} + \frac{3.5 \times 10^{-6} V}{V_{shunt}[V]})^2 + (0.0014)^2} \quad \text{(A.24)}$$

A.2.9 SMA Wire Strain

The SMA wire strain is calculated by converting the resistance signal measured by the Bourns Square Single-Turn Panel control potentiometer the resistance signal readings was through the Keithley data acquisition system. The uncertainty in the strain measurements is determined as

$$\frac{\delta \varepsilon}{\varepsilon} = \pm \sqrt{(\frac{\delta C}{C})^2 + (\frac{\delta R}{R})^2 + (\frac{\delta D}{D})^2 + (\frac{\delta l}{l})^2} \quad \text{(A.25)}$$

where $\frac{\delta C}{C}$ is the accuracy of the potentiometer which is determined from specification as

$$\frac{\delta C}{C} = \pm \text{ 5\% of full scale}$$

The potentiometer full scale used in this work is 10 kΩ, therefore the uncertainty for the potentiometer is

(A.26)

$$\frac{\delta C}{C} = \pm \frac{500\Omega}{R[\Omega]}$$

$\frac{\delta R}{R}$ is the uncertainty for the Keithley data acquisition system which according to its specifications for 10 kΩ range is

(A.27)

$$\frac{\delta R}{R} = \pm \left(10^{-4} + \frac{6 \times 10^{-2}\Omega}{R[\Omega]}\right)$$

$\frac{\delta D}{D}$ and $\frac{\delta l}{l}$ are the uncertainty in measured pulley diameter and wire length as introduced in section A.2.5.

Therefore, based on Equation (A.18) and (A.26) and (A.27) the uncertainty in wire strain can be shown as

(A.28)

$$\frac{\delta \varepsilon}{\varepsilon} = \pm \sqrt{(10^{-4} + \frac{6 \times 10^{-2}\Omega}{R[\Omega]})^2 + (\frac{500\Omega}{R[\Omega]})^2 + (\frac{0.01mm}{D[mm]})^2}$$

A.3 Uncertainty in Calculated Quantities

A.3.1 Radiation Heat Transfer Q_{rad}

The radiation heat transfer rate from the wire is calculated as

$$Q_{rad} = V_{SMA} I_{shunt(vacuum)} \tag{A.29}$$

The uncertainty in Q_{rad} can be shown as

$$\frac{\delta Q_{rad}}{Q_{rad}} = \pm \sqrt{(\frac{\delta V_{SMA(Vacuum)}}{V_{SMA(Vacuum)}})^2 + (\frac{\delta I_{shunt(vacuum)}}{I_{shunt(vacuum)}})^2} \tag{A.30}$$

By substituting Equations (A.7) and (A.11) into Equation (A.30) the uncertainty in Q_{rad} can be shown as

$$\frac{\delta Q_{rad}}{Q_{rad}} = \pm \sqrt{(3.0 \times 10^{-5} + \frac{7.0 \times 10^{-6} V}{V_{SMA}[V]})^2 + (3.0 \times 10^{-5} + \frac{3.5 \times 10^{-6} V}{V_{shunt}[V]})^2 + (0.0014)^2} \tag{A.31}$$

A.3.2 Convection Heat Transfer Q_{conv}

The convection heat transfer from the SMA wire is calculated as

$$Q_{conv} = V_{SMA} I_{SMA} - Q_{rad} \tag{A.32}$$

The uncertainty in Q_{conv} based on Equation (A.31) and (A.32) can be shown as

(A.33)

$$\frac{\delta Q_{conv}}{Q_{conv}} = \pm\sqrt{(\frac{\delta V_{SMA}}{V_{SMA}})^2 + (\frac{\delta I_{SMA}}{I_{SMA}})^2 + (\frac{\delta V_{SMA(Vacuum)}}{V_{SMA(Vacuum)}})^2 + (\frac{\delta I_{shunt(vacuum)}}{I_{shunt(vacuum)}})^2}$$

$$= \pm\sqrt{2(\frac{\delta V_{SMA}}{V_{SMA}})^2 + 2(\frac{\delta I_{SMA}}{I_{SMA}})^2}$$

By substituting Equations (A.7) and (A.11) into Equation (A.33) the uncertainty in Q_{conv} can be shown as

(A.34)

$$\frac{\delta Q_{conv}}{Q_{conv}}$$

$$= \pm\sqrt{2(3.0 \times 10^{-5} + \frac{7.0 \times 10^{-6} V}{V_{SMA}[V]})^2 + 2(3.0 \times 10^{-5} + \frac{3.5 \times 10^{-6} V}{V_{shunt}[V]})^2 + 3.92 \times 10^{-6}}$$

A.3.3 Rayleigh Number

The Rayleigh number for the SMA wire is calculated as

$$Ra_D = \frac{g\beta(T_{SMA} - T_\infty)D^3}{v^2}.Pr = \frac{g(T_{SMA} - T_\infty)D^3P^2}{\mu^2 T_\infty R^2 Z^2 {T_m}^2}.Pr$$

By neglecting the uncertainty in g and R the uncertainties in the Rayleigh number can be shown as [73, 76]

(A.35)

$$\frac{\delta Ra_D}{Ra_D} = \pm \sqrt{\begin{array}{c}(\frac{\delta T_{SMA}}{T_{SMA} - T_\infty})^2 + (\frac{\delta T_\infty}{T_{SMA} - T_\infty})^2 + (3\frac{\delta D}{D})^2 + (2\frac{\delta P}{P})^2 + (\frac{\delta Pr}{Pr})^2 + \\ (2\frac{\delta \mu}{\mu})^2 + (\frac{\delta T_\infty}{T_\infty})^2 + (2\frac{\delta T_m}{T_m})^2\end{array}}$$

where the uncertainty in T_m can be shown as

(A.36)

$$\frac{\delta T_m}{T_m} = \pm \sqrt{(\frac{\delta T_{SMA}}{T_{SMA}})^2 + (\frac{\delta T_\infty}{T_\infty})^2}$$

A.3.4 Nusselt Number

The Nusselt number for the SMA wire is calculated as

$$Nu_D = \frac{Q_{conv} D}{k A_{SMA} (T_{SMA} - T_\infty)}$$

The Nusselt number uncertainty based an Equation (A.34) can be shown as [73, 76]

(A.37)

$$\frac{\delta Nu_D}{Nu_D} = \sqrt{2\left(\frac{\delta V_{SMA}}{V_{SMA}}\right)^2 + 2\left(\frac{\delta I_{SMA}}{I_{SMA}}\right)^2 + \left(\frac{\delta T_{SMA}}{T_{SMA} - T_\infty}\right)^2 + \left(\frac{\delta T_\infty}{T_{SMA} - T_\infty}\right)^2 + \left(\frac{\delta D}{D}\right)^2 \left(\frac{\delta k}{k}\right)^2 + \left(\frac{\delta A_{SMA}}{A_{SMA}}\right)^2}$$

A.4 Uncertainty of Experimental Results

The summaries of calculated uncertainties for presented experimental data are tabulated from Table (A-1) to (A-15).

Table A-1 Uncertainty in experimental variables

Variables	Range	± Uncertainty (%)
T_{SMA}	(23 ℃ - 150 ℃)	(1% - 4%)
M_s, M_f, A_s, A_f	(40 ℃ - 95 ℃)	(2% - 5%)
R_{SMA}	(0.55 Ω – 0.93 Ω)	(1% - 2%)
I_{SMA}	(0.06 A – 1.3 A)	(2% - 7%)
ε	(0 – 0.045 mm)	(8% - 10 %)
P	(0.00002 MPa - 0.1 MPa)	(1% - 7%)
Ra_D	($2.6 \times 10^{-8} - 0.6$)	(11%-12%)
Nu_D	(0.2-0.9)	(5%-9%)

References

[1] Wayman,C.M., Duerig, T.W. 1990 “An Introduction to Martensite and Shape Memory”, Duerig, T. W., Melton, K. N., Stockel, D., Wayman, C.M. (Eds.) “Engineering Aspects of Shape Memory Alloys” (3), Butterworth-Heinemann, Essex.

[2] Trivedi, B.P. (2011, May) “Waste Recovery Heat Engines”, 7 Radical Energy Solutions, Scientific American, issue 304 (38).

[3] Stoeckel,D. 1990 “Shape Memory Actuators for Automative Applications”, Duerig, T. W., Melton, K. N., Stockel, D., Wayman, C.M. (Eds.) “Engineering Aspects of Shape Memory Alloys” (283), Butterworth-Heinemann, Essex.

[4] Cui, D., Song, G., Li, H. 2010 “Modeling of the Electrical Resistance of Shape Memory Alloy Wires”, Smart Materials and Structures, Vol. 19, No 5 (1).

[5] Kirkpatrick, K., Valasek, J. 2009 “Reinforcement Learning for Characterizing Hysteresis Behavior of Shape Memory Alloys”, Journal of Aerospace Computing, Information and Communication, Vol. 6 (227).

[6] Dutta, S.M., Ghorbel, F. H. 2005 “Differential Hysteresis Modeling of a Shape Memory Alloy Wire Actuator”, IEEE Transactions on Mechatronics, Vol. 10 (189).

[7] Shahin, A.R., Meckl, P.H., Jones, J.D. 1994 “Enhanced Cooling of Shape Memory Alloy Wires Using Semiconductor Heat Pump Modules”, Journal of Intelligent Material Systems and Structures, Vol. 5 (95).

[8] Pathak, A., Brei, D., Luntz, J. 2010 “Transformation Strain Based Method for Characterization of Convective Heat Transfer from Shape Memory Alloy Wires”, Smart Materials and Structures Vol.19, No 3 (1).

[9] Nascimento M., Araujo, J., Neto, J., Lima A. 2006 “Electro-Thermomechanical Characterization of Ti-Ni Shape Memory Alloy Thin Wires”, Materials Research, Vol. 9, No. 1, (15).

[10] Jena, A. K., Chaturvedi, M. C. 1992 “Phase Transformations in Materials”, Prentice-Hall Inc., New Jersey.

[11] Mittemeijer, E.J. 2010 “Fundamentals of Materials Science” Springer-Verlag Berlin Heidelberg.

[12] Christian, J. W. 2002 “The Theory of Transformations in Metals and Alloys”, Part I, Elsevier Science Ltd., Oxford.

[13] Callister, W. D. 1991 “Materials Science and Engineering an Introduction”, John Wiley and Sons, New Jersey.
[14] Sorby, H. C. 1890 “ On the Microscopical Structure of Iron and Steel”; as cited in Nishiyama, Z. 1978 “Martensitic Transformation” Edited by Fine, M., Meshii, M., Wayman, C., Academic Press Inc., London.
[15] Christian, J. W. 2002 “The Theory of Transformations in Metals and Alloys”, Part II, Elsevier Science Ltd., Oxford.
[16] Christian, J. W. 1965 “Military Transformation: An Introductory Survey”, Physical Properties of Martensite and Bainite, Special Report 93.
[17] Kurdjumov, G. V., Maximova, O. P. 1948 “ O Kinetike Prevrashcheniya Austenia V Martensit Prinizkikh Temperaturakh ”, Doklady Akademii Nauk, SSSR Vol.61 (83).
[18] Bunshah, R.F., Mehl, R. F. 1953 “Rate of Propagation of Martensite”, Journal of Metals, Vol. 5 (1251).
[19] Patoor, E., Lagoudas, D.C., Entchev, P.B., Brinson, L.C., Gao, X. 2006 “Shape Memory Alloys, Part I: General Properties and Modeling of Single Crystals”, Mechanics of Materials, Vol. 38 (391).
[20] Wang, Z., Kirkpatrick, S.R., Adams, T., Siahmakoun, A. 2004 “TiNi MEMS Heat Engine” Proceedings of SEM X International Congress and Exposition on Experimental and Applied Mechanics.
[21] Urbina, C., De la Flor, S., Ferrando, F. 2010 “ R-phase Influence on Different Two-way Shape Memory Training Methods in NiTi Shape Memory Alloys”, Journal of Alloys and Compounds, Vol. 490 (499).
[22] Zhou, Y., Fan, G., Zhang, J., Ding, X., Ren, X., Sun, J., Otsuka, K. 2006 “Understanding of Multi-Stage R-Phase Transformation in Aged Ni- Rich Ti-Ni Shape Memory Alloys”, Material Science and Engineering A 438-440 (602).
[23] Otsuka, K. 1990 “Introduction to the R-Phase Transition”, Duerig, T. W., Melton, K. N., Stockel, D., Wayman, C.M. (Eds.) “Engineering Aspects of Shape Memory Alloys” (36), Butterworth-Heinemann, Essex.
[24] Lukas, P., Sittner, P., Lugovoy, D., Neov, D., Ceretti, M. 2002 “In Situ Neutron Diffraction Studies of the R-Phase Transformation in the NiTi Shape Memory Alloy”, Applied Physics A 74 (1121).

[25] Fukuda, T., Saburi, T., Doi, K., Nenno, S. 1992 “Nucleation and Self-Accommodation of R-Phase in Ti-Ni Alloys”, Materials Transaction Vol.33, No.3 (271).
[26] Kumar, P.K., Lagoudas, D.G. 2008 “Introduction to Shape Memory Alloys”, Springer Science, Texas.
[27] Olander, A. 1932 “An Electrochemical Investigation of Solid Cadmium-Gold Alloys”, Journal of the American Chemical Society, Vol.54 (3819).
[28] Greninger, A.B., Mooradian, V.G. 1938 “Strain Transformation in Metastable Beta Copper-Zinc and Beta Copper-Tin Alloys”, Trans. AIME 128 (337).
[29] Kurdjumov, G. V., Khandros, L. G. 1949 “First Reports of the Thermoelastic Behaviour of the Martensitic Phase of Au-Cd Alloys”, Doklady Akademii Nauk, SSSR Vol.66 (211).
[30] Buehler, W. J., Gilfrich, J. V., Wiley, R. C. 1963 “Effects of Low-temperature Phase Changes on the Mechanical Properties of Alloys Near Composition TiNi”, Journal of Applied Physics, Vol. 34 (1475).
[31] He, Z., Gall, K.R., Brinson, L.C. 2006 “Use of Electrical Resistance Testing to Redefine the Transformation Kinetics and Phase Diagram for Shape-Memory Alloys”, Metallurgical and Materials Transactions 37A(579).
[32] Keeley, A., Stockel, D., Duerig, T.W. 1990 “Actuator and Work Production Devices”, Duerig, T. W., Melton, K. N., Stockel, D., Wayman, C.M. (Eds.) “Engineering Aspects of Shape Memory Alloys” (181), Butterworth-Heinemann, Essex.
[33] Waram, T. 1990 “Design Principles for Ni-Ti Actuators”, Duerig, T. W., Melton, K. N., Stockel, D., Wayman, C.M. (Eds.) “Engineering Aspects of Shape Memory Alloys” (234), Butterworth-Heinemann, Essex.
[34] Tautzenberger, P. 1990 “Thermal Actuators: A Comparison of Shape Memory Alloys with Thermostatic Bimetals and Wax Actuators”, Duerig, T. W., Melton, K. N., Stockel, D., Wayman, C.M. (Eds.) “Engineering Aspects of Shape Memory Alloys” (207), Butterworth-Heinemann, Essex.
[35] Fosdick,R., Ketema,Y. 1998 “ Shape Memory for Passive Vibration Damping”, Journal of Intelligent Material Systems and Structures, Vol. 9 (854).
[36] Humbeeck, J.V., Kustov, S. 2005 “Active and Passive Damping of Noise and Vibration Through Shape Memory Alloys: Applications and Mechanisms” Journal of Smart Materials and Structures, Vol.14 (171).

[37] Calkins, T., Polt, W., Mabe, J. 2006, Not So Loud, Boeing Frontiers Vol. 4 iss.10 http://www.boeing.com/news/frontiers/archive/2006/march/i_tt.html
[38] Hartl, D., Lagoudas, D.C. 2007 "Aerospace Applications of Shape Memory Alloys" Journal of Aerospace Engineering, Vol.221, No. 4 (535).
[39] NASA Glenn Research Center, Shape Effect on Lift, http://www.grc.nasa.gov/WWW/k-12/airplane/shape.html
[40] Gil, F.J., Planell, J. A. 1998 "Shape Memory Alloys for Medical Applications", Journal of Engineering in Medicine, Vol. 212 (473).
[41] Carballo, M., Pu, Z.J., Wu, K. H. 1995 "Variation of Electrical Resistance and the Elastic Modulus of Shape Memory Alloys under Different Loading and Temperature Conditions", Journal of Intelligent Material Systems and Structures, Vol. 6 (557).
[42] Wu, X. D., Wu, J.S., Wang, Z. 1999 "The Variation of Electrical Resistance of Near Stoichiometric NiTi During Thermo-mechanic Procedures", Smart Materials and Structures Vol. 8 (574).
[43] Ikuta, K., Tsukamoto, M., Hirose, S. 1991 "Mathematical Model And Experimental Verification of Shape Memory Alloy For Designing Micro Actuator", Proceedings of An Investigation of Micro Structures, Sensors, Actuators, Machines and Robots IEEE (103).
[44] Novak,V., Sittner, P., Dayananda, G.N., Braz-Fernandes, F.M., Mahesh, K.K. 2008 "Electric Variation of NiTi Shape Memory Alloy Wires in Thermomechanical Tests: Experiments and Simulation" , Materials Science and Engineering A 481-482 (127).
[45] Incropera, F.P., DeWitt, D.P. 1996 "Fundamentals of Heat and Mass Transfer", John Wiley and Sons, New York.
[46] Morgan, V.T. 1975 "The Overall Convective Heat Transfer from Smooth Circular Cylinders", Advances in Heat Transfer, Vol. 11 (199).
[47] Churchill, S.W., Chu, H.H.S. 1975 "Correlating Equations for Laminar and Turbulent Free Convection from a Horizontal Cylinder", International Journal of Heat and Mass Transfer, Vol. 18 (1049).
[48] Jaluria, Y. 1980 "Natural Convection Heat and Mass Transfer", Pergamon Press, Beccles and London.
[49] McAdams, W.H. 1954 "Heat Transmission", McGraw Hill, New York.
[50] Kyte, J.R., Madden, A.J., Piret, E.L. 1953 "Natural-Convection Heat Transfer at Reduced Pressure", Chemical Engineering Progress, Vol.49, No.12 (653).

[51] Tsubouchi, T., Masuda, H. 1968 “Heat Transfer by Natural Convection from Horizontal Cylinders at Low Rayleigh Numbers”, Sci. Rep. Res. Inst., Tohoku University, Ser. B 19 (205).
[52] Fujii, T., Fujii, M., Honda, T. 1982 “Theoretical and Experimental Studies of the Free Convection Round a Long Horizontal Thin Wire in Air”, 7th International Heat Transfer Conference, Munich, Vol.2 (311).
[53] Yang, S.M., 1985 “General Correlating Equations for Free Convection Heat Transfer from a Vertical Cylinder”, Proceedings of International Symposium on Heat Transfer (153).
[54] Mueller, A. C. 1942 “Heat Transfer from Wires to Air in Parallel Flow”, Transactions of the American Institute of Chemical Engineers, Vol. 38 (613).
[55] Nagendra, H.R., Tirunarayanan, M.A., Ramachandran, A. 1969 “Free Convection Heat Transfer from Vertical Cylinders and Wires”, Chemical Engineering Science, Vol.24 (1491).
[56] Fujii, T., Koyama, Sh., Fujii, M. 1986 “Experimental Study of Free Convection Heat Transfer from Convection Heat Transfer from an Inclined Fine Wire To Air”, Proceeding 8th International Heat Transfer Conference, Vol.3 (1323).
[57] Janna,W.S. 1986 “ Engineering Heat Transfer”, PWS Publishers, Boston.
[58] Oosthuizen, P. H. 1976 “Experimental Study of Free Convection Heat Transfer from Inclined Cylinders”, Journal of Heat Transfer, Vol. 98 (672).
[59] Chand, J., Vir, D. 1980 “A Unified Approach to Natural Convection Heat Transfer in the Laminar Region from Horizontal and Inclined Cylinders”, Letters in Heat and Mass Transfer, Vol.7 (213).
[60] Raithby, G.D., Hollands, K.G.T. 1976 “Laminar and Turbulent Free Convection from Elliptic Cylinders, With a Vertical Plate and Horizontal Circular Cylinder as Special Cases”, Trans. ASME, Ser. C, Journal of Heat and Mass Transfer, Vol. 98 (72).
[61] Ma, H. 2010 “Thermal Modeling of Shape Memory Alloy Wire Actuators for Automotive Applications ” M.Sc. Thesis, Department of Mechanical and Mechatronics Engineering, University of Waterloo, Waterloo, Ontario, Canada.
[62] Omega, Technical references, Physical Properties of Thermoelement Materials, http://www.omega.com/temperature/Z/pdf/z016.pdf
[63] Morgan, N.B., Friend, C.M. 2001 “Stress/Temperature Phase Diagrams As a Tool for Shape Memory Alloy Selection and Processing”, Journal of Physics IV France Vol.11 (503).
[64] Bhattacharya, K. 1992 “Self- Accommodation in Martensite” Communicated by Kinderlehrer D., Archive for Rational Mechanics and Analysis Vol.120 (201).

[65] Saburi, T., Wayman, C.M. 1979 “Crystallographic Similarities in Shape Memory Martensites”, Acta Metallurgica, Vol. 27 (979).
[66] Ma, N., Song, G., Lee, H.J. 2004 “Position Control of Shape Memory Alloy Actuators With Internal Electrical Resistance Feedback Using Neural Networks”, Smart Materials and Structures, Vol. 13 (777).
[67] Johnson Matthey Medical 2011 “Measuring Transformation Temperatures in Nitinol Alloys” http://jmmedical.com/resources/211/Measuring-Transformation-Temperatures-in-Nitinol-Alloys.html.
[68] Khandelwal,A., Buravalla, V. 2009 “Models for Shape Memory Alloy: An Overview of Modeling Approaches”, The International Journal of Structural Changes in Solids, Vol.1 NO. 1.
[69] Choon, T.W., Salleh, A.S., Jamian, S., Ghazali, M.I. 2007 “Phase Transformation Temperatures for Shape Memory Alloy Wire”, World Academy of Science, Engineering and Technology Vol. 25 (304).
[70] ASTM International 2010 “Standard Test Method for Transformation Temperature of Nickel-Titanium Alloys by Thermal Analysis”, F2004-05.
[71] Tobushi, H., Shimeno, Y., Hachisuka, T., Tanaka, K. 1998 “Influence of Strain Rate on Superelastic Properties of NiTi Shape Memory Alloy” Mechanics of Materials Vol.30 (141).
[72] Dynalloy Inc., Flexinol Technical and Design Data, http://www.dynalloy.com/TechData_Metric.html
[73] Moffat, R.J. 1988 “Describing The Uncertainties in Experimental Results”, Experimental Thermal and Fluid Science Vol.1 (3) Elsevier Science Publishing Co. Inc.
[74]Teertstra, P. 2003 “Models and Experiments for Laminar Natural Convection from Heated Bodies in Enclosures,” Ph.D. Thesis, Department of Mechanical and Mechatronics Engineering, University of Waterloo, Waterloo, Ontario, Canada.
[75] Jafarpur, K. 1992“ Analytical and Experimental Study of Laminar Free Convective Heat Transfer From Isothermal Convex Bodies of Arbitrary Shape”, Ph.D. Thesis, Department of Mechanical and Mechatronics Engineering, University of Waterloo, Waterloo, Ontario, Canada.
[76] Coleman, H., Steele, W. 1989 “Experimentation and Uncertainty Analysis for Engineers”, John Wiley & Sons, New York.